Chapter 7

AHTR One-Third Assembly Optimization Results

This chapter reports the Advanced High-Temperature Reactor (AHTR) one-third assembly's Reactor evOLutionary aLgorithm Optimizer (ROLLO) optimization results. I vary the following AHTR one-third assembly input parameters:

- Tristructural Isotropic (TRISO) packing fraction distribution ($\rho_{TRISO}(\vec{r})$)
- Total fuel packing fraction (PF_{total})
- Coolant channel shape (r_1, r_2, r_3, r_4, and r_5)

Section 5.3.1 detailed how I vary these AHTR one-third assembly's input parameters. I optimize the AHTR one-third assembly for the following objectives:

- Minimize total fuel packing fraction (PF_{total})
- Minimize maximum one-third assembly temperature (T_{max})
- Minimize fuel-normalized power peaking factor (PPF_{fuel})

Table 5.1 outlined these objectives and their motivation. Chapter 5 detailed the methodology for AHTR one-third assembly modeling and ROLLO optimization.

The subsequent sections outline the AHTR one-third assembly's optimization simulations, describe the single-objective and multi-objective ROLLO optimization simulations' results, report each simulation's computational cost, and discuss the results' significance.

7.1 ROLLO AHTR One-Third Assembly Optimization Simulations Overview

Table 7.1 details the ROLLO optimization problems explored in this chapter. I first conducted sin-

Table 7.1: Reactor evOLutionary aLgorithm Optimizer (ROLLO) simulations for optimizing Advanced High-Temperature Reactor (AHTR) one-third assembly. PF_{total}: Total Fuel Packing Fraction, T_{max}: Maximum one-third assembly Temperature, PPF_{fuel}: Normalized Power Peaking Factor, $\rho_{TRISO}(\vec{r})$: TRISO packing fraction distribution

Num of Objs	**Sim**	**Objectives**	**Constraints**	**Varying Parameters**	**Coupled Nuclear Software**
1	a-1a	• $\min(PF_{total})$	• $k_{eff} \geq 1.38$	• $\rho_{TRISO}(\vec{r})$ • PF_{total}	OpenMC
	a-1b	• $\min(T_{max})$	• $k_{eff} \geq 1.38$	• $\rho_{TRISO}(\vec{r})$	OpenMC, Moltres
	a-1c	• $\min(PPF_{fuel})$	• $k_{eff} \geq 1.38$	• $\rho_{TRISO}(\vec{r})$	OpenMC
	a-1d	• $\min(PF_{total})$	• $k_{eff} \geq 1.0$	• Coolant channel shape • PF_{total}	OpenMC
	a-1e	• $\min(T_{max})$	• $k_{eff} \geq 1.38$	• Coolant channel shape	OpenMC, Moltres
	a-1f	• $\min(PPF_{fuel})$	• $k_{eff} \geq 1.0$	• Coolant channel shape	OpenMC
2	a-2a	• $\min(PF_{total})$ • $\min(T_{max})$	• $k_{eff} \geq 1.38$	• $\rho_{TRISO}(\vec{r})$ • PF_{total}	OpenMC, Moltres
	a-2b	• $\min(PF_{total})$ • $\min(PPF_{fuel})$	• $k_{eff} \geq 1.38$	• $\rho_{TRISO}(\vec{r})$ • PF_{total}	OpenMC
	a-2c	• $\min(T_{max})$ • $\min(PPF_{fuel})$	• $k_{eff} \geq 1.38$	• $\rho_{TRISO}(\vec{r})$	OpenMC, Moltres
3	a-3a	• $\min(PF_{total})$ • $\min(PPF_{fuel})$ • $\min(T_{max})$	• $k_{eff} \geq 1.38$	• $\rho_{TRISO}(\vec{r})$ • PF_{total}	OpenMC, Moltres
	a-3b	• $\min(PF_{total})$ • $\min(PPF_{fuel})$ • $\min(T_{max})$	• $k_{eff} \geq 1.38$	• $\rho_{TRISO}(\vec{r})$ • PF_{total} • Coolant channel shape	OpenMC, Moltres

gle objective, single input parameter ROLLO optimizations to understand the individual impacts of each objective on each input parameter. Their results will inform the multi-objective optimization simulation setup.

Simulations are run on the Theta supercomputer at the Argonne Leadership Computing Facility under the Director's Discretionary Allocation Program [108]. Section 7.5 details each optimization simulation's computational cost.

7.2 AHTR One-Third Assembly: Single-Objective Optimization Results

This section reports the AHTR one-third assembly's ROLLO single-objective optimization results. Table 7.1 summarized the one-objective simulations: a-1a, a-1b, a-1c, a-1d, a-1e, and a-1f. In the following subsections, I describe the single-objective optimization results grouped by the minimized objective.

If a single-objective optimization problem's objective converges earlier than the five generations I intended to run (determined in Section 5.5.2), I stop the simulation at that generation. Section 4.5.1 described how reactor designers use ROLLO to determine problem convergence.

7.2.1 Objective: Minimize Total Packing Fraction (PF_{total})

This section reports results from the minimize total fuel packing fraction (PF_{total}) single-objective optimization simulations: a-1a and a-1d. Simulation a-1a varies the PF_{total} and TRISO packing fraction distribution ($\rho_{TRISO}(\vec{r})$), and simulation a-1d varies the PF_{total} and coolant channel shape (r_1, r_2, r_3, r_4, and r_5).

Simulation a-1a: Variation of PF_{total} and $\rho_{TRISO}(\vec{r})$

Table 7.2 shows simulation a-1a's optimization problem parameters.

The one-third assembly's TRISO distribution is varied based on sine distributions, as described in Section 5.3.1. If the simulation used the FHR benchmark equivalent PF_{total} = 0.153, at certain sine distributions, some fuel cells would have PF > 0.3. OpenMC's random sequential packing

Table 7.2: Simulation a-1a Optimization Problem Parameters

Single Objective: Simulation a-1a	
Objectives	Minimize PF_{total}
Input Parameter Variations	$0.05 \leq PF_{total} \leq 0.07$ $\rho_{TRISO}(\vec{r})$: $0 \leq a \leq 2$, $0 \leq d \leq 2$ $\rho_{TRISO}(\vec{r})$: $0 \leq b \leq \frac{\pi}{2}$, $0 \leq e \leq \frac{\pi}{2}$ $\rho_{TRISO}(\vec{r})$: $0 \leq c \leq 2\pi$, $0 \leq f \leq 2\pi$
Constraints	$k_{eff} \geq 1.38$
Genetic Algorithm Parameters	Population size: 128 Generations: 3

algorithm becomes prohibitively slow at $PF > 0.3$, resulting in long runtimes. Therefore, I used $PF_{total} = 0.06$ because it is approximately the smallest PF_{total} that enables $k_{eff} \geq 1.38$ and will avoid fuel cells with $PF > 0.3$ occurrences. I use $PF_{total} = 0.06$ for all optimization simulations that do not vary PF_{total}: a-1b, a-1c, a-1e, a-1f, and a-2c. I vary PF_{total} between 0.05 and 0.07 for all optimization simulations that vary PF_{total}: a-1a, a-1d, a-2a, a-2b, a-3a, and a-3b.

Figure 7.1a shows the PF_{total} evolution. Figure 7.1b shows four unique TRISO packing fraction distributions in the final generation with the most-minimized PF_{total}. Figure 7.1c illustrates the AHTR one-third assembly model with the most-minimized PF_{total}.

Figure 7.1a shows that the minimum and average PF_{total} converged to approximately 0.057 in the final generation. In Figure 7.1b, the four unique TRISO packing fraction distributions in the final generation that most-minimized PF_{total} have various oscillating TRISO distribution patterns.

The one-third assembly model with the most-minimized PF_{total} has a $PF_{total} = 0.0559$, an oscillating TRISO distribution along the x-axis and y-axis, and a packing fraction standard deviation of 0.04 across the one-third assembly. Along the x-axis, the distribution peaks on the even fuel cell columns (at 8.2cm, 12.3cm, 16.4cm, 20.5cm, and 24.5cm). The even columns have the largest y-axis variation of ~ 0.05 with peaks of $PF \approx 0.12$. The odd columns have the smallest y-axis variation of ~ 0.01 with minimums of $PF \approx 0.01$. Along the y-axis, the distribution peaks on the 2nd and 5th fuel cell rows (at 6.8cm and 16.5cm). The 2nd and 5th row have the largest x-axis variation of ~ 0.10 with peaks of $PF \approx 0.12$. The middle 3rd and 4th rows have the smallest x-axis variation of ~ 0.06 with minimums of $PF \approx 0.01$. Section 7.6.1 discusses the driving factors for the minimize PF_{total} objective and explains simulation a-1a's most-minimized PF_{total} oscillating TRISO distribution.

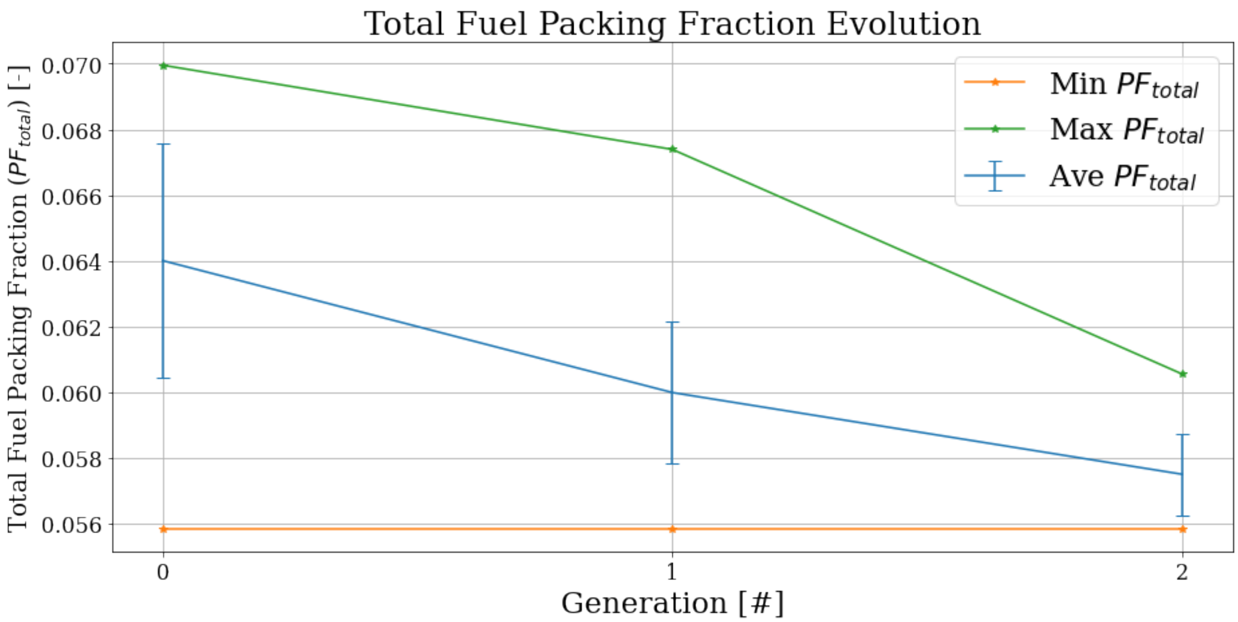

(a) Minimum, average, and maximum PF_{total} evolution.

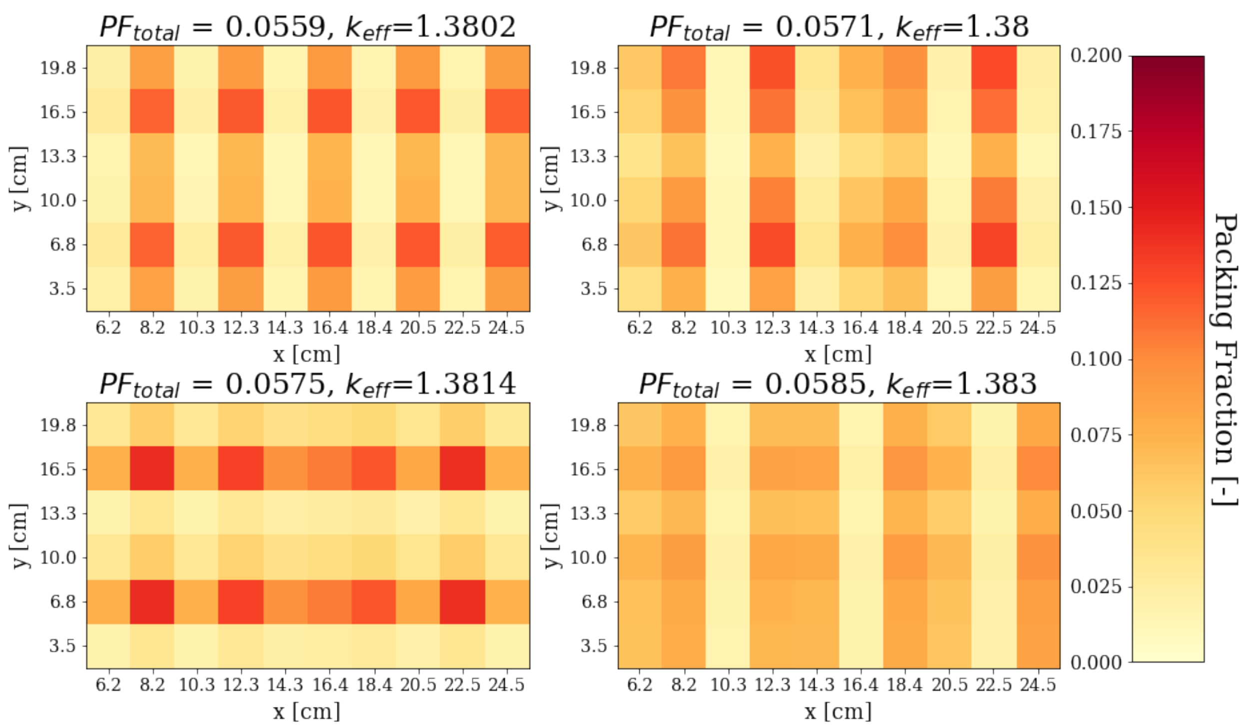

(b) TRISO packing fraction distribution for four unique reactor models with the smallest PF_{total} in the final generation.

Figure 7.1: Simulation a-1a – ROLLO single-objective optimization to minimize total fuel packing fraction (PF_{total}) in AHTR one-third assembly. Input parameters varied: PF_{total}, TRISO packing fraction distribution ($\rho_{TRISO}(\vec{r})$).

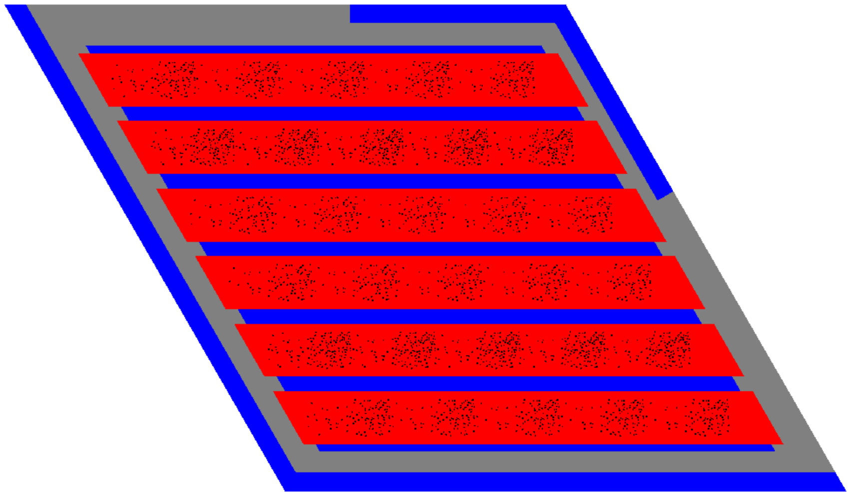

(c) AHTR one-third assembly model with the most-minimized PF_{total}, corresponding to the first TRISO distribution in Figure 7.1b. The reactor model has PF_{total} = 0.0559 and k_{eff} = 1.3802.

Figure 7.1: (contd.) Simulation a-1a – ROLLO single-objective optimization to minimize total fuel packing fraction (PF_{total}) in AHTR one-third assembly. Input parameters varied: total fuel packing fraction (PF_{total}), TRISO packing fraction distribution ($\rho_{TRISO}(\vec{r})$).

Simulation a-1d: Variation of PF_{total} and Coolant channel shape

Table 7.3 shows simulation a-1d's optimization problem parameters.

Table 7.3: Simulation a-1d Optimization Problem Parameters

Single Objective: Simulation a-1d	
Objectives	Minimize PF_{total}
Input Parameter variations	$0.01 < PF_{total} < 0.04$
	coolant channel shape: $0.05 < r_1 < 0.35$
	coolant channel shape: $0.05 < r_2 < 0.35$
	coolant channel shape: $0.05 < r_3 < 0.35$
	coolant channel shape: $0.05 < r_4 < 0.35$
	coolant channel shape: $0.05 < r_5 < 0.35$
Constraints	$k_{eff} \geq 1.0$
Genetic Algorithm Parameters	Population size: 64
	Generations: 2

Figure 7.2 shows the plots of coolant channel shape's r_1, r_2, r_3, r_4, and r_5 values against PF_{total}. Figure 7.2 demonstrates that there is no correlation between PF_{total} and coolant channel shape's r_1, r_2, r_3, r_4, and r_5.

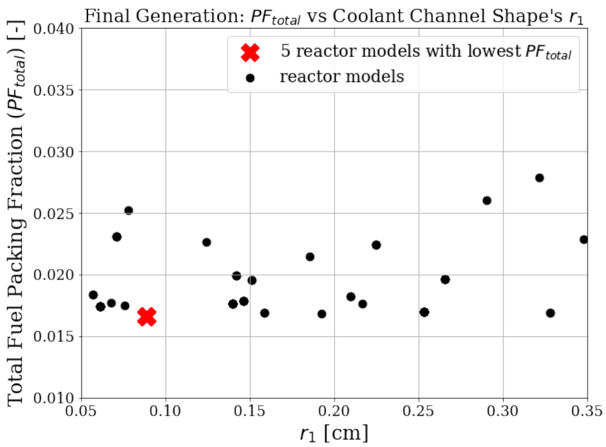

(a) Plot of PF_{total} against r_1.

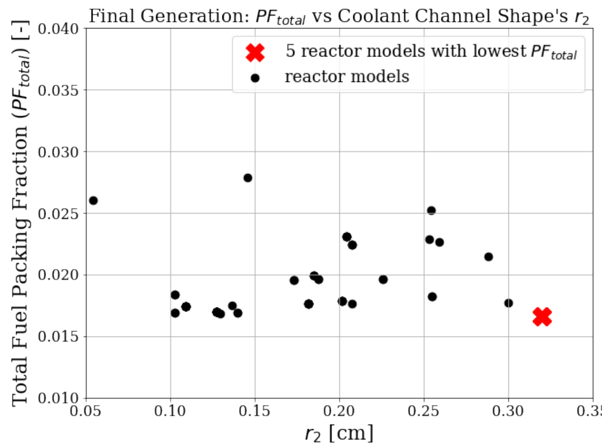

(b) Plot of PF_{total} against r_2.

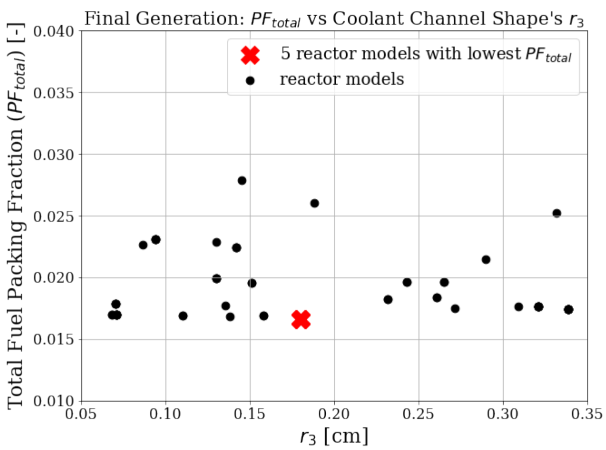

(c) Plot of PF_{total} against r_3.

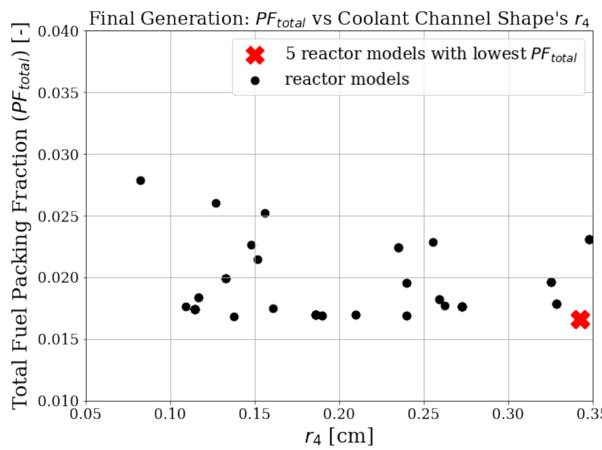

(d) Plot of PF_{total} against r_4.

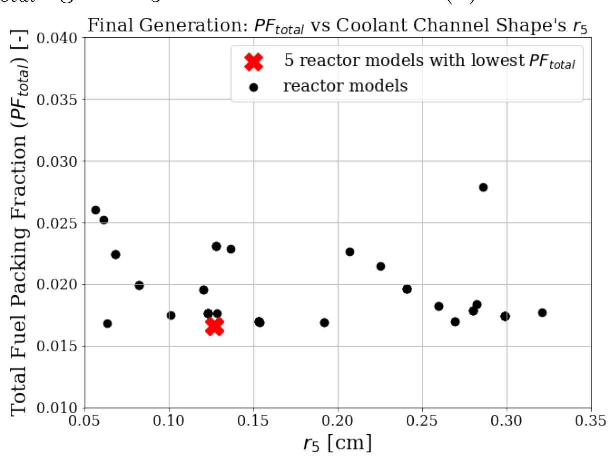

(e) Plot of PF_{total} against r_5.

Figure 7.2: Simulation a-1d – ROLLO single-objective optimization to minimize total fuel packing fraction (PF_{total}). Plots of simulation a-1d final generation's reactor models PF_{total} against coolant channel shape input parameters. Red crosses indicate the five reactor models with the lowest PF_{total}. Input parameters varied: PF_{total} and coolant channel shape $(r_1, r_2, r_3, r_4, r_5)$.

7.2.2 Objective: Minimize Maximum Temperature (T_{max})

This section reports results from the minimize maximum one-third assembly temperature (T_{max}) single-objective optimization simulations: a-1b and a-1e. Simulation a-1b varies TRISO packing fraction distribution ($\rho_{TRISO}(\vec{r})$), and simulation a-1e varies the coolant channel shape (r_1, r_2, r_3, r_4, and r_5).

Simulation a-1b: Variation of $\rho_{TRISO}(\vec{r})$

Table 7.4 shows simulation a-1b's optimization problem parameters.

Table 7.4: Simulation a-1b Optimization Problem Parameters

Single Objective: Simulation a-1b	
Objectives	Minimize T_{max}
Input Parameter variations	$\rho_{TRISO}(\vec{r})$: $0 \leq a \leq 2$, $0 \leq d \leq 2$ $\rho_{TRISO}(\vec{r})$: $0 \leq b \leq \frac{\pi}{2}$, $0 \leq e \leq \frac{\pi}{2}$ $\rho_{TRISO}(\vec{r})$: $0 \leq c \leq 2\pi$, $0 \leq f \leq 2\pi$
Constraints	$k_{eff} \geq 1.38$ $PF_{total} = 0.06$
Genetic Algorithm Parameters	Population size: 128 Generations: 3

Figure 7.3a shows the one-third assembly's T_{max} evolution. Figure 7.3b shows four unique TRISO packing fraction distributions in the final generation with the most minimized T_{max}. Figure 7.3c illustrates the AHTR one-third assembly model with the most-minimized T_{max}.

Figure 7.3a shows that the minimum and average one-third assembly's T_{max} converged to approximately 1200 K. In Figure 7.3b, the one-third assembly model with the most-minimized T_{max} has a T_{max} = 1186.5K and an almost constant TRISO packing fraction distribution with packing fraction standard deviation of 0.0009 across the one-third assembly. Section 7.6.2 discusses and explains simulation a-1b's most-minimized T_{max} almost constant TRISO distribution.

Simulation a-1e: Variation of Coolant channel shape

Table 7.5 shows simulation a-1e's optimization problem parameters.

Figure 7.4a shows the one-third assembly's T_{max} evolution. Figure 7.4b illustrates the AHTR one-third assembly model with the most-minimized T_{max}. Figures 7.4c, 7.4d, 7.4e, 7.4f, and 7.4g

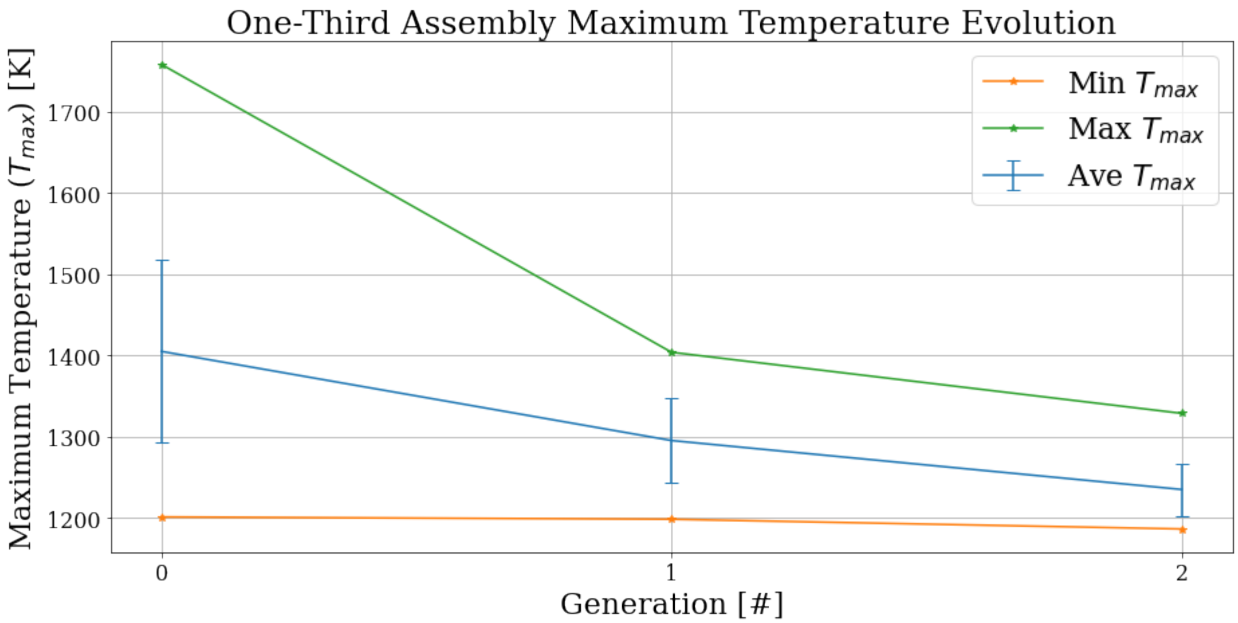

(a) Minimum, average, and maximum T_{max} evolution.

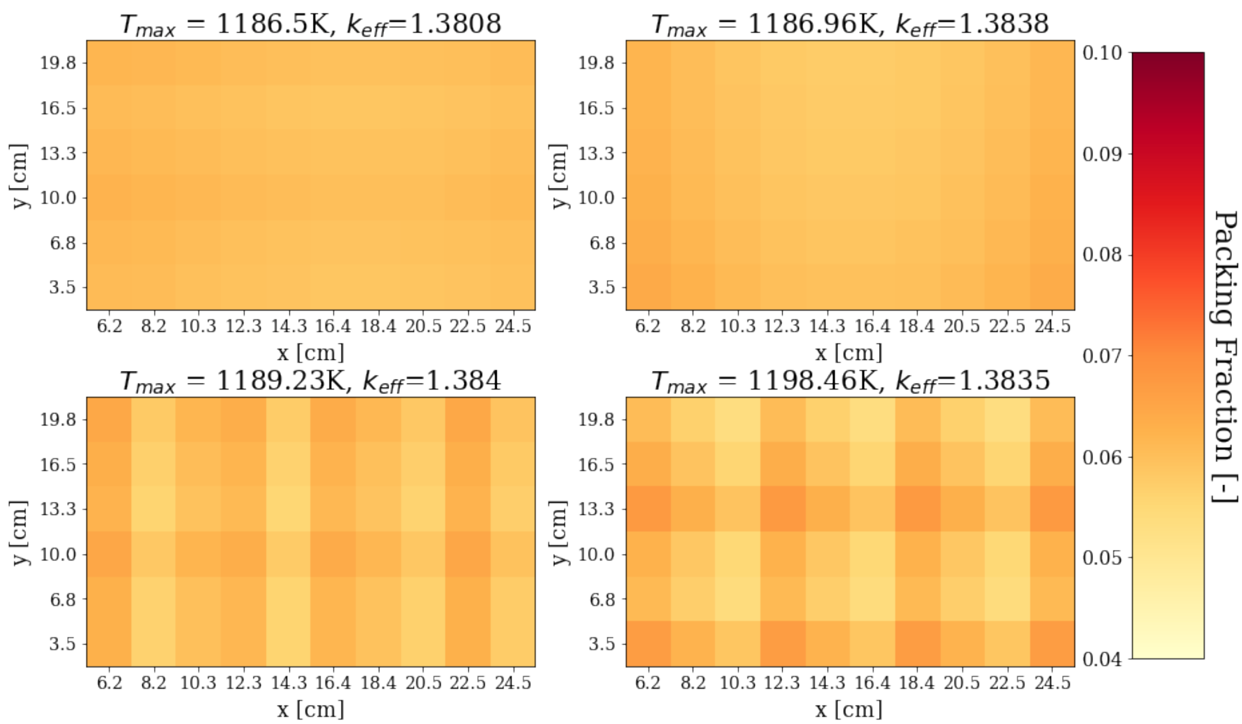

(b) TRISO packing fraction distribution for four unique reactor models with the smallest T_{max} in the final generation.

Figure 7.3: Simulation a-1b – ROLLO single-objective optimization to minimize maximum temperature (T_{max}) in the AHTR one-third assembly. Input parameters varied: TRISO packing fraction distribution ($\rho_{TRISO}(\vec{r})$).

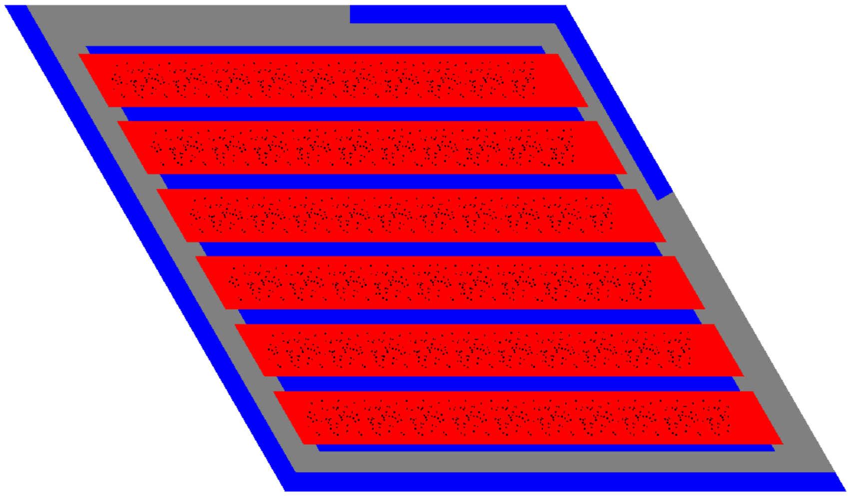

(c) AHTR one-third assembly model with the most-minimized T_{max}, corresponding to the first TRISO distribution in Figure 7.3b. The reactor model has T_{max} = 1180.29K and k_{eff} = 1.3046.

Figure 7.3: Simulation a-1b – ROLLO single-objective optimization to minimize maximum temperature (T_{max}) in AHTR one-third assembly. Input parameters varied: TRISO packing fraction distribution ($\rho_{TRISO}(\vec{r})$).

Table 7.5: Simulation a-1e Optimization Problem Parameters

Single Objective: Simulation a-1e	
Objectives	Minimize T_{max}
Input Parameter variations	coolant channel shape: $0.05 < r_1 < 0.35$
	coolant channel shape: $0.05 < r_2 < 0.35$
	coolant channel shape: $0.05 < r_3 < 0.35$
	coolant channel shape: $0.05 < r_4 < 0.35$
	coolant channel shape: $0.05 < r_5 < 0.35$
Constraints	$k_{eff} \geq 1.38$
	$PF_{total} = 0.06$
Genetic Algorithm Parameters	Population size: 128
	Generations: 2

show the plots of coolant channel shape's r_1, r_2, r_3, r_4, and r_5 values against T_{max}.

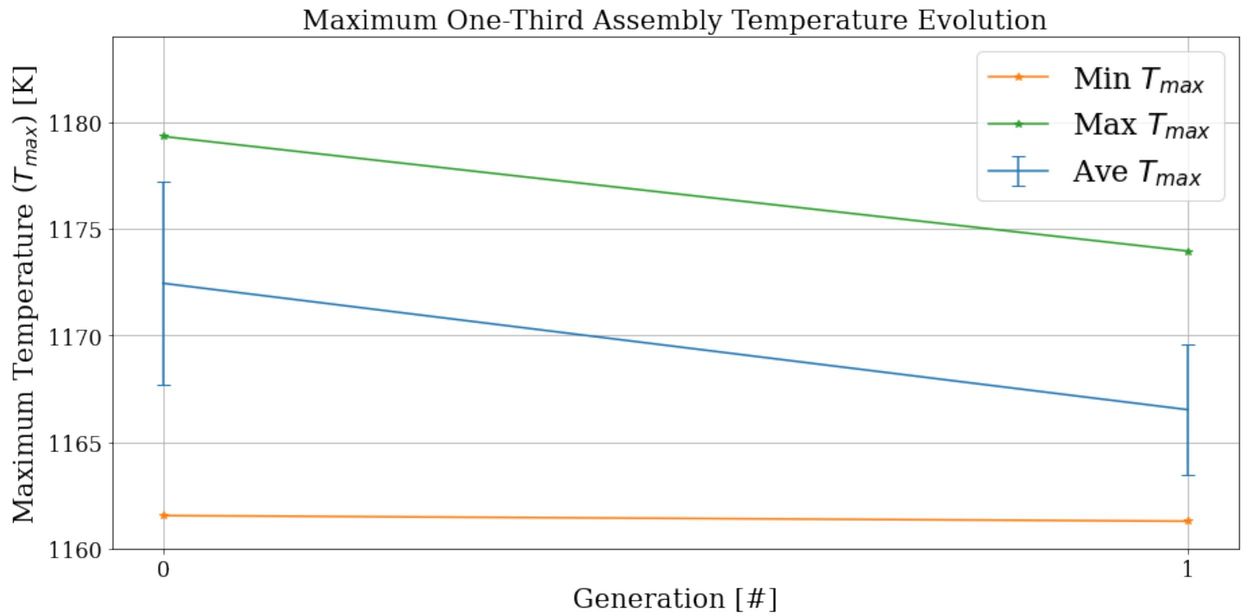

(a) Minimum, average, and maximum evolution of AHTR one-third assembly's T_{max}.

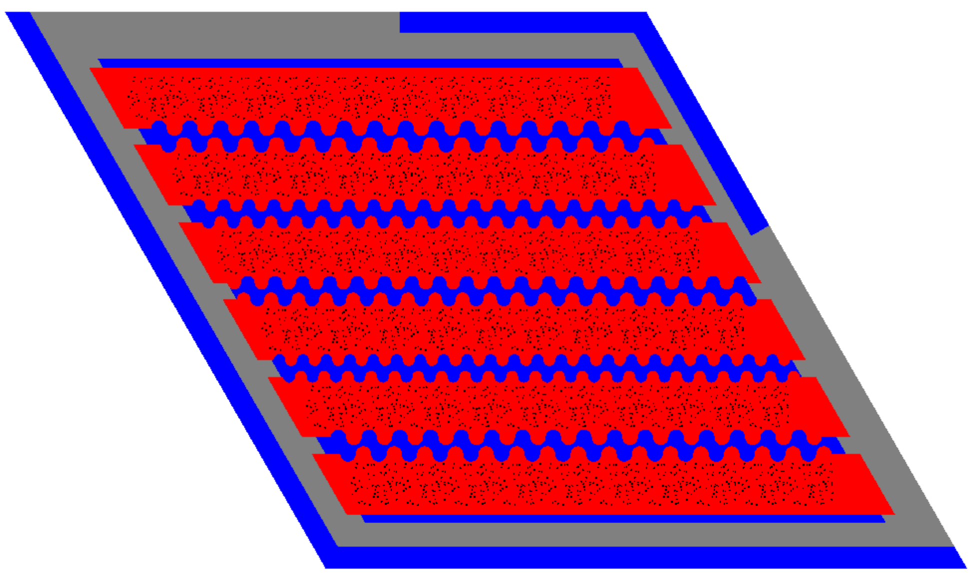

(b) AHTR one-third assembly model with the most-minimized T_{max}. The reactor model has T_{max} = 1161.28K, r_1 = 0.32cm, r_2 = 0.26cm, r_3 = 0.28cm, r_4 = 0.24cm, and r_5 = 0.32cm.

Figure 7.4: Simulation a-1e – ROLLO single-objective optimization to minimize maximum one-third assembly temperature (T_{max}). Plots of final generation's reactor models T_{max} against coolant channel shape input parameters. Red crosses indicate the five reactor models with the lowest T_{max}. Input parameters varied: coolant channel shape (r_1, r_2, r_3, r_4, r_5).

Figures 7.4c and 7.4g demonstrate negative linear correlations between the one-third assembly's T_{max} with r_1 and r_5. Figures 7.4d, 7.4e and 7.4f demonstrate that there is no correlation between T_{max} with r_2, r_3, and r_4. Section 7.6.2 discusses and explains the relationship between T_{max} and coolant channel shape.

7.2.3 Objective: Minimize Fuel-Normalized Power Peaking Factor (PPF_{fuel})

This section reports the minimize fuel-normalized power peaking factor (PPF_{fuel}) single-objective optimization simulation results: a-1c and a-1f. Simulation a-1c varies TRISO packing fraction distribution ($\rho_{TRISO}(\vec{r})$), and simulation a-1f varies the coolant channel shape (r_1, r_2, r_3, r_4, and r_5).

Simulation a-1c: Variation of $\rho_{TRISO}(\vec{r})$

Table 7.6 shows simulation a-1c's optimization problem parameters.

Table 7.6: Simulation a-1c Optimization Problem Parameters

Single Objective: Simulation a-1c	
Objectives	Minimize PPF_{fuel}
Input Parameter variations	$\rho_{TRISO}(\vec{r})$: $0 \leq a \leq 2$, $0 \leq d \leq 2$ $\rho_{TRISO}(\vec{r})$: $0 \leq b \leq \frac{\pi}{2}$, $0 \leq e \leq \frac{\pi}{2}$ $\rho_{TRISO}(\vec{r})$: $0 \leq c \leq 2\pi$, $0 \leq f \leq 2\pi$
Constraints	$k_{eff} \geq 1.38$ $PF_{total} = 0.06$
Genetic Algorithm Parameters	Population size: 128 Generations: 2

Figure 7.5a shows the one-third assembly's PPF_{fuel} evolution. Figure 7.5b shows the four unique TRISO packing fraction distributions in the final generation with the most minimized PPF_{fuel}. Figure 7.5c illustrates the AHTR one-third assembly model with the most-minimized PPF_{fuel}.

Figure 7.5a shows that the minimum and average one-third assembly's T_{max} converged to approximately 1.1. In Figure 7.5b, the most-minimized TRISO distribution has a PPF_{fuel} = 1.0872 and an oscillating TRISO distribution along the x-axis and a packing fraction standard deviation of 0.017 across the one-third assembly. Along the x-axis, the distribution peaks at the 2nd, 5th, and 9th fuel cell columns (at 8.2cm, 14.3cm, and 22.5cm) with $PF \approx 0.08$ and has minimum points

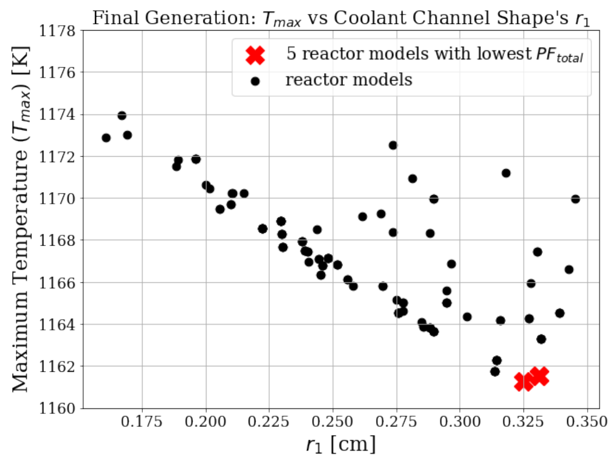

(c) Plot of PF_{total} against r_1.

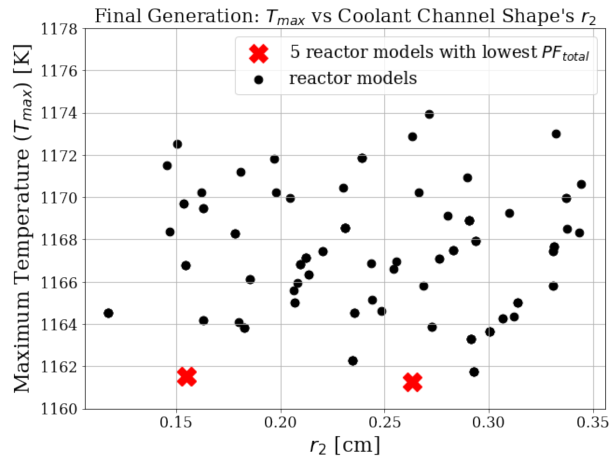

(d) Plot of PF_{total} against r_2.

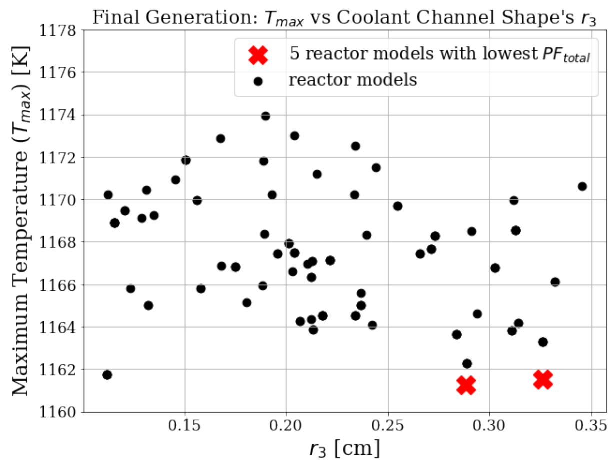

(e) Plot of PF_{total} against r_3.

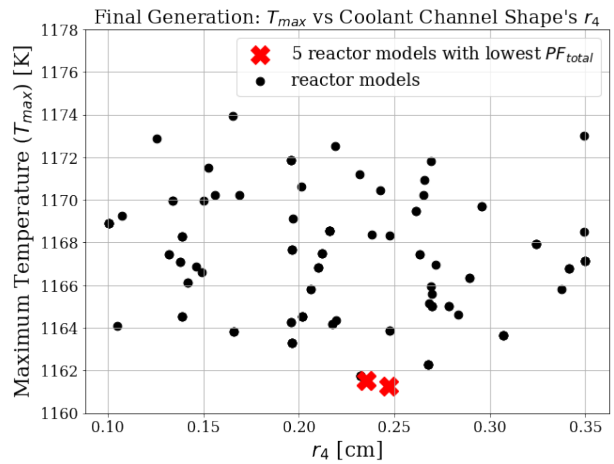

(f) Plot of PF_{total} against r_4.

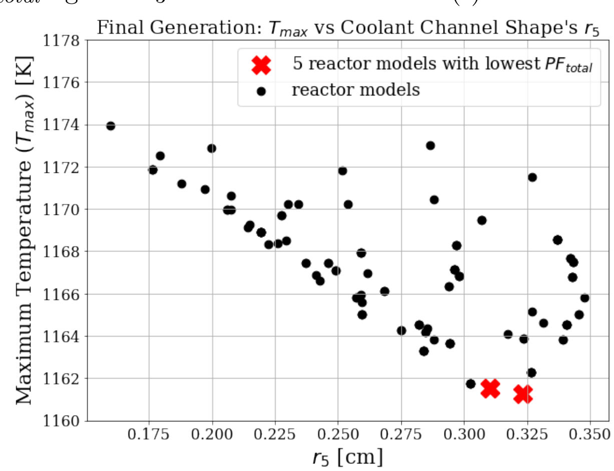

(g) Plot of PF_{total} against r_5.

Figure 7.4: Simulation a-1e – ROLLO single-objective optimization to minimize maximum one-third assembly temperature (T_{max}). Plots of final generation's reactor models T_{max} against coolant channel shape input parameters. Red crosses indicate the five reactor models with the lowest T_{max}. Input parameters varied: coolant channel shape $(r_1, r_2, r_3, r_4, r_5)$.

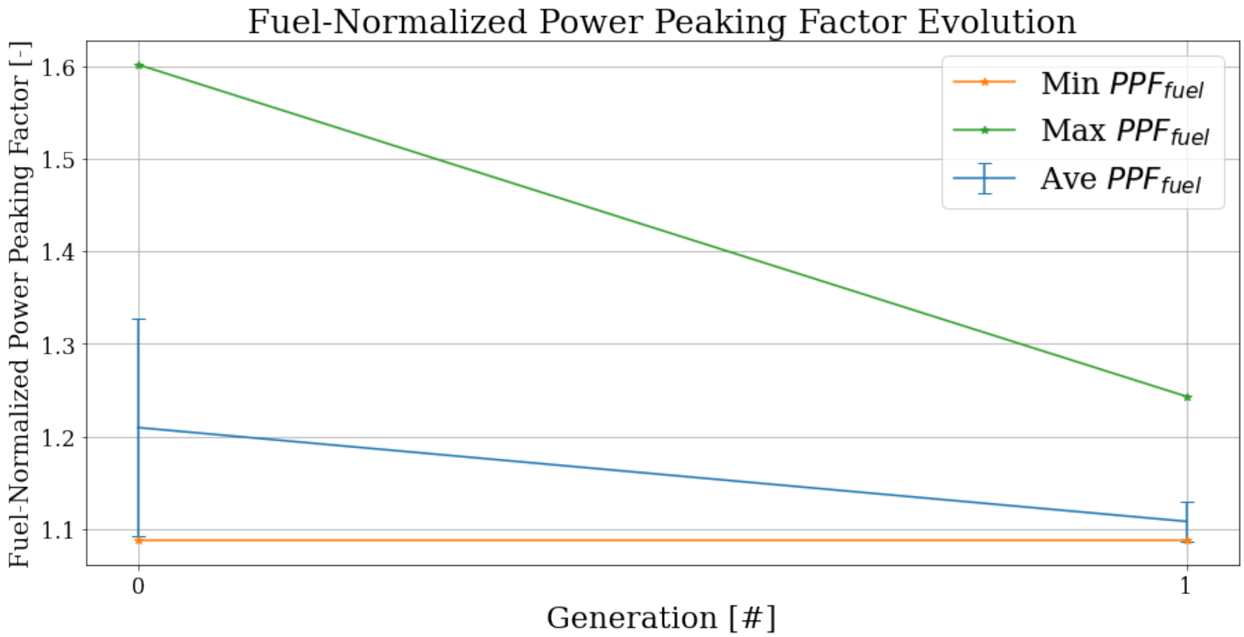

(a) Minimum, average, and maximum evolution of PPF_{fuel} in the AHTR one-third assembly.

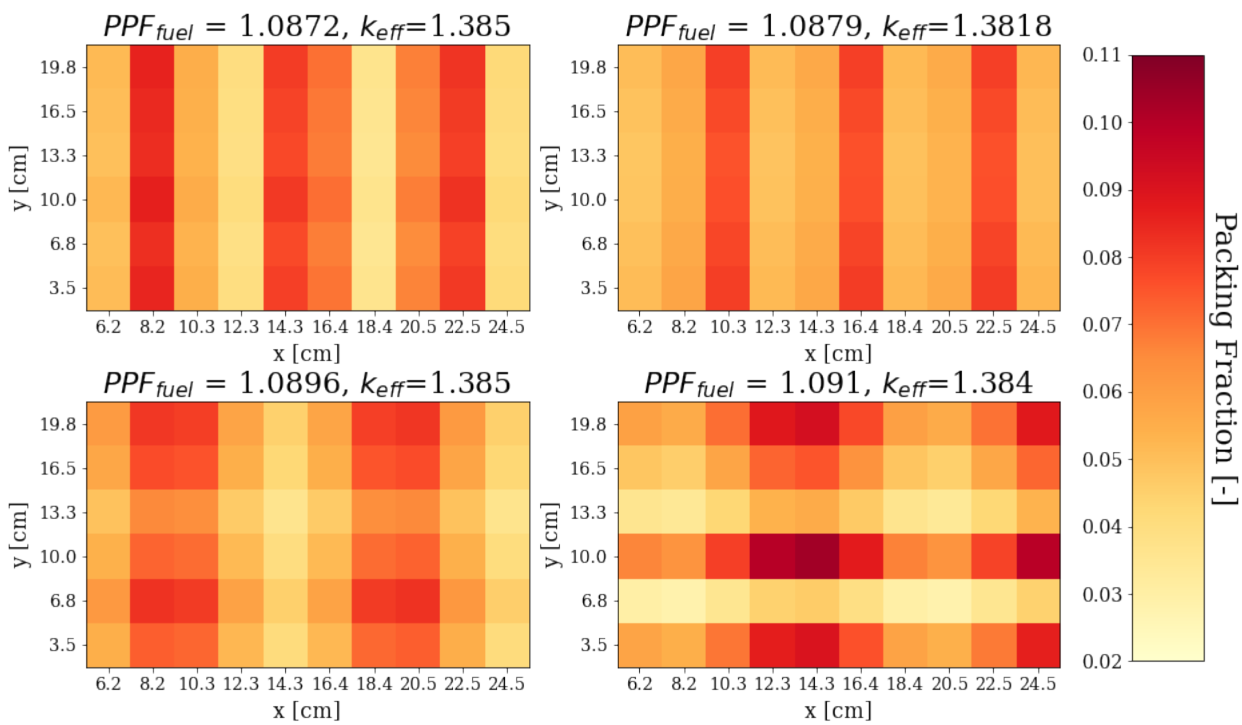

(b) TRISO distribution for the four unique reactor models with the lowest PPF_{fuel} in the AHTR one-third assembly at the final generation.

Figure 7.5: Simulation a-1c – ROLLO single-objective optimization to minimize AHTR one-third assembly's fuel-normalized power peaking factor (PPF_{fuel}). Input parameters varied: TRISO distribution ($\rho_{TRISO}(\vec{r})$). $PF_{total} = 0.06$.

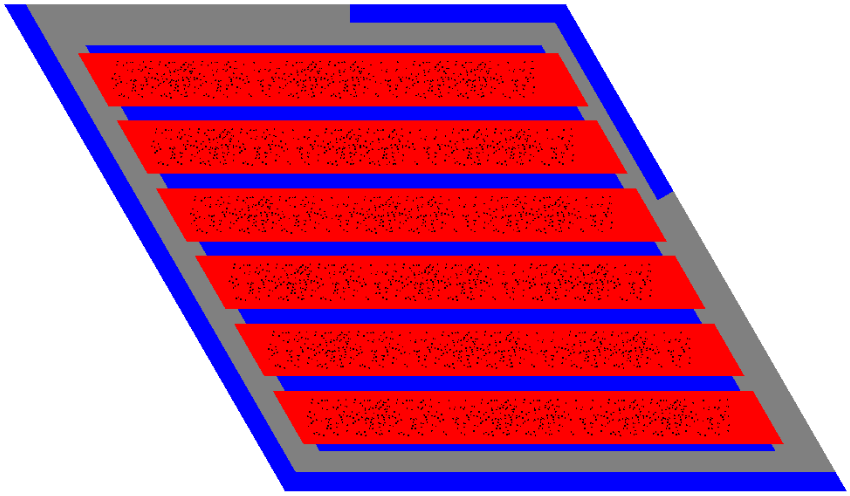

(c) AHTR one-third assembly model with the most-minimized PPF_{fuel}, corresponding to the first TRISO distribution in Figure 7.5b. The reactor model has $PPF_{fuel} = 1.0872$ and $k_{eff} = 1.385$.

Figure 7.5: Simulation a-1c – ROLLO single-objective optimization to minimize AHTR one-third assembly's fuel-normalized power peaking factor (PPF_{fuel}). Input parameters varied: TRISO distribution ($\rho_{TRISO}(\vec{r})$). $PF_{total} = 0.06$.

at the 4th and 7th fuel cell columns (at 12.3cm and 18.4cm) with $PF \approx 0.035$. Section 7.6.3 discusses the driving factors for the minimize PPF_{fuel} objective and explains simulation a-1c's most-minimized PPF_{fuel} TRISO distribution.

Simulation a-1f: Variation of Coolant channel shape

Table 7.7 shows simulation a-1f's optimization problem parameters.

Figure 7.6 shows the plots of coolant channel shape's r_1, r_2, r_3, r_4, and r_5 values against PPF_{fuel}. Figure 7.6 demonstrates that there is no correlation between PPF_{fuel} and coolant channel shape's r_1, r_2, r_3, r_4, and r_5.

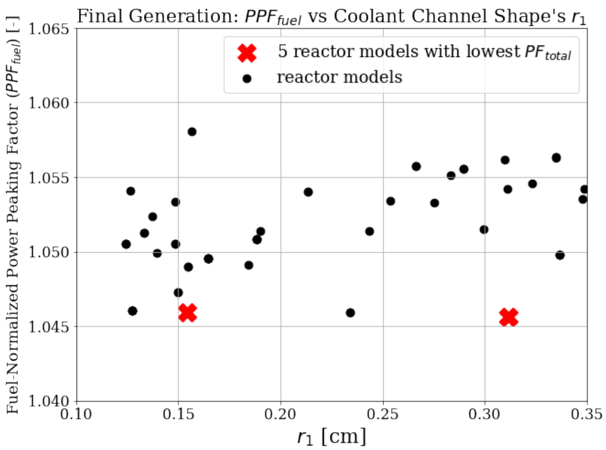

(a) Plot of PF_{total} against r_1.

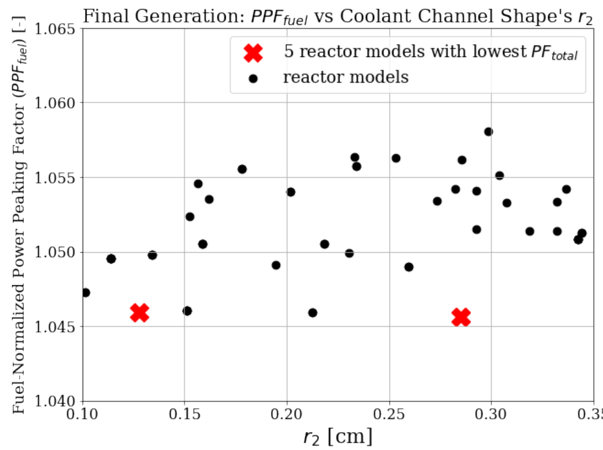

(b) Plot of PF_{total} against r_2.

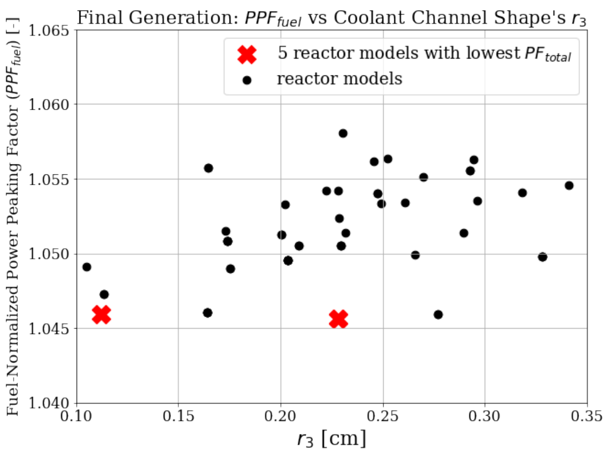

(c) Plot of PF_{total} against r_3.

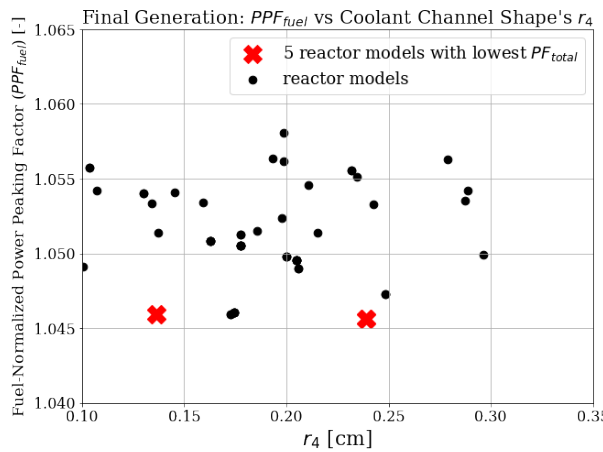

(d) Plot of PF_{total} against r_4.

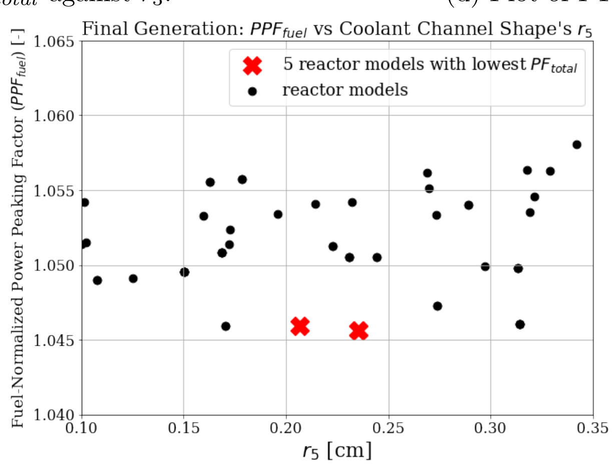

(e) Plot of PF_{total} against r_5.

Figure 7.6: Simulation a-1f – ROLLO single-objective optimization to minimize AHTR one-third assembly's fuel-normalized power peaking factor (PPF_{fuel}). Plots of simulation a-1f final generation's reactor models PPF_{fuel} against coolant channel shape input parameters. Red crosses indicate the five reactor models with the lowest PPF_{fuel}. Input parameters varied: total fuel packing fraction (PPF_{fuel}), and coolant channel shape (r_1, r_2, r_3, r_4, r_5).

Table 7.7: Simulation a-1f Optimization Problem Parameters

Single Objective: Simulation a-1f	
Objectives	Minimize PPF_{fuel}
Input Parameter variations	coolant channel shape: $0.05 < r_1 < 0.35$
	coolant channel shape: $0.05 < r_2 < 0.35$
	coolant channel shape: $0.05 < r_3 < 0.35$
	coolant channel shape: $0.05 < r_4 < 0.35$
	coolant channel shape: $0.05 < r_5 < 0.35$
Constraints	$k_{eff} \geq 1.0$
	$PF_{total} = 0.04$
Genetic Algorithm Parameters	Population size: 64
	Generations: 2

7.3 AHTR One-Third Assembly: Two-Objective Optimization Results

This section reports the AHTR one-third assembly's ROLLO two-objective optimization results. The previous section's one-objective optimization results inform the multi-objective optimization simulations in this section and Section 7.4. Since the variations in coolant channel shape only impact one objective: minimize one-third assembly's maximum temperature (T_{max}), I do not conduct two-objective optimization for coolant channel shape variations. Table 7.1 summarized the two-objective simulations: a-2a, a-2b, and a-2c.

As described in Section 2.3, multi-objective optimization returns multiple optimal solutions that meet each objective to varying degrees; this set of solutions is the Pareto front [67]. For each solution in the Pareto front, none of the objective functions can be improved without degrading another objective. An ideal optimization method for a multi-objective problem like reactor design optimization should find widely spread out reactor model solutions in the Pareto front [67]. Thus, I report on the optimal reactor models on the Pareto front for the multi-objective optimization problems in this section and Section 7.4.

To ensure that the multi-objective optimization problems are converged, I report the hypervolume values for each generation. As previously described in Section 4.4.2, the hypervolume indicator quantifies the Pareto front's goodness (bigger = better). I use a different reference point for each optimization problem. If a multi-objective optimization problem's hypervolume converges earlier than the five generations I intended to run (determined in Section 5.5.2), I stop the simulation at that generation.

7.3.1 a-2a: Minimize PF_{total} and T_{max}

This section reports results from the two-objective optimization simulation a-2a; minimized objectives are total fuel packing fraction (PF_{total}) and maximum temperature (T_{max}) in the one-third assembly. Table 7.8 shows simulation a-2a's optimization problem parameters.

Table 7.8: Simulation a-2a Optimization Problem Parameters

Two Objectives: Simulation a-2a	
Objectives	Minimize PF_{total} Minimize T_{max}
Input parameter variations	$0.05 \leq PF_{total} \leq 0.07$ $\rho_{TRISO}(\vec{r})$: $0 \leq a \leq 2$, $0 \leq d \leq 2$ $\rho_{TRISO}(\vec{r})$: $0 \leq b \leq \frac{\pi}{2}$, $0 \leq e \leq \frac{\pi}{2}$ $\rho_{TRISO}(\vec{r})$: $0 \leq c \leq 2\pi$, $0 \leq f \leq 2\pi$
Constraints	$k_{eff} \geq 1.38$
Genetic algorithm parameters	Population size: 128 Generations: 5

Table 7.9 shows the hypervolume value at each generation, confirming that simulation a-2a converges by generation 5.

Table 7.9: Simulation a-2a hypervolume values at each generation.

Two Objectives: Simulation a-2a Reference point: (0.07, 1700)	
Generation	**Hypervolume [-]**
1	6.0090
2	6.0859
3	6.2220
4	6.3379
5	6.4664

Figure 7.7a shows a plot of the final generation's reactor models' PF_{total} against T_{max}; crosses mark the reactor models that fall on the Pareto front. Figure 7.7b shows the 22 TRISO packing fraction distributions in the final generation that fall on the Pareto front.

Figure 7.7a shows that minimize PF_{total} and minimize T_{max} are contrasting objectives. In Figure 7.7, the one-third assembly model with the most-minimized PF_{total} and highest T_{max} are reactor models 13 to 20. These models have an oscillating TRISO distribution along the x-axis and

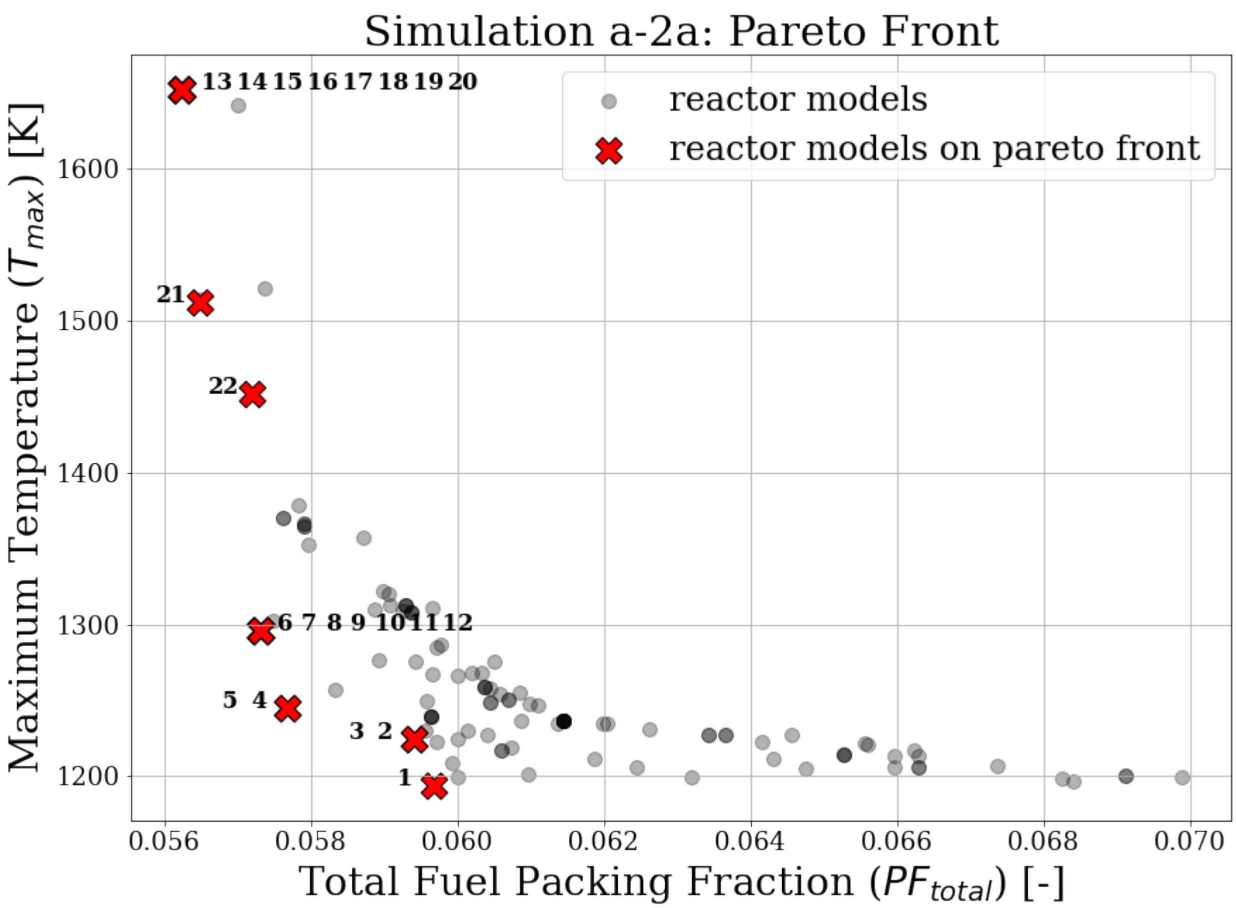

(a) Plot of final generation's reactor models' PF_{total} against T_{max}. Crosses indicate the reactor models on the Pareto front. Annotated numbers on each cross correspond to TRISO distributions in the plot below.

Figure 7.7: Simulation a-2a – ROLLO two-objective optimization to minimize total fuel packing fraction (PF_{total}) and maximum temperature (T_{max}) in the one-third assembly. Input parameters varied: total fuel packing fraction (PF_{total}) and TRISO packing fraction distribution ($\rho_{TRISO}(\vec{r})$).

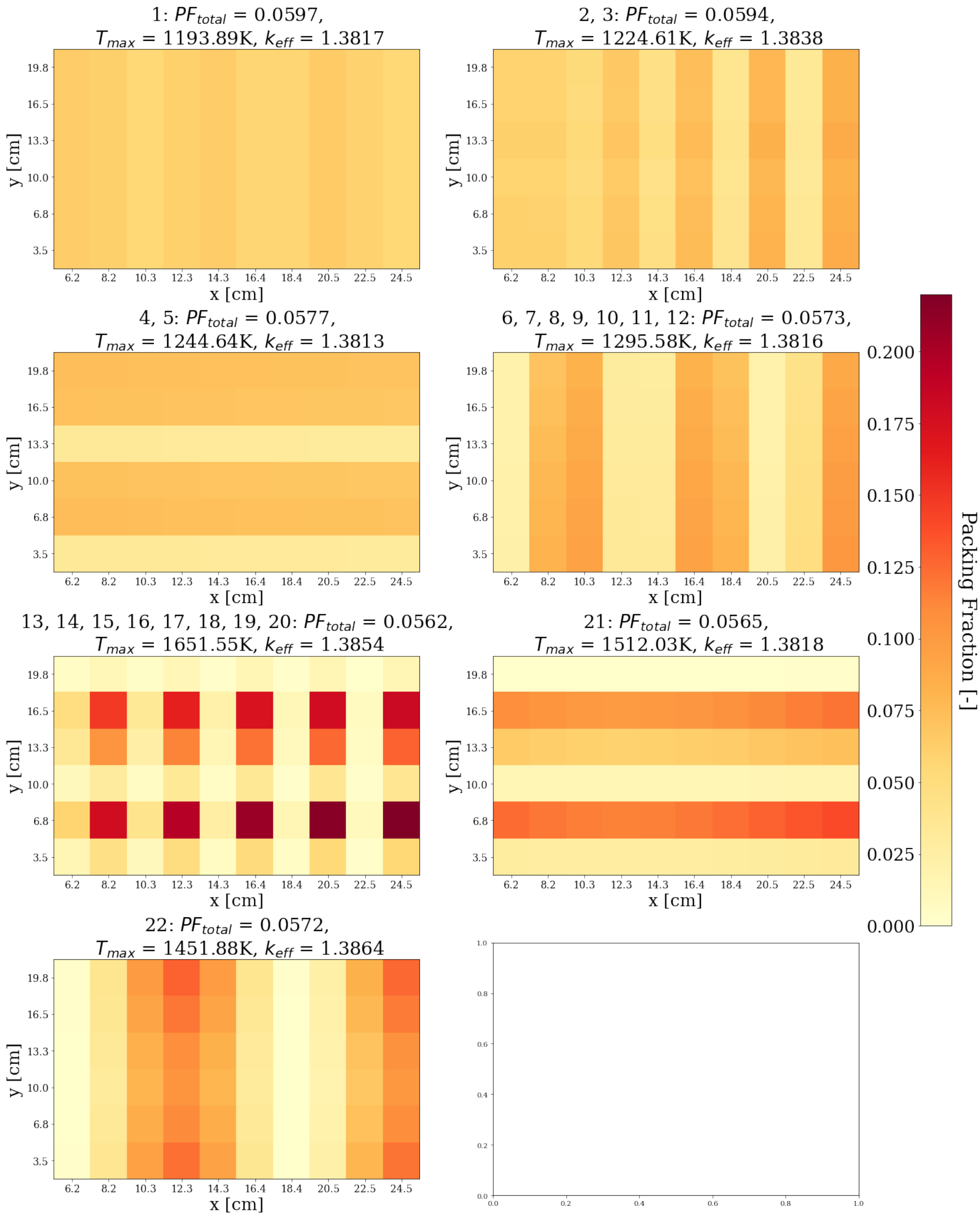

(b) TRISO distribution for the 22 reactor models on the Pareto front. Numbered reactor models correspond to numbered crosses in the plot above.

Figure 7.7: (contd.) Simulation a-2a – ROLLO two-objective optimization to minimize total fuel packing fraction (PF_{total}) and maximum temperature (T_{max}) in the one-third assembly. Input parameters varied: total fuel packing fraction (PF_{total}) and TRISO packing fraction distribution ($\rho_{TRISO}(\vec{r})$).

y-axis, and a packing fraction standard deviation of 0.066 across the one-third assembly. Along the x-axis, the distribution peaks at the even fuel cell columns (at 8.2cm, and 12.3cm, 16.4cm, 20.5cm, and 24.5cm) and has minimum points at the odd fuel cell columns (at 6.2cm, 10.3cm, 14.3cm, 18.4cm, and 22.5cm). The even fuel cell columns have a ~ 0.18 y-axis variation with peaks of $PF \approx 0.21$.

In Figure 7.7, the one-third assembly model with the most-minimized T_{max} and highest PF_{total} is reactor model 1. Reactor model 1 has an almost constant TRISO packing fraction distribution with a packing fraction standard deviation of 0.004 across the one-third assembly. The one-third assembly model that visually from the Pareto Front (Figure 7.7a) minimizes both PF_{total} and T_{max} to an equal extent are reactor models 4 and 5. Reactor models 4 and 5 have an oscillating TRISO distribution along the y-axis and a packing fraction standard deviation of 0.018 across the one-third assembly. Along the y-axis, the distribution peaks at the 2nd, 3rd, 5th, and 6th rows (at 6.8cm, 10.0cm, 16.5cm, and 19.8cm) with $PF \approx 0.07$ and has minimum points at the 1st and 4th rows (at 3.5cm and 13.3cm) with $PF \approx 0.03$. Section 7.6.4 discusses and explains simulation a-2a's results.

7.3.2 a-2b: Minimize PF_{total} and PPF_{fuel}

This section reports results from the two-objective optimization simulation a-2b; the objectives minimized are total fuel packing fraction (PF_{total}) and fuel-normalized power peaking factor (PPF_{fuel}) in the one-third assembly. Table 7.10 shows simulation a-2b's optimization problem parameters.

Table 7.10: Simulation a-2b Optimization Problem Parameters

Two Objectives: Simulation a-2b	
Objectives	Minimize PF_{total}
	Minimize PPF_{fuel}
Input parameter variations	$0.05 \leq PF_{total} \leq 0.07$
	$\rho_{TRISO}(\vec{r})$: $0 \leq a \leq 2$, $0 \leq d \leq 2$
	$\rho_{TRISO}(\vec{r})$: $0 \leq b \leq \frac{\pi}{2}$, $0 \leq e \leq \frac{\pi}{2}$
	$\rho_{TRISO}(\vec{r})$: $0 \leq c \leq 2\pi$, $0 \leq f \leq 2\pi$
Constraints	$k_{eff} \geq 1.38$
Genetic algorithm parameters	Population size: 128
	Generations: 5

Table 7.11 shows the hypervolume value at each generation, confirming that simulation a-2b converges by generation 5.

Table 7.11: Simulation a-2b hypervolume values at each generation.

Two Objectives: Simulation a-2b	
Reference point: (0.07, 1.9)	
Generation	**Hypervolume [-]**
1	0.00989
2	0.00991
3	0.00997
4	0.01054
5	0.01058

Figure 7.8a shows a plot of the final generation's reactor models' PF_{total} against PPF_{fuel}; crosses mark the reactor models that fall on the Pareto front. Figure 7.8b shows the 12 TRISO packing fraction distributions that fall on the Pareto front.

Figure 7.8a shows that minimize PF_{total} and minimize PPF_{fuel} are contrasting objectives. In Figure 7.8, the one-third assembly model with the most-minimized PF_{total} and highest PPF_{fuel} is reactor model 11. Reactor model 11 has an oscillating TRISO distribution along the x-axis and y-axis, and a packing fraction standard deviation of 0.053 across the one-third assembly. Along the y-axis, the distribution peaks at the 3rd and 4th fuel cell rows (at 10.0cm amd 13.3cm) and has minimum points at the 1st, 5th, and 6th fuel cell rows (at 3.5cm, 16.5cm, 19.8cm). The 3rd and 4th rows have the largest x-axis variation of ~ 0.14 with peaks of $PF \approx 0.17$. The 1st, 5th, and 6th row has the smallest x-axis variation of ~ 0.02 with minimums of $PF \approx 0.005$.

In Figure 7.8, the one-third assembly model with the most-minimized PPF_{fuel} and highest PF_{total} is reactor model 1. Reactor model 1 has an oscillating TRISO distribution along the x-axis and y-axis and a packing fraction standard deviation of 0.013 across the one-third assembly. Along the x-axis, the distribution peaks at the 2nd, 5th, and 8th fuel cell columns (at 8.2cm, 14.3cm, and 20.5cm) and has minimum points at the 1st, 6th, and 9th (at 6.2cm, 16.4cm, and 22.5cm). The 2nd, 5th, and 8th columns have the largest y-axis variation of ~ 0.034 with peaks of $PF \approx 0.08$. The 1st, 6th, and 9th columns have the smallest y-axis variation of ~ 0.027 with minimums of $PF \approx 0.038$. On the y-axis, the distribution has peaks at the top and bottom row (at 3.5cm and 19.8cm) and has a minimum point in the center rows (at 10.0cm and 13.3cm). The top and bottom row have the largest x-axis variation of ~ 0.018 with peaks of $PF \approx 0.08$. The center rows have the smallest x-axis variation of ~ 0.011 with minimums of $PF \approx 0.038$.

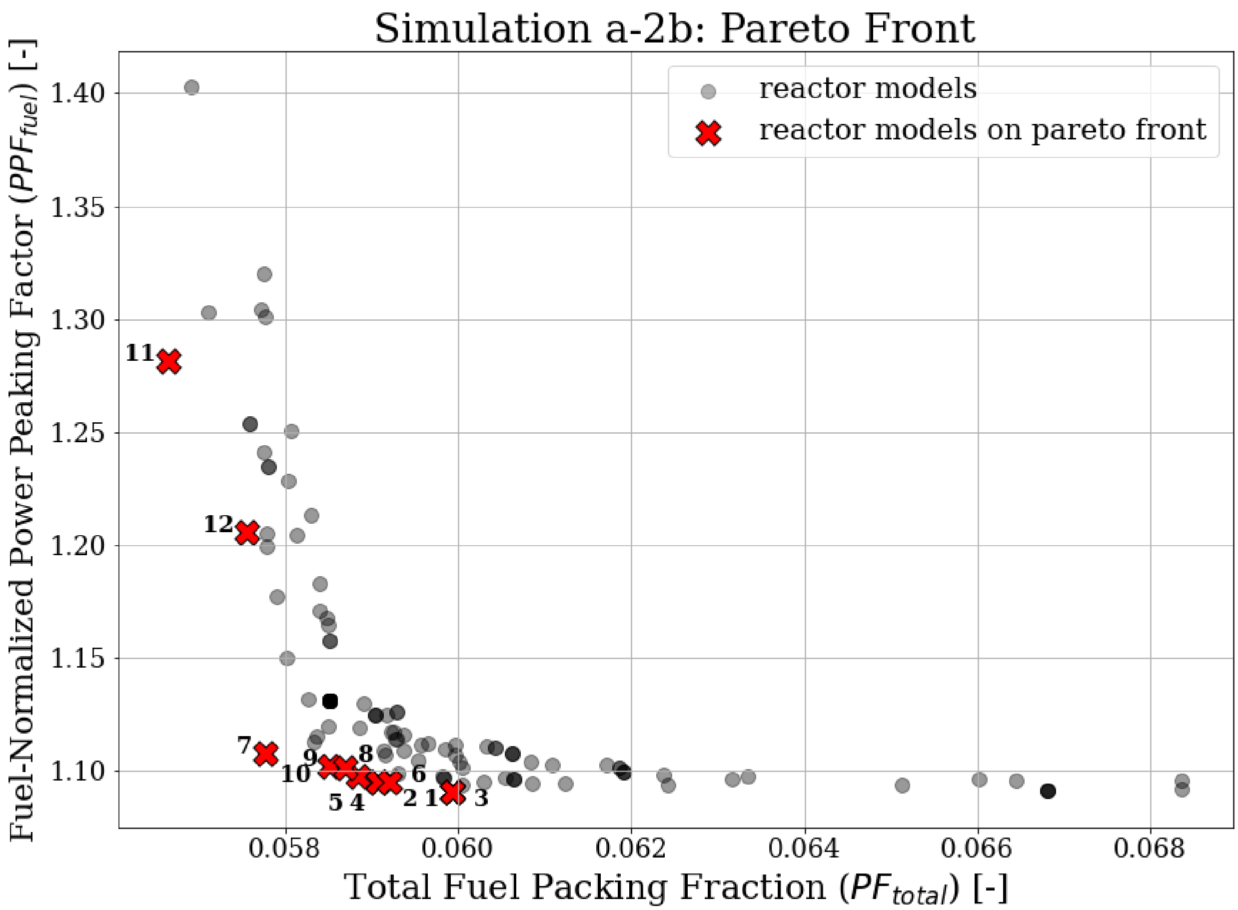

(a) Plot of final generation's reactor models' PF_{total} against PPF_{fuel}. Crosses indicate the reactor models on the Pareto front. Annotated numbers on each cross correspond to TRISO distributions in Figure 7.8b.

Figure 7.8: Simulation a-2b – ROLLO two-objective optimization to minimize total fuel packing fraction (PF_{total}) and normalized power peaking factor (PPF_{fuel}) in the AHTR one-third assembly. Input parameters varied: PF_{total} and TRISO packing fraction distribution ($\rho_{TRISO}(\vec{r})$).

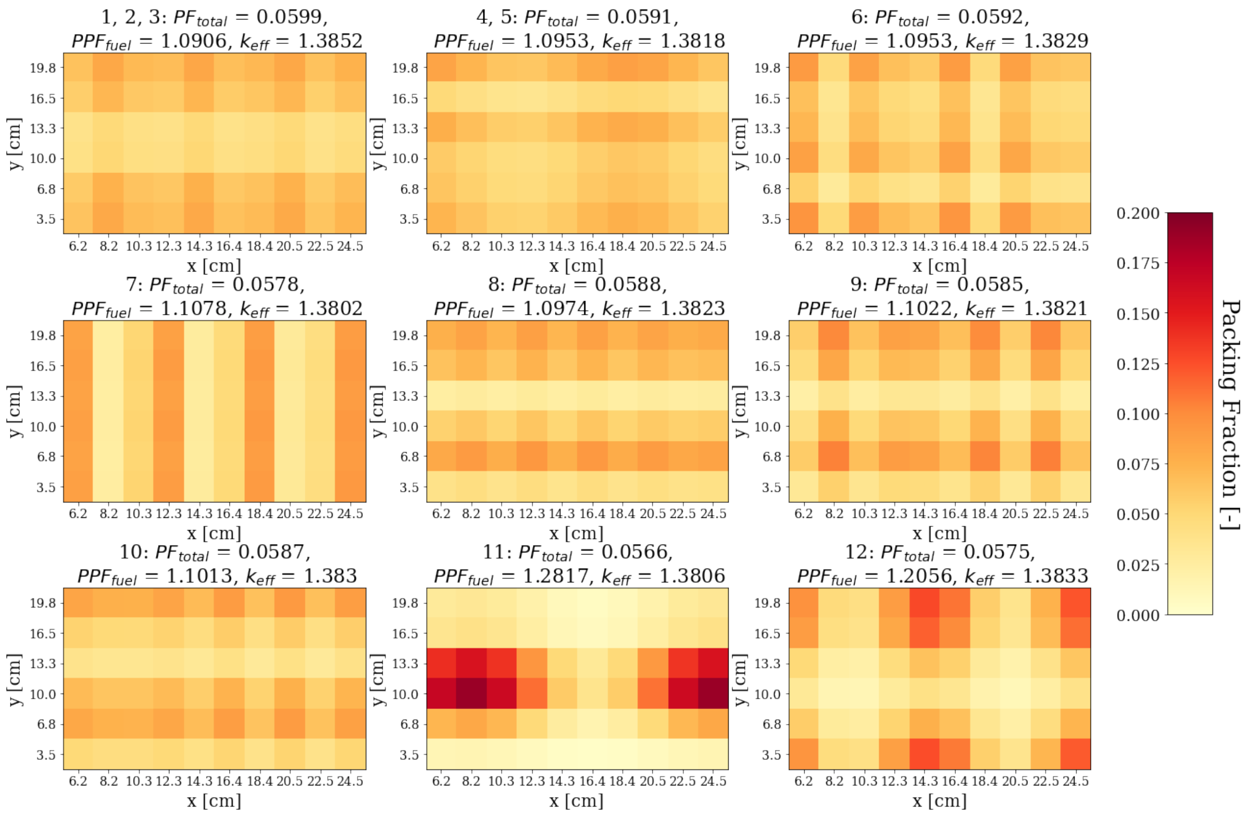

(b) TRISO distribution for the 12 reactor models on the Pareto front. Numbered reactor models correspond to numbered crosses in Figure 7.8a.

Figure 7.8: (contd.) Simulation a-2b – ROLLO two-objective optimization to minimize total fuel packing fraction (PF_{total}) and normalized power peaking factor (PPF_{fuel}) in the AHTR one-third assembly. Input parameters varied: PF_{total} and TRISO packing fraction distribution ($\rho_{TRISO}(\vec{r})$).

The one-third assembly model that visually from the Pareto Front (Figure 7.8a) minimizes both PF_{total} and PPF_{fuel} to an equal extent is reactor model 5. Like reactor models 11 and 1, reactor model 5 has an oscillating TRISO distribution along the x-axis and y-axis. Reactor model 5 has a packing fraction standard deviation of 0.013 across the one-third assembly. Along the x-axis, the distribution peaks at the 1st and 7th fuel cell columns (at 6.2cm and 18.4cm) and has minimum points in the 3rd, 4th, and 10th fuel cell columns (at 10.3cm, 12.3cm, and 24.5cm). Along the x-axis, all the columns have a similar x-axis variation of ~ 0.03. Along the y-axis, the distribution peaks at the 4th and 6th fuel cell rows (at 13.3cm and 19.8cm) and has minimum points at the 5th fuel row (at 16.5cm). The 4th and 6th rows have the largest x-axis variation of ~ 0.024 with peaks of $PF \approx 0.08$. The 5th row has the smallest x-axis variation of ~ 0.015 with minimums of $PF \approx 0.035$. Sections 7.6.4 discusses and explains simulation a-2b's results.

7.3.3 a-2c: Minimize T_{max} and PPF_{fuel}

This section reports results from the two-objective optimization simulation a-2c; minimized objectives are maximum temperature (T_{max}) and fuel-normalized power peaking factor (PPF_{fuel}) in the one-third assembly. Table 7.12 shows simulation a-2c's optimization problem parameters.

Table 7.12: Simulation a-2c Optimization Problem Parameters

Two Objectives: Simulation a-2c	
Objectives	Minimize T_{max} Minimize PPF_{fuel}
Input parameter variations	$\rho_{TRISO}(\vec{r})$: $0 \le a \le 2$, $0 \le d \le 2$ $\rho_{TRISO}(\vec{r})$: $0 \le b \le \frac{\pi}{2}$, $0 \le e \le \frac{\pi}{2}$ $\rho_{TRISO}(\vec{r})$: $0 \le c \le 2\pi$, $0 \le f \le 2\pi$
Constraints	$k_{eff} \ge 1.38$ $PF_{total} = 0.06$
Genetic algorithm parameters	Population size: 128 Generations: 2

Table 7.13 shows the hypervolume value at each generation, confirming that simulation a-2c converges by generation 2.

Figure 7.9a shows a plot of the final generation's reactor models' T_{max} against PPF_{fuel}; crosses mark the reactor models that fall on the Pareto front. Figure 7.9b shows the one TRISO packing fraction distribution in the final generation that falls on the Pareto front. Figure 7.9c illustrates

Table 7.13: Simulation a-2c hypervolume values at each generation.

Two Objectives: Simulation a-2c	
Reference point: (1700, 1.5)	
Generation	**Hypervolume** [-]
1	210.685
2	210.685

the one AHTR one-third assembly model on the Pareto front.

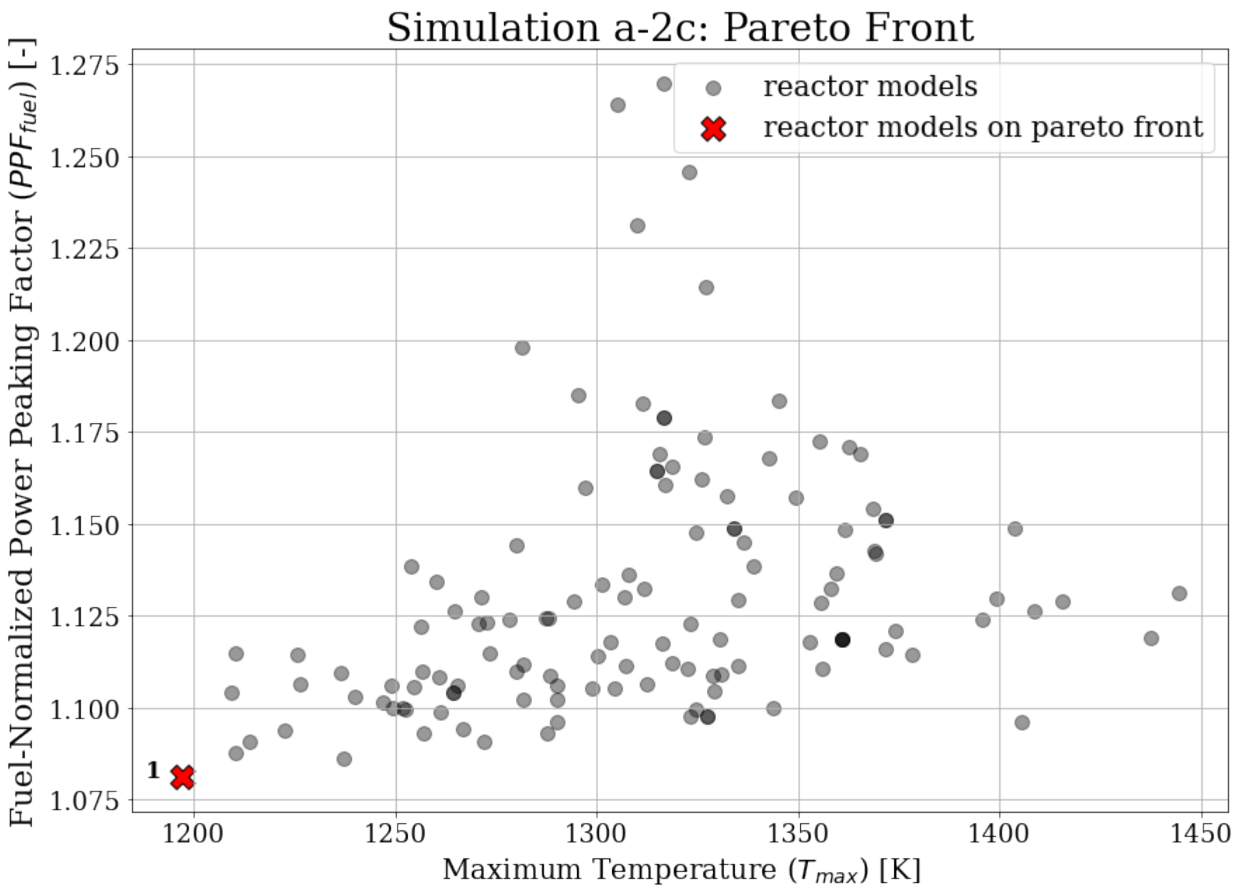

(a) Plot of final generation's reactor models' T_{max} against PPF_{fuel}. Crosses indicate the reactor models on the Pareto front. Annotated numbers on each cross correspond to TRISO distributions in the plot below.

Figure 7.9: Simulation a-2c – ROLLO two-objective optimization to minimize one-third assembly's maximum temperature (T_{max}) and fuel-normalized power peaking factor (PPF_{fuel}) in the AHTR one-third assembly. Input parameters varied: TRISO packing fraction distribution ($\rho_{TRISO}(\vec{r})$).

Figure 7.9a shows that minimize T_{max} and minimize PPF_{fuel} are non-contrasting objectives, resulting in a single reactor model on the Pareto Front. Figure 7.9b shows the TRISO distribution

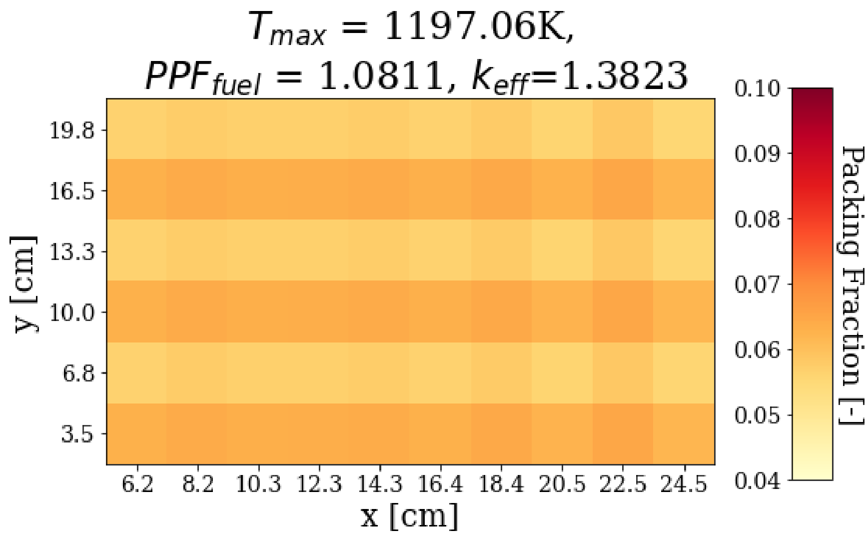

(b) TRISO distribution for the 1 reactor model on the Pareto front. Numbered reactor models correspond to numbered crosses in the plot above.

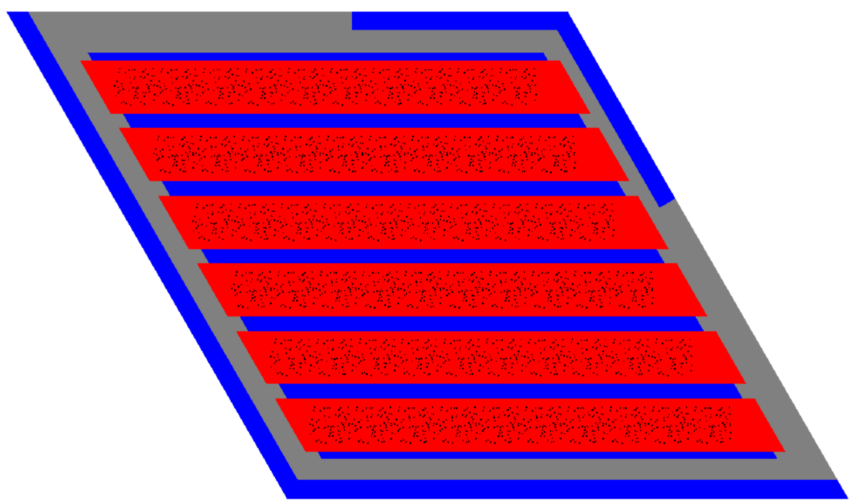

(c) AHTR one-third assembly model with the most-minimized T_{max} and PPF_{fuel} (corresponds to the TRISO distribution in the above plot).

Figure 7.9: (contd.) Simulation a-2c – ROLLO two-objective optimization to minimize one-third assembly's maximum temperature (T_{max}) and fuel-normalized power peaking factor (PPF_{fuel}) in the AHTR one-third assembly. Input parameters varied: TRISO packing fraction distribution ($\rho_{TRISO}(\vec{r})$).

that best minimizes both T_{max} and PPF_{fuel}. The reactor model has a TRISO distribution that oscillates along the y-axis and slightly on the x-axis, and a packing fraction standard deviation of 0.033 across the one-third assembly. Along the y-axis, the distribution peaks at the odd rows (at 3.5cm, 10.0cm, and 16.5cm) with $PF \approx 0.06$ and has minimum points at the even rows (at 6.8cm, 13.3cm, and 19.8cm) with $PF \approx 0.055$. Sections 7.6.4 discusses and explains simulation a-2c's results.

7.4 AHTR One-Third Assembly: Three-Objective Optimization Results

This section reports the AHTR one-third assembly's ROLLO three-objective optimization results. Table 7.1 summarized the three-objective simulations in this section: a-3a and a-3b.

7.4.1 a-3a: Variation of PF_{total} and $\rho_{TRISO}(\vec{r})$

This section reports results from the three-objective optimization simulation a-3a, with all objectives minimized: total fuel packing fraction (PF_{total}), maximum temperature (T_{max}), and fuel-normalized power peaking factor (PPF_{fuel}) in the one-third assembly. The input parameters varied are PF_{total} and TRISO packing fraction distribution ($\rho_{TRISO}(\vec{r})$). Table 7.14 shows simulation a-3a's optimization problem parameters.

Table 7.14: Simulation a-3a optimization problem parameters.

Three Objectives: Simulation a-3a	
Objectives	Minimize PF_{total} Minimize T_{max} Minimize PPF_{fuel}
Input parameter variations	$0.05 \le PF_{total} \le 0.07$ $\rho_{TRISO}(\vec{r})$: $0 \le a \le 2$, $0 \le d \le 2$ $\rho_{TRISO}(\vec{r})$: $0 \le b \le \frac{\pi}{2}$, $0 \le e \le \frac{\pi}{2}$ $\rho_{TRISO}(\vec{r})$: $0 \le c \le 2\pi$, $0 \le f \le 2\pi$
Constraints	$k_{eff} \ge 1.38$
Genetic algorithm parameters	Population size: 128 Generations: 5

Table 7.15 shows the hypervolume value at each generation, confirming that simulation a-3a converges by generation 5.

Table 7.15: Simulation a-3a hypervolume values at each generation.

Three Objectives: Simulation a-3a	
Reference point: (0.07, 1700,1.8)	
Generation	**Hypervolume** [-]
1	4.0925
2	4.2233
3	4.4002
4	4.4250
5	4.5312

Figure 7.10a shows a plot of the final generation's reactor models' PF_{total} against T_{max} against PPF_{fuel}; crosses mark the reactor models that fall on the Pareto front. Figure 7.10b shows the 32 TRISO packing fraction distributions in the final generation that fall on the Pareto front.

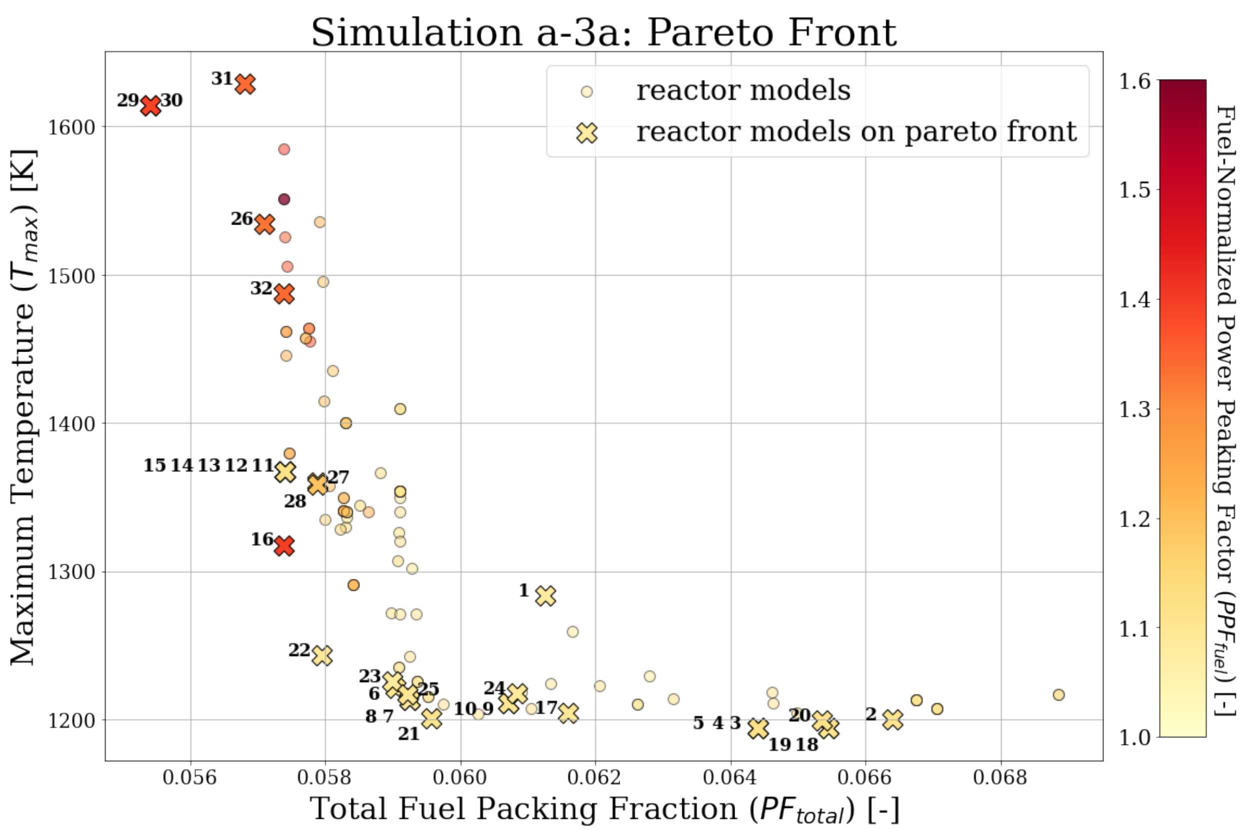

(a) Plot of final generation's reactor models' PF_{total} against T_{max} against PPF_{fuel} as a color dimension. Crosses indicate the reactor models on the Pareto front. Cross numbering corresponds to TRISO distributions in Figure 7.10b.

Figure 7.10: Simulation a-3a – ROLLO three-objective optimization to minimize total fuel packing fraction (PF_{total}), maximum temperature (T_{max}), and fuel-normalized power peaking factor (PPF_{fuel}) in the one-third assembly. Input parameters varied: PF_{total}, TRISO packing fraction distribution ($\rho_{TRISO}(\vec{r})$).

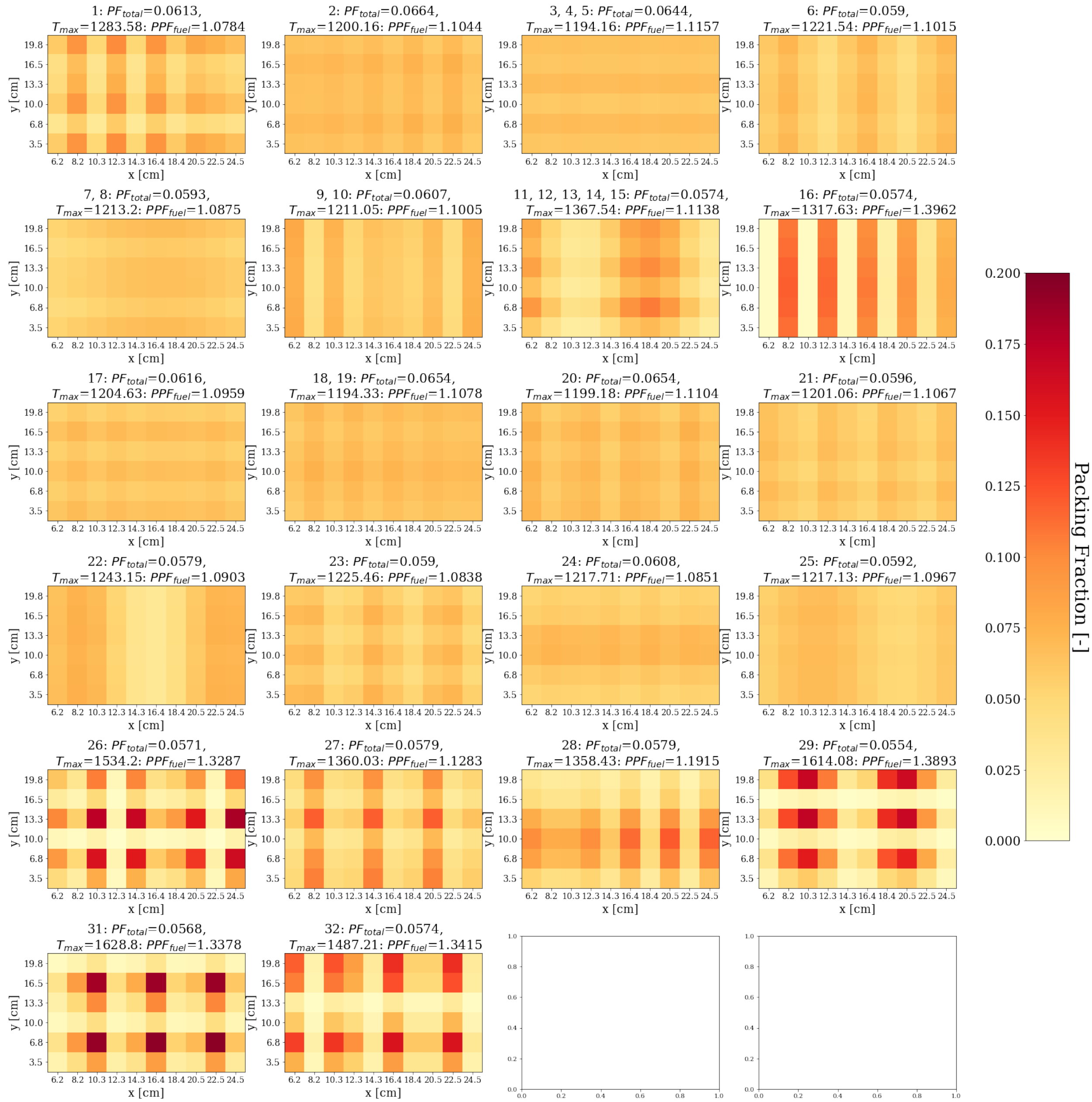

(b) TRISO distributions for the 32 reactor models on the Pareto front. Numbered reactor models correspond to numbered crosses in Figure 7.10a.

Figure 7.10: (contd.) Simulation a-3a – ROLLO three-objective optimization to minimize total fuel packing fraction (PF_{total}), maximum temperature (T_{max}), and fuel-normalized power peaking factor (PPF_{fuel}) in the one-third assembly. Input parameters varied: PF_{total}, TRISO packing fraction distribution ($\rho_{TRISO}(\vec{r})$).

Figure 7.10 demonstrates that ROLLO found 32 reactor models on simulation a-3a final generation's Pareto front. Figure 7.11 shows three reactor models on the Pareto front that most minimized each objective and one reactor model on the Pareto front that equally minimized all three objectives. I selected the equally minimized reactor model by visually studying Figure 7.10 and selecting a reactor model close to the origin with a light yellow color dimension. Reactor model 30 most-minimized PF_{total}, reactor model 3 most-minimized T_{max}, reactor model 1 most-minimized PPF_{fuel}, and reactor model 22 equally minimized all three objectives.

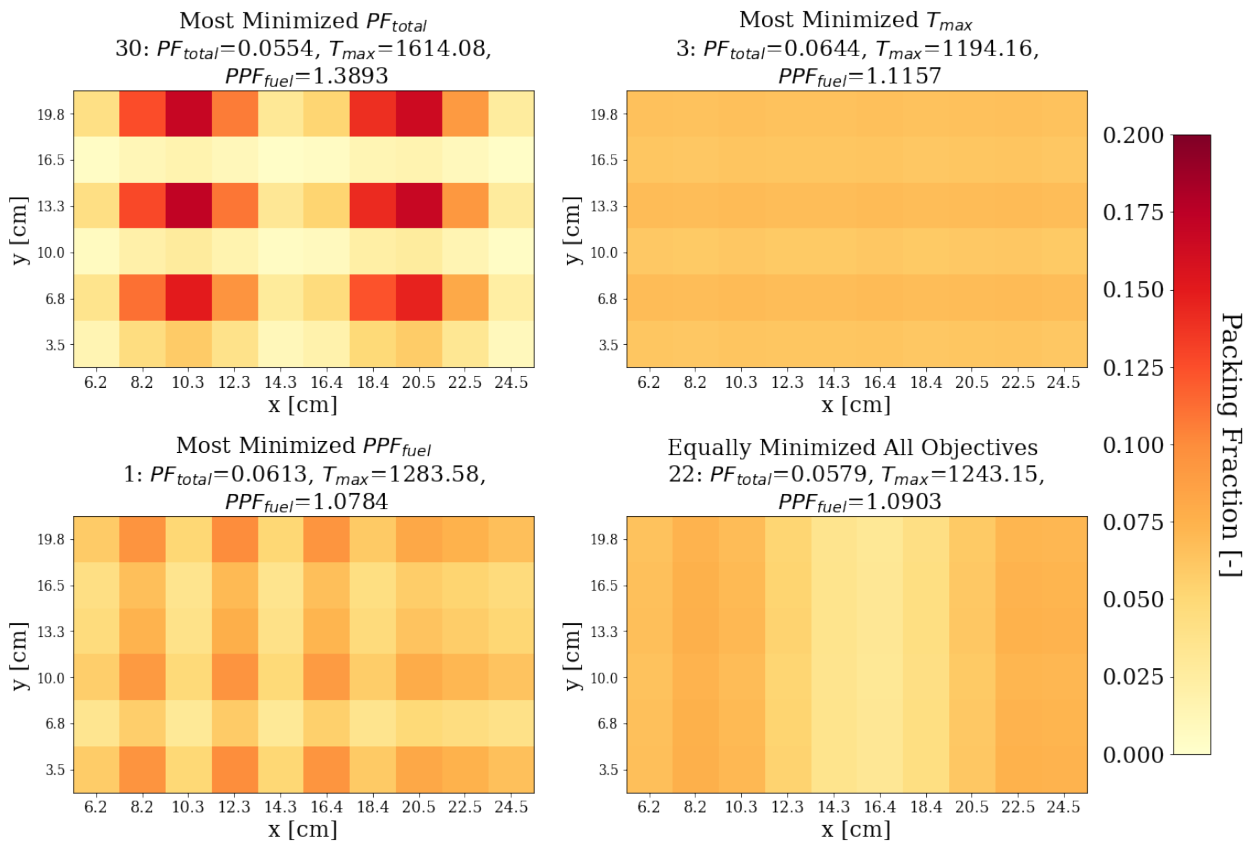

(a) TRISO packing fraction distributions.

Figure 7.11: AHTR one-third assembly models and TRISO distributions for the three reactor models on simulation a-3a's Pareto front that most minimized each objective, and one reactor model that equally minimized all three objectives. Simulation a-3a – ROLLO three-objective optimization to minimize total fuel packing fraction (PF_{total}), maximum temperature (T_{max}) and normalized power peaking factor (PPF_{fuel}) in the one-third assembly. Input parameters varied: PF_{total}, TRISO packing fraction distribution ($\rho_{TRISO}(\vec{r})$).

In Figure 7.11a, the one-third assembly model with the most-minimized PF_{total} is reactor model 30 (also illustrated in Figure 7.11b). Reactor model 30 has an oscillating TRISO distribution along the x-axis and y-axis, and a packing fraction standard deviation of 0.052 across the one-third assembly. Along the y-axis, the distribution peaks at the even fuel cell rows (at 6.8cm, 13.3cm,

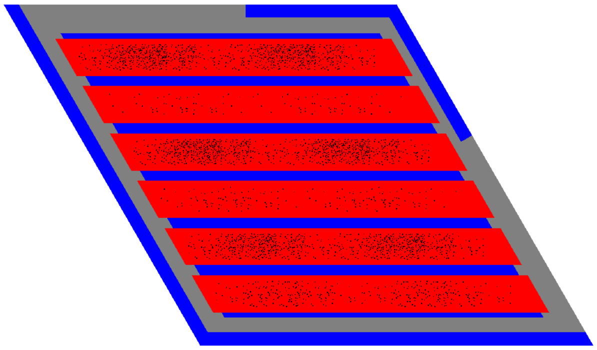

(b) AHTR one-third assembly model with the most-minimized PF_{total} (reactor model 30).

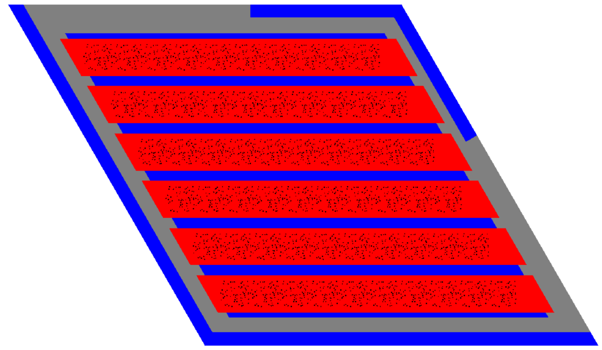

(c) AHTR one-third assembly model with the most-minimized T_{max} (reactor model 3).

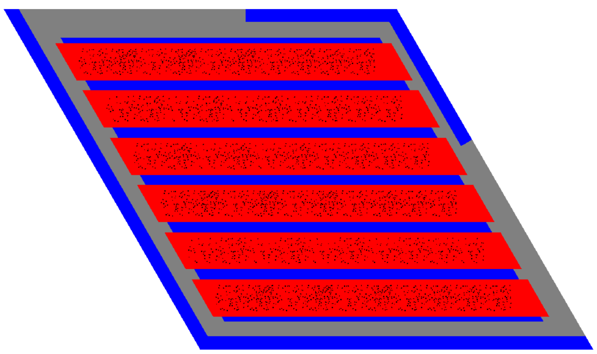

(d) AHTR one-third assembly model with the most-minimized PPF_{fuel} (reactor model 1).

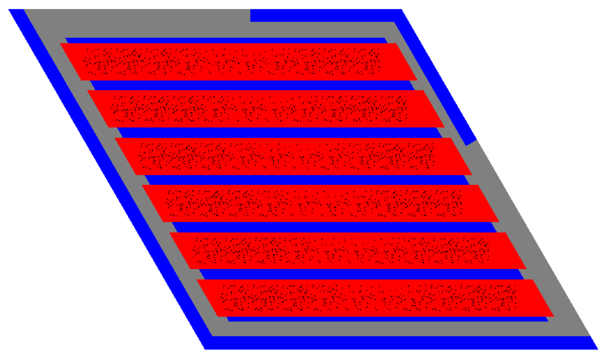

(e) AHTR one-third assembly model that equally minimized all objectives (reactor model 22).

Fluoride-Lithium-Beryllium (FLiBe)
Graphite (Structure)
Graphite (Fuel Plank)
TRISO particle

Figure 7.11: (contd.) AHTR one-third assembly models and TRISO distributions for the three reactor models on simulation a-3a's Pareto front that most-minimized each objective, and one reactor model that equally minimized all three objectives. Simulation a-3a – ROLLO three-objective optimization to minimize total fuel packing fraction (PF_{total}), maximum temperature (T_{max}) and normalized power peaking factor (PPF_{fuel}) in the one-third assembly. Input parameters varied: PF_{total}, TRISO packing fraction distribution ($\rho_{TRISO}(\vec{r})$).

and 19.8cm) and has minimum points at the odd fuel cell rows (at 3.5cm, 10.0cm, and 16.5cm). The even fuel cell rows have a ~ 0.14 x-axis variation with peaks of $PF \approx 0.16$. The odd fuel cell rows have a ~ 0.02 x-axis variation with minimums of $PF \approx 0.005$.

In Figure 7.11a, the one-third assembly model with the most-minimized T_{max} is reactor model 3 (also illustrated in Figure 7.11c). Reactor model 3 has an almost constant TRISO packing fraction distribution with a packing fraction standard deviation of 0.003 across the one-third assembly. In Figure 7.11a, the one-third assembly model with the most-minimized PPF_{fuel} is reactor model 1 (also illustrated in Figure 7.11d). Reactor model 1 has an oscillating TRISO distribution along the x-axis and y-axis and a packing fraction standard deviation of 0.019 across the one-third assembly. Along the x-axis, the distribution peaks at the 2nd, 4th, and 6th fuel cell columns (at 8.2cm, 12.3cm, and 16.4cm). These three fuel cell columns have a ~ 0.04 y-axis variation with peaks of $PF \approx 0.1$. Along the y-axis, the distribution peaks at the 1st, 3rd, and 6th fuel cell rows (at 3.5cm, 10.0cm, and 19.8cm). These three fuel cell rows have a ~ 0.05 x-axis variation with peaks of $PF \approx 0.1$.

In Figure 7.11a, the one-third assembly model that equally minimized all three objectives is reactor model 22 (also illustrated in Figure 7.11e). Reactor model 22 has an oscillating TRISO distribution along x-axis and a packing fraction standard deviation of 0.015 across the one-third assembly. Along the x-axis, the distribution peaks at the 2nd, 9th, and 10th fuel cell columns (at 8.2cm, 22.5cm, and 24.5cm) with $PF \approx 0.07$. The distribution has minimum points at the 5th and 6th fuel cell columns (at 14.3cm, 16.4cm) with $PF \approx 0.03$. Section 7.6.4 discusses and explains simulation a-3a's results.

7.4.2 a-3b: Variation of PF_{total}, $\rho_{TRISO}(\vec{r})$, and Coolant Channel Shape

This section reports results from the three-objective optimization simulation a-3b, with all objectives minimized: total fuel packing fraction (PF_{total}), maximum temperature (T_{max}), and fuel-normalized power peaking factor (PPF_{fuel}) in the one-third assembly. The input parameters varied are PF_{total}, TRISO packing fraction distribution ($\rho_{TRISO}(\vec{r})$), and coolant channel shape (r_1, r_2, r_3, r_4, and r_5). Table 7.16 shows simulation a-3b's optimization problem parameters.

Table 7.17 shows the hypervolume value at each generation, confirming that simulation a-3b

Table 7.16: Simulation a-3b optimization problem parameters.

Three Objectives: Simulation a-3b	
Objectives	Minimize PF_{total}
	Minimize T_{max}
	Minimize PPF_{fuel}
Input parameter variations	$0.05 \leq PF_{total} \leq 0.07$
	$\rho_{TRISO}(\vec{r})$: $0 \leq a \leq 2$, $0 \leq d \leq 2$
	$\rho_{TRISO}(\vec{r})$: $0 \leq b \leq \frac{\pi}{2}$, $0 \leq e \leq \frac{\pi}{2}$
	$\rho_{TRISO}(\vec{r})$: $0 \leq c \leq 2\pi$, $0 \leq f \leq 2\pi$
	coolant channel shape: $0.1 < r_1 < 0.35$
	coolant channel shape: $0.1 < r_2 < 0.35$
	coolant channel shape: $0.1 < r_3 < 0.35$
	coolant channel shape: $0.1 < r_4 < 0.35$
	coolant channel shape: $0.1 < r_5 < 0.35$
Constraints	$k_{eff} \geq 1.38$
Genetic algorithm parameters	Population size: 128
	Generations: 6

converges by generation 6.

Table 7.17: Simulation a-3b hypervolume values at each generation.

Three Objectives: Simulation a-3b	
Reference point: (0.06, 1260,1.5)	
Generation	**Hypervolume [-]**
1	5.4961
2	5.6739
3	5.6876
4	5.8104
5	6.0023
6	6.0093

Figure 7.12a shows a plot of the final generation's reactor models' PF_{total} against T_{max} against PPF_{fuel}; crosses mark the reactor models that fall on the Pareto front. Figure 7.12b shows the 12 TRISO packing fraction distributions in the final generation that fall on the Pareto front.

Figure 7.12 demonstrates that ROLLO found 12 reactor models on simulation a-3b final generation's Pareto front. Figure 7.13 shows three reactor models on the Pareto front that most minimized each objective and one reactor model on the Pareto front that equally minimized all three objectives. I selected the equally minimized reactor model by visually studying Figure 7.12 and selecting a reactor model close to the origin with a light yellow color dimension. Reactor model 11 most-minimized PF_{total}, reactor model 1 most-minimized T_{max}, reactor model 4 most-minimized

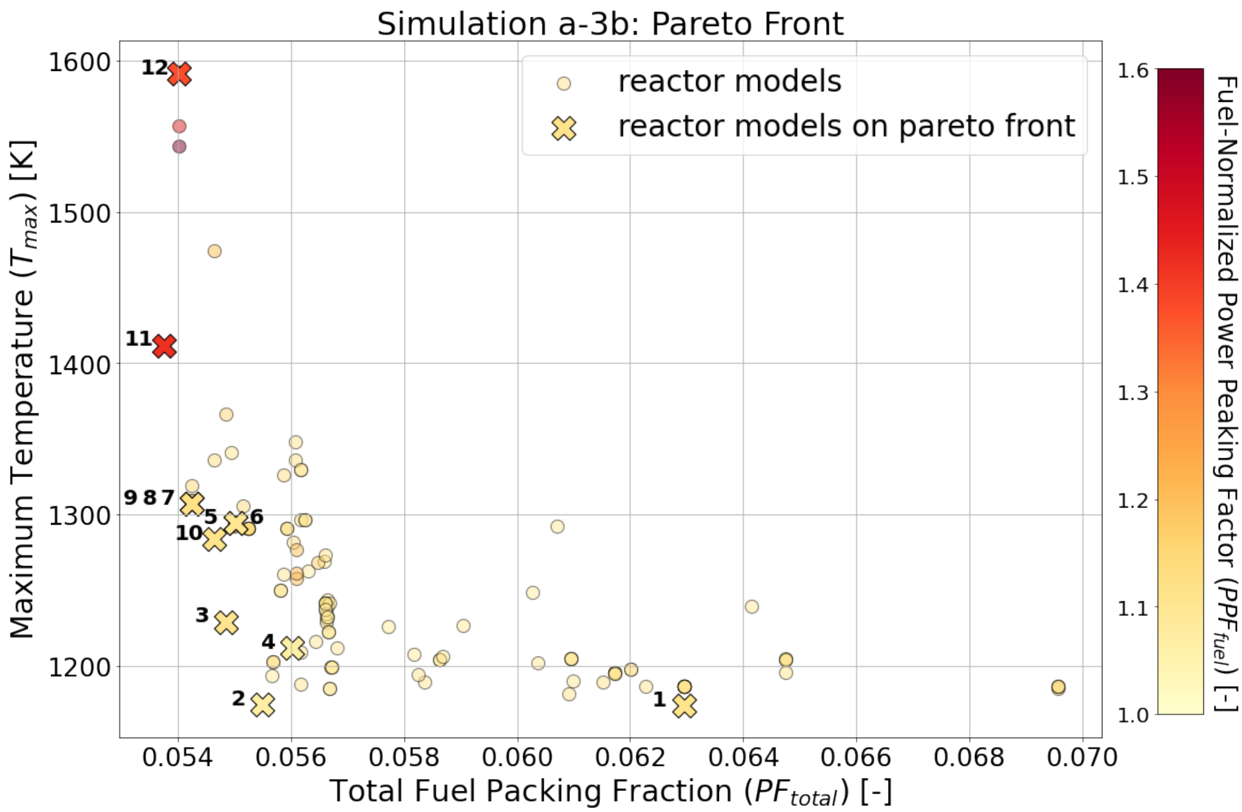

(a) Plot of final generation's reactor models' PF_{total} against T_{max} against PPF_{fuel} as a color dimension. Crosses indicate the reactor models on the Pareto front. Cross numbering correspond to TRISO distributions in Figure 7.12b.

Figure 7.12: Simulation a-3b – ROLLO three-objective optimization to minimize total fuel packing fraction (PF_{total}), maximum temperature (T_{max}), and fuel-normalized power peaking factor (PPF_{fuel}) in the one-third assembly. Input parameters varied: total fuel packing fraction PF_{total}, TRISO packing fraction distribution ($\rho_{TRISO}(\vec{r})$), coolant channel shape (r_1, r_2, r_3, r_4, r_5).

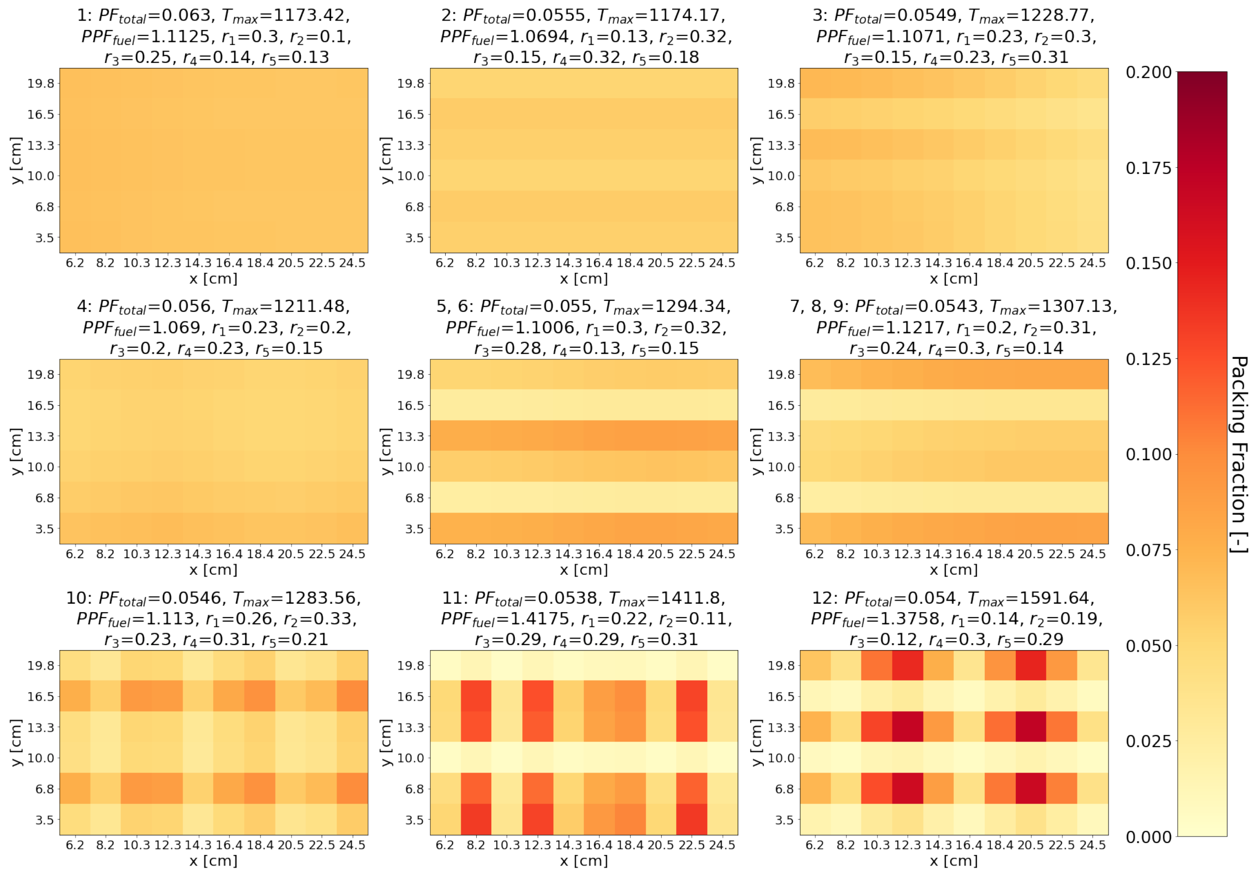

(b) TRISO distributions for the 12 reactor models on the Pareto front. Numbered reactor models correspond to numbered crosses in Figure 7.12a.

Figure 7.12: (contd.) Simulation a-3b – ROLLO three-objective optimization to minimize total fuel packing fraction (PF_{total}), maximum temperature (T_{max}), and fuel-normalized power peaking factor (PPF_{fuel}) in the one-third assembly. Input parameters varied: total fuel packing fraction PF_{total}, TRISO packing fraction distribution ($\rho_{TRISO}(\vec{r})$), coolant channel shape $(r_1, r_2, r_3, r_4, r_5)$.

PPF_{fuel}, and reactor model 2 equally minimized all three objectives.

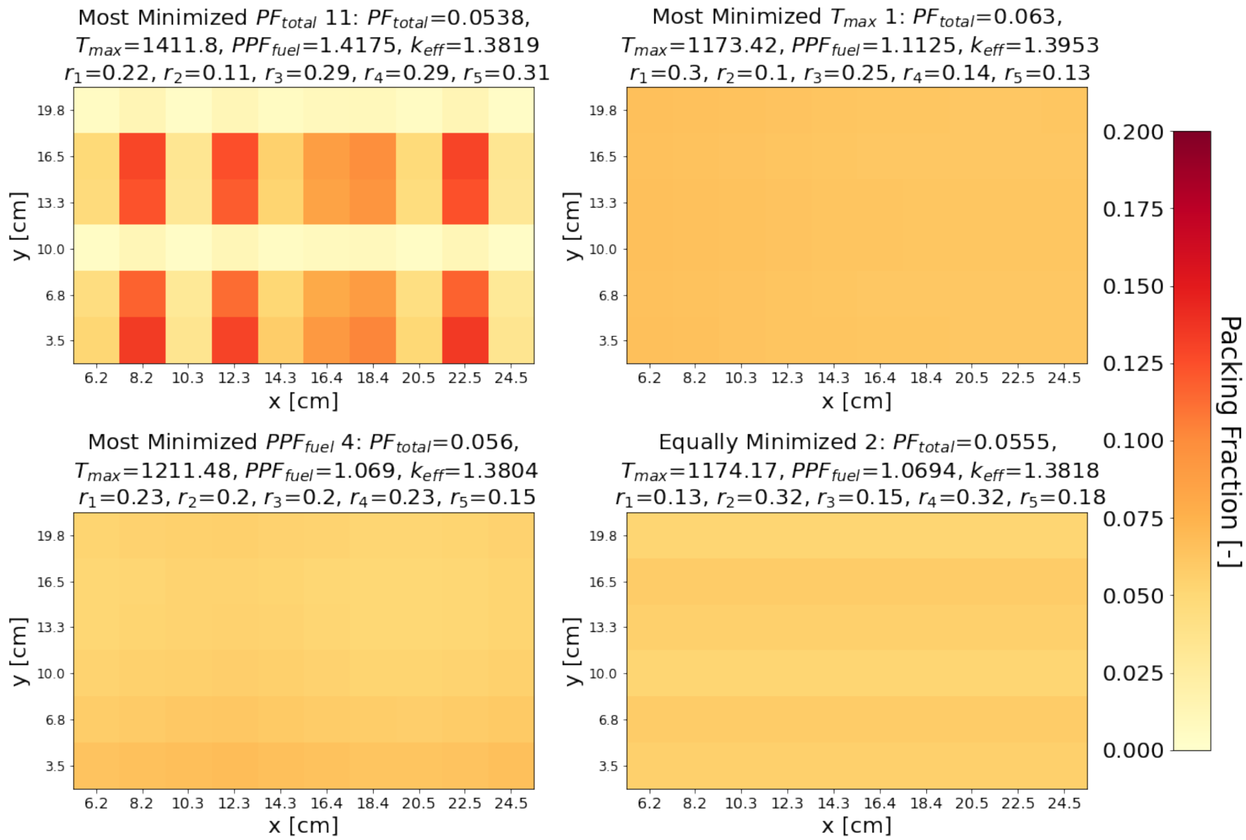

(a) TRISO packing fraction distributions.

Figure 7.13: AHTR one-third assembly models and TRISO distributions for the 3 reactor models on simulation a-3b's Pareto front that most minimized each objective, and 1 reactor model that equally minimized all three objectives. Simulation a-3b – ROLLO three-objective optimization to minimize total fuel packing fraction (PF_{total}), maximum temperature (T_{max}), and fuel-normalized power peaking factor (PPF_{fuel}) in the one-third assembly. Input parameters varied: total fuel packing fraction PF_{total}, TRISO packing fraction distribution ($\rho_{TRISO}(\vec{r})$), coolant channel shape (r_1, r_2, r_3, r_4, r_5).

In Figure 7.13a, the one-third assembly model with the most-minimized PF_{total} is reactor model 11 (also illustrated in Figure 7.13b). Reactor model 11's TRISO distribution oscillates along the x-axis, slightly oscillates along the y-axis, and has a packing fraction standard deviation of 0.044 across the one-third assembly. Along the x-axis, the distribution peaks at the 2nd and 9th fuel cell columns (at 8.2cm, 12.3cm, and 22.5cm), and minimum points at the 1st and 8th fuel cell columns (at 10.3cm and 24.5cm). The 2nd and 9th columns have ~ 0.12 y-axis variation with peaks of $PF \approx 0.13$. The 1st and 8th columns have ~ 0.03 y-axis variation with minimums of $PF \approx 0.003$.

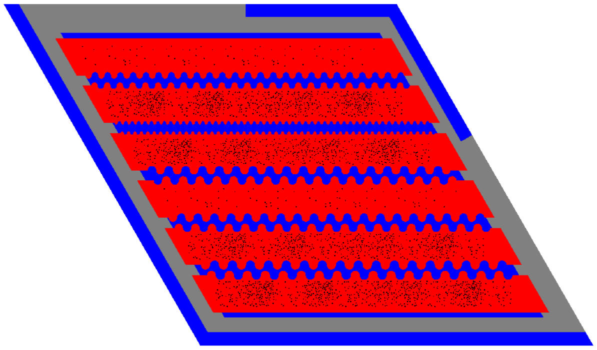

(b) AHTR one-third assembly model with the most-minimized PF_{total} (reactor model 11).

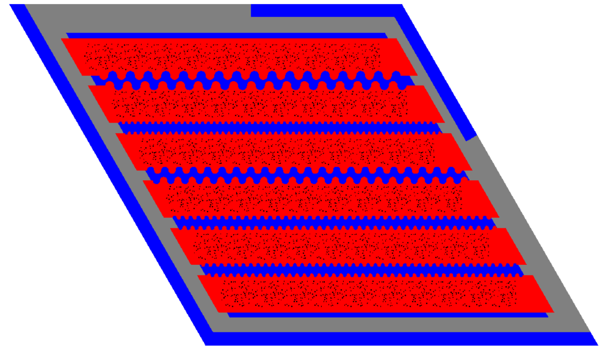

(c) AHTR one-third assembly model with the most-minimized T_{max} (reactor model 1).

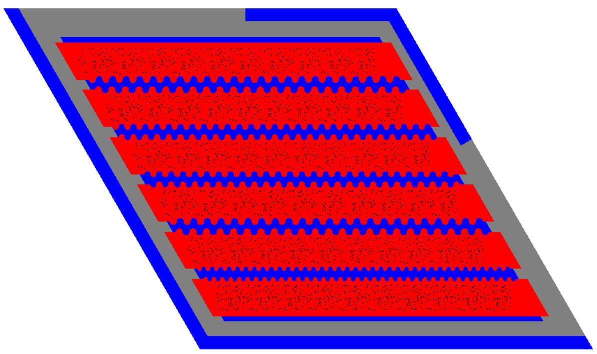

(d) AHTR one-third assembly model with the most-minimized PPF_{fuel} (reactor model 4).

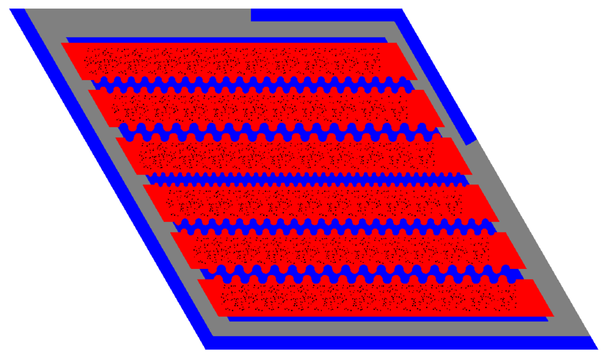

(e) AHTR one-third assembly model that equally minimized all objectives (reactor model 3).

■ FLiBe
■ Graphite (Structure)
■ Graphite (Fuel Plank)
■ TRISO particle

Figure 7.13: (contd.) AHTR one-third assembly models and TRISO distributions for the 3 reactor models on simulation a-3b's Pareto front that most-minimized each objective, and 1 reactor model that equally minimized all three objectives. Simulation a-3b – ROLLO three-objective optimization to minimize total fuel packing fraction (PF_{total}), maximum temperature (T_{max}), and fuel-normalized power peaking factor (PPF_{fuel}) in the one-third assembly. Input parameters varied: total fuel packing fraction PF_{total}, TRISO packing fraction distribution ($\rho_{TRISO}(\vec{r})$), coolant channel shape (r_1, r_2, r_3, r_4, r_5).

In Figure 7.13a, the one-third assembly model with the most-minimized T_{max} is reactor model 1 (also illustrated in Figure 7.13c). Reactor model 1 has an almost constant TRISO packing fraction distribution with a packing fraction standard deviation of 0.001 across the one-third assembly. In Figure 7.13a, the one-third assembly model with the most-minimized PPF_{fuel} is reactor model 4 (also illustrated in Figure 7.13d). Reactor model 4's TRISO distribution oscillates slightly along the y-axis, and has a packing fraction standard deviation of 0.005 across the one-third assembly. Along the y-axis, the distribution peaks at the 1st fuel cell row (at 3.5cm) with $PF \approx 0.065$. The distribution has minimums at the 4th, 5th, and 6th fuel cell rows (at 13.3cm, 16.5cm, and 19.8cm) with $PF \approx 0.052$.

In Figure 7.13a, the one-third assembly model that equally minimized all three objectives is reactor model 2 (also illustrated in Figure 7.13e). Reactor model 2's TRISO distribution oscillates slightly along the y-axis, and has a packing fraction standard deviation of 0.003 across the one-third assembly. Along the y-axis, the distribution peaks at the 2nd and 5th fuel cell row (at 6.8cm and 16.5cm) with $PF \approx 0.058$. The distribution has minimums at the 3rd and 6th fuel cell rows (at 10.0cm and 19.8cm) with $PF \approx 0.052$. Section 7.6.4 discusses and explains simulation a-3b's results.

7.5 AHTR One-Third Assembly: Computational Cost Summary

Optimization simulations are run on the Theta supercomputer at the Argonne Leadership Computing Facility under the Director's Discretionary Allocation Program [108]. Each Theta compute node has 64 processor cores with a nominal clock speed of 1.5GHz [108].

Each optimization simulation takes a different amount of node-hours due to differences in simulation software, tallies, and intermediate steps required. Table 7.18 reports the computational cost for each optimization simulation. Table 7.1 detailed the simulation parameters.

Table 7.18: Computational cost of Reactor evOLutionary aLgorithm Optimizer (ROLLO) simulations for optimizing Advanced High-Temperature Reactor (AHTR) one-third assembly. BW: BlueWaters Supercomputer, Theta: Theta supercomputer.

Num of Objs	**Sim**	**Machine**	**Compute Cost Per Gen [node-hours]**	**Generations [#]**	**Total Compute Cost [node-hours]**
1	a-1a	Theta	95.3	3	285.8
	a-1b	Theta	247.0	3	740.9
	a-1c	Theta	115.0	2	230.0
	a-1d	Theta	167.3	2	334.6
	a-1e	Theta	346.1	2	692.3
	a-1f	Theta	111.5	2	222.9
2	a-2a	Theta	250.2	5	1250.9
	a-2b	Theta	98.3	5	491.7
	a-2c	Theta	268.8	2	537.7
3	a-3a	Theta	273.6	5	1367.9
	a-3b	Theta	305.8	5	1528.9
	a-3b-256	Theta	839.8	4	3359.3

7.6 AHTR One-Third Assembly Optimization Results Discussion

Chapter 6 characterized the AHTR plank model's reactor optimization objectives' driving factors and their relationship with one another. This section utilizes the previous AHTR plank characterizations and conducts a deep dive to verify if the same driving factors apply to the AHTR one-third assembly model's optimization objectives. I also analyze how their combined effects result in the optimal reactor models found by the multi-objective optimization simulations.

7.6.1 Discussion: Minimize PF_{total} Objective

Simulation a-1a In Section 7.2.1's simulation a-1a, I conducted a single-objective optimization simulation to minimize the one-third assembly's total fuel packing fraction (PF_{total}) by varying PF_{total} and TRISO distribution. ROLLO found that an AHTR one-third assembly model with the most-minimized PF_{total} has a PF_{total} = 0.0559 and an oscillating TRISO distribution along the x-axis and y-axis, and a packing fraction standard deviation of 0.04 across the one-third assembly (Figure 7.1b).

Section 6.6.1 concluded that for the AHTR plank model, the minimize PF_{total} objective is driven by maximizing the total fission reaction rates. I ran a simulation for constant PF_{total} = 0.0559 TRISO distribution and compared its fission reaction rate with simulation a-1a's oscillating TRISO distribution that most-minimized PF_{total}. Figure 7.14 shows the TRISO distributions for the two compared reactor models: Figure 7.1b's most-minimized PF_{total} and the constant PF_{total} = 0.0559. The reactor model with the most-minimized PF_{total} has k_{eff} = 1.3802, and the reactor model with constant TRISO distribution has k_{eff} = 1.3736.

Table 7.19 compares the total fission reaction rate (OpenMC's `fission` tally) between the most-minimized PF_{total} TRISO distribution and a constant PF_{total} = 0.0559 TRISO distribution (both shown in Figure 7.14). The most-minimized PF_{total} TRISO distribution has 0.65% higher total fission reaction rate than the constant PF_{total} = 0.0559 TRISO distribution. For the same PF_{total}, the oscillating TRISO distribution enabled 660pcm higher k_{eff} than the constant TRISO distribution. The minimize PF_{total} objective is driven by maximizing the total fission reaction rates

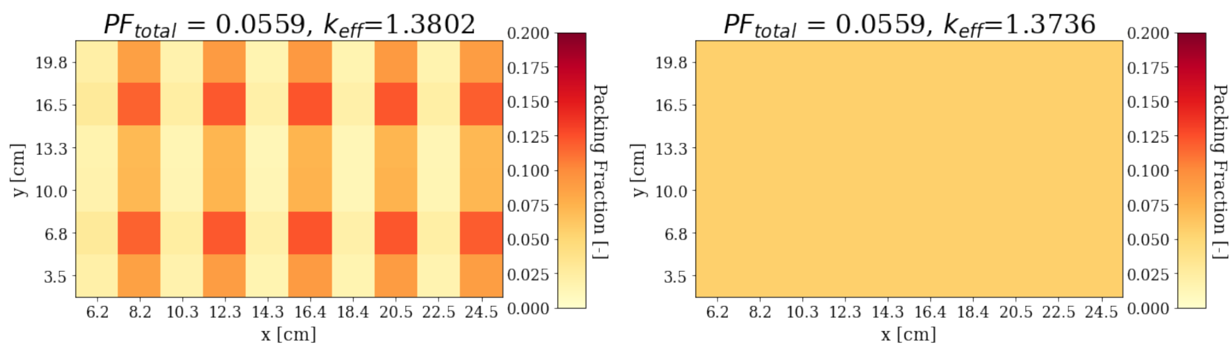

Figure 7.14: Simulation a-1a's most-minimized PF_{total} TRISO distribution (oscillating TRISO distribution) from Figure 7.1 (left) and the constant PF_{total} = 0.0559 TRISO distribution (right).

Table 7.19: Total fission reaction rate comparison between simulation a-1a's most-minimized PF_{total} TRISO distribution and a constant PF_{total} = 0.0559 TRISO distribution. Both distributions shown in Figure 7.14.

Energy Group	**% of Total**	**Most-minimized PF_{total} Fission [reactions/src]**	**Flat PF_{total} Fission [reactions/src]**	**% Fission Difference**
1	00.28	0.00165	0.00162	+2.01
2	01.56	0.00886	0.00884	+0.21
3	01.51	0.00854	0.00852	+0.23
4	96.63	0.54813	0.54465	+0.63
Total	-	0.52998	0.52656	+0.65

to find a reactor model with lower PF_{total} that meets k_{eff} constraints.

Simulation a-1d In Section 7.2.1's simulation a-1d, I conducted a single-objective optimization simulation to minimize total fuel packing fraction (PF_{total}) by varying PF_{total} and coolant channel shape. In simulation a-1d, ROLLO found no correlation between PF_{total} and coolant channel shape (demonstrated in Figure 7.2).

Summary I verified that the minimize PF_{total} objective for the AHTR one-third assembly model is also driven by maximizing the total fission reaction rates. The minimize PF_{total} objective influences oscillations in the TRISO distribution. The objective does not correlate with the coolant channel shape.

7.6.2 Discussion: Minimize T_{max} Objective

Simulation a-1b In Section 7.2.2's simulation a-1b, I conducted a single-objective optimization simulation to minimize the one-third assembly's maximum temperature (T_{max}) by varying TRISO distribution. In simulation a-1b, ROLLO found that for $PF_{total} = 0.06$, the reactor model with the most-minimized T_{max} has a T_{max} = $1161.28K$ with an almost constant TRISO distribution (Figure 7.3b).

Simulation a-1e In Section 7.2.2's simulation a-1e, I conducted a single-objective optimization simulation to minimize the one-third assembly's maximum temperature (T_{max}) by varying coolant channel shape. In simulation a-1e, ROLLO found a negative linear correlation between the one-third assembly's T_{max} and r_1 and r_5, but no correlation with r_2, r_3, and r_4, shown in Figure 7.4.

Figures 7.15a and 7.15b show the 2D temperature distribution and centerline temperature for simulation a-1e's one-third assembly model with the most-minimized T_{max} (Figure 7.4b). Figure 7.15 demonstrates that for simulation a-1e's most-minimized T_{max} reactor model, the temperature peaks in the top and bottom graphite planks. r_1 and r_5 control the coolant channel shape of the FLiBe channels closest to the top and bottom graphite planks. This explains why ROLLO found a negative linear correlation between the one-third assembly's T_{max} and r_1 and r_5. To

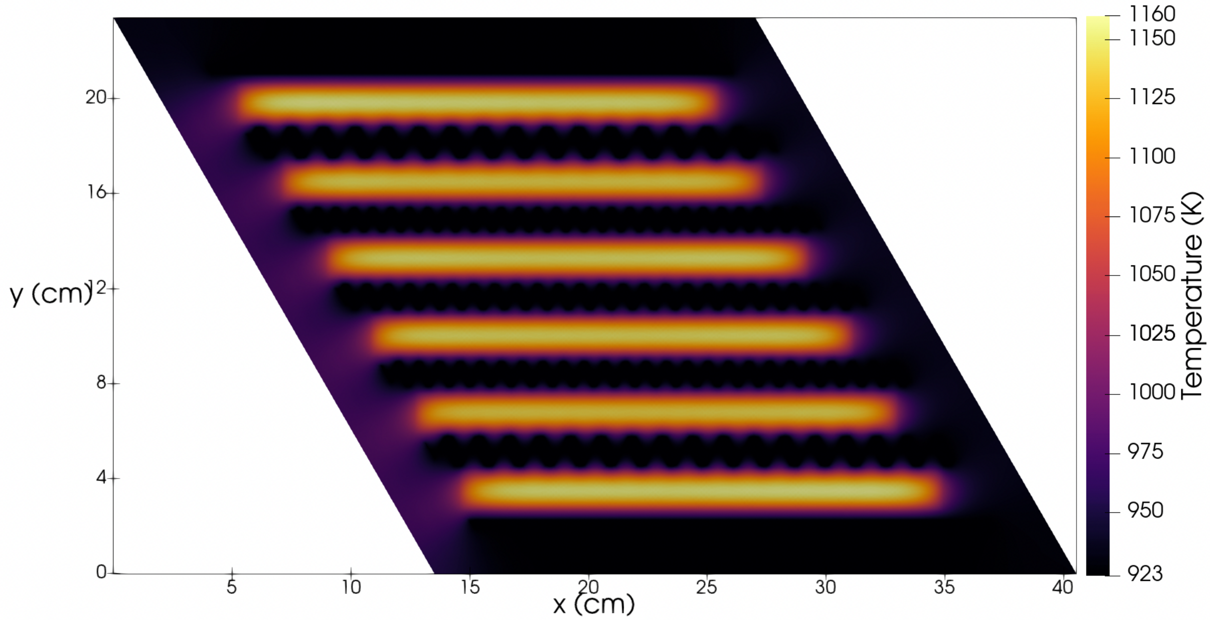

(a) 2D temperature distribution.

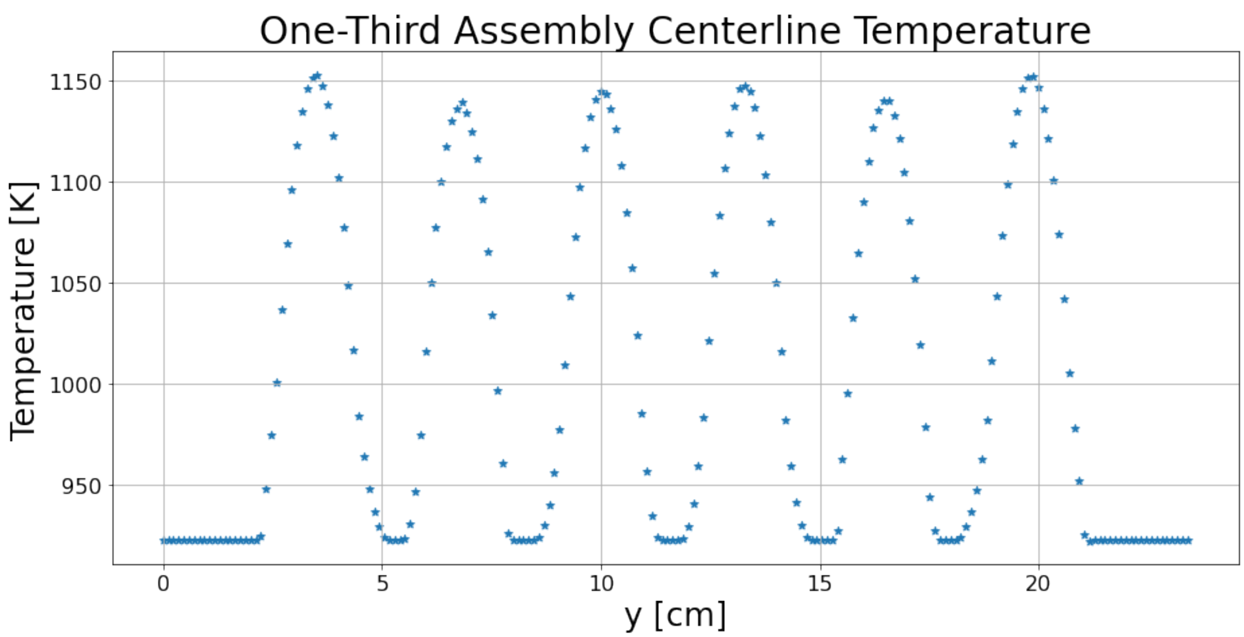

(b) Centerline temperature. AHTR assembly's centerline is the white line in Figure 5.14.

Figure 7.15: Simulation a-1e's most-minimized T_{max} one-third assembly reactor model's temperature distribution.

minimize the maximum one-third assembly temperature, ROLLO maximized r_1 and r_5 to enable enhanced cooling in the top and bottom graphite planks. Thus, depending on the temperature distribution in a one-third assembly, the FLiBe channels (corresponding to r_1, r_2, r_3, r_4, r_5) closest to the temperature peaks will be most important to minimizing T_{max}.

Comparison of simulation a-1b and a-1e's results in Figures 7.3a and 7.4a show that coolant channel shape variation does not have as high of an impact on T_{max} as TRISO distribution variation: the average T_{max} due to TRISO variation decreased by ~ $150K$ over 3 generations, while average T_{max} due to coolant channel shape variation only decreased by ~ $10K$ over 3 generations.

Summary I verified that, similar to the AHTR plank model, a flatter TRISO distribution minimizes the one-third assembly's T_{max}. For the one-third assembly, the FLiBe channels (corresponding to r_1, r_2, r_3, r_4, r_5) closest to the temperature peaks will be most important to minimizing maximum one-third assembly temperature and thus, will show a negative correlation with T_{max}. Simulation a-1b and a-1e suggest that TRISO distribution influences the minimize T_{max} objective more than the coolant channel shape.

7.6.3 Discussion: Minimize PPF_{fuel} Objective

Simulation a-1c In Section 7.2.3's simulation a-1c, I conducted a single-objective optimization simulation to minimize fuel-normalized power peaking factor (PPF_{fuel}) by varying TRISO distribution. In simulation a-1c, ROLLO found that for $PF_{total} = 0.06$, the reactor model with the most-minimized PPF_{fuel} has a PPF_{fuel} = 1.0872, an oscillating TRISO distribution along the x-axis, and a packing fraction standard deviation of 0.017 across the one-third assembly (Figure 7.5b).

Section 6.6.1 concluded that for the AHTR plank model, the minimize PPF_{fuel} objective is driven by flattening thermal (Group 4) flux distribution. I compare the flux distributions for simulation a-1c's most-minimized PPF_{fuel} reactor model (PPF_{fuel} = 1.0872) and the reactor model in simulation a-1c's final generation with the highest PPF_{fuel} = 1.2431. Figure 7.16 shows the TRISO distributions for the compared reactor models.

Figure 7.17 compares the 4 energy group flux distributions between simulation a-1c's most-minimized PPF_{fuel} TRISO distribution and highest PPF_{fuel} TRISO distribution (both shown in

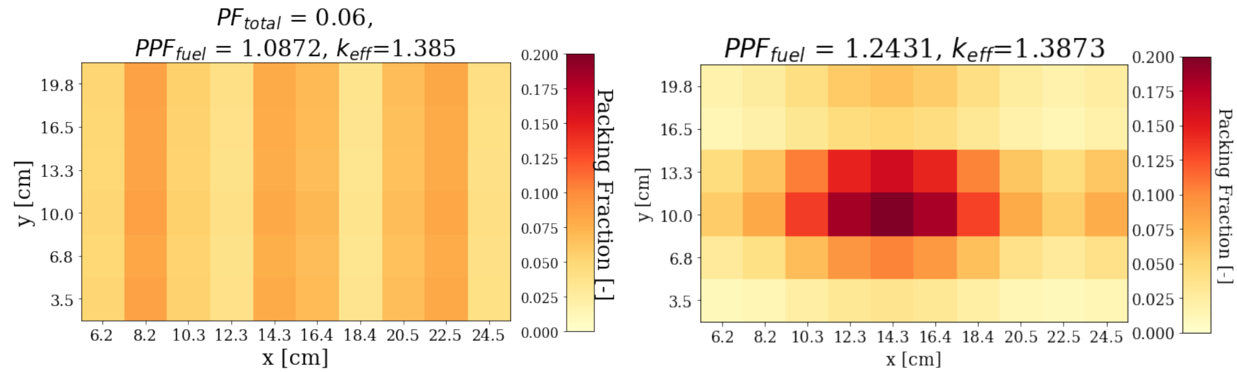

Figure 7.16: Simulation a-1c's most-minimized PPF_{fuel} TRISO distribution from Figure 7.5 (left) and the highest PPF_{fuel} TRISO distribution (right).

Figure 7.16). In Figure 7.17, the reactor model with the highest PPF_{fuel} = 1.2431's Group 4 flux dips in the center of the one-third assembly due to spatial self-shielding effects. In the highest PPF_{fuel} = 1.2431 reactor model's Group 1 flux, there is a peak in fast neutrons born in the one-third assembly's center. The fast neutrons are moderated in the graphite matrix and graphite structure (AHTR one-third assembly geometry: Figure 5.2). The moderated neutrons are more likely absorbed in the fuel regions nearer to the outer pure graphite structure moderating regions.

Table 7.20 quantifies the total flux differences per energy group between the reactor models. I used a 100 x 100 mesh to tally the flux values for each energy group within the one-third assembly model.

Table 7.20: Flux value comparison between the two reactor models in Figure 7.16: simulation a-1c's most-minimized PPF_{fuel} reactor model with PPF_{fuel} = 1.0872 and simulation a-1c's reactor model with the highest PPF_{fuel} = 1.2431. Energy Group 1: E > 9.1188×10^{-3} MeV, Energy Group 2: $2.9023 \times 10^{-5} < E < 9.1188 \times 10^{-3}$ MeV, Energy Group 3: $1.8556 \times 10^{-5} < E < 2.9023 \times 10^{-5}$ MeV, Energy Group 4: $1.0 \times 10^{-12} < E < 1.8554 \times 10^{-6}$ MeV.

Energy Group	$max(\phi)/min(\phi)$ **Most-minimized** PPF_{fuel} **TRISO Distribution**	$max(\phi)/min(\phi)$ **Highest** PPF_{fuel} **TRISO Distribution**	**% Difference**
1	1.825	2.608	-30.00
2	1.341	1.386	-3.18
3	1.302	1.334	-2.43
4	1.319	1.331	-0.85

In energy group 4, the most-minimized PPF_{fuel} flux distribution is 0.85% flatter than the reactor model with the highest PPF_{fuel} = 1.2431. These results verify that, similar to the AHTR

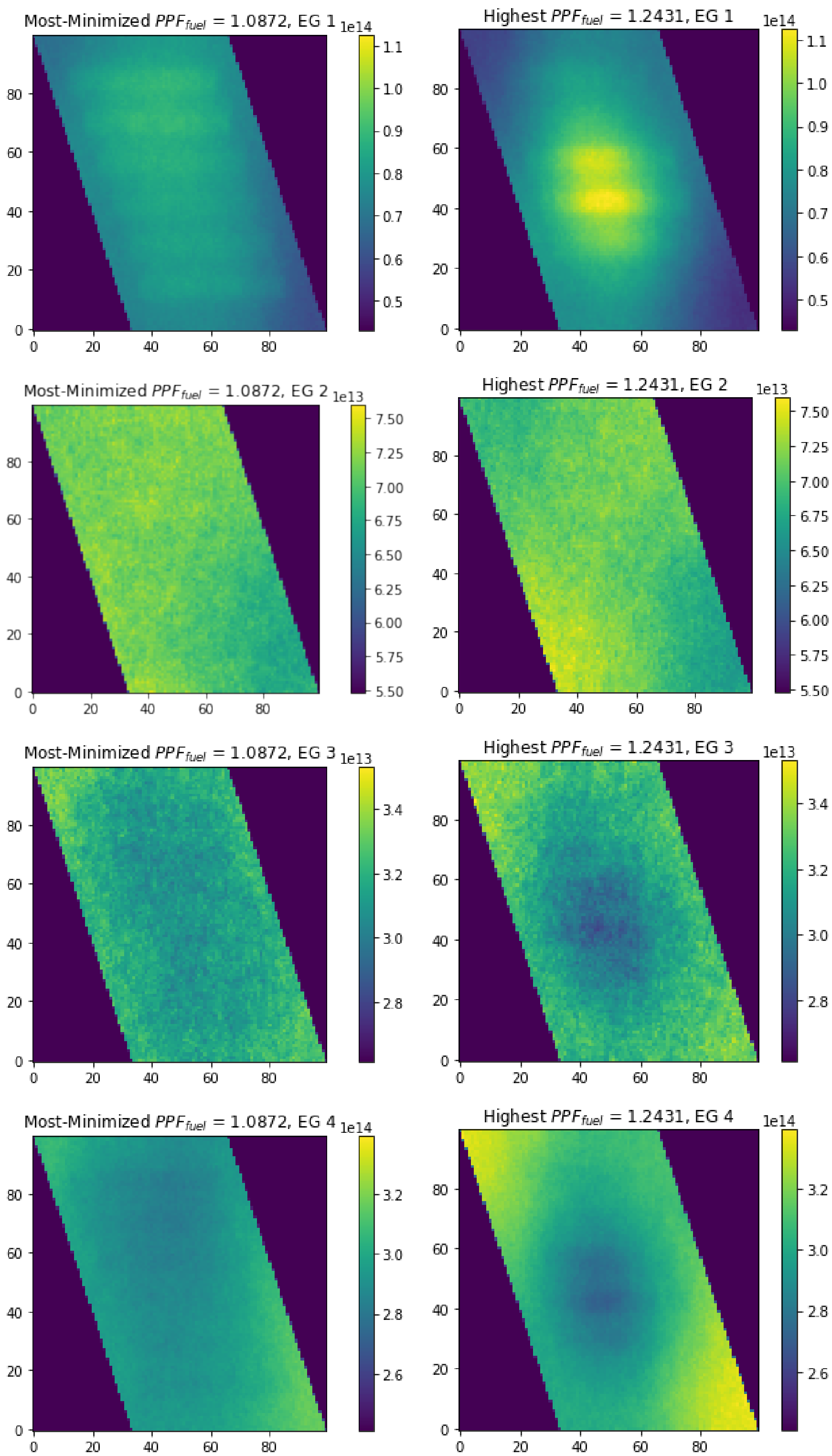

Figure 7.17: AHTR one-third assembly's flux comparison between the two reactor models in Figure 7.16: simulation a-1c's most-minimized PPF_{fuel} reactor model with PPF_{fuel} = 1.0872 and simulation a-1c's reactor model with the highest PPF_{fuel} = 1.2431. Energy Group 1: E $> 9.1188 \times 10^{-3}$ MeV, Energy Group 2: $2.9023 \times 10^{-5} < E < 9.1188 \times 10^{-3}$ MeV, Energy Group 3: $1.8556 \times 10^{-5} < E < 2.9023 \times 10^{-5}$ MeV, Energy Group 4: $1.0 \times 10^{-12} < E < 1.8554 \times 10^{-6}$ MeV.

plank model, the AHTR one-third assembly model's minimize PPF_{fuel} objective is also driven by flattening thermal (Group 4) flux distribution since $max(\Phi_j) \div ave(\Phi_j) \propto PPF_{fuel}$ (Equation 6.5).

Simulation p-1f In Section 7.2.3's simulation a-1f, I conducted a single-objective optimization simulation to minimize fuel-normalized power peaking factor (PPF_{fuel}) by varying coolant channel shape. In simulation a-1f, ROLLO found no correlation between PPF_{fuel} and coolant channel shape (demonstrated in Figure 7.6).

Summary I verified that the minimize PPF_{fuel} objective for the AHTR one-third assembly model is also driven by flattening thermal (Group 4) flux distribution. The minimize PPF_{fuel} objective influences PF_{total} and oscillations in the TRISO distribution. The objective does not correlate with the coolant channel shape.

7.6.4 Discussion: Multi-Objective Optimization

ROLLO successfully found widely spread out reactor model solutions in each multi-objective optimization simulation's final generation Pareto fronts. In this section, I explain how the driving factors and phenomena observed in the previous single-objective discussions (Sections 7.6.1, 7.6.2, and 7.6.3) combine to result in the optimal reactor models found by the multi-objective optimization simulations.

Simulation a-2a

In Section 7.3.1's simulation a-2a, I conducted a two-objective optimization simulation to minimize total fuel packing fraction (PF_{total}) and maximum temperature (T_{max}) in a one-third assembly model by varying PF_{total} and TRISO distribution. In simulation a-2a, ROLLO found 13 reactor models on the Pareto Front (Figure 7.7a).

In simulation a-2a, ROLLO found that the one-third assembly models with the most-minimized PF_{total} objective are reactor models 3 and 4 (Figure 7.7b). Both reactor models have an oscillating TRISO distribution along the x-axis and y-axis. Figure 7.18 compares simulation a-2a's most-minimized PF_{total} reactor model 3 and simulation a-1a's most-minimized PF_{total} reactor model. Figure 7.18 shows that simulation a-2a's most-minimized PF_{total} reactor model, and simulation

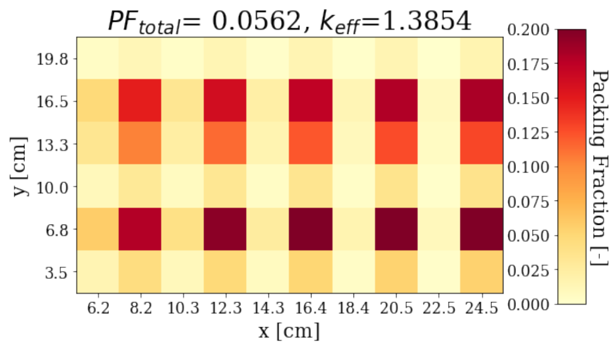

Figure 7.18: Simulation a-2a's most-minimized PF_{total} TRISO distribution from Figure 7.7 (left) and simulation a-1a's most-minimized PF_{total} TRISO distribution from Figure 7.1 (right).

a-1a's most-minimized PF_{total} reactor model have similar distributions with peaks on the even fuel cell columns but at different amplitudes.

In simulation a-2a, ROLLO found that the one-third assembly model with the most-minimized T_{max} objective, reactor model 9 (Figure 7.7b), has an almost constant TRISO distribution. Figure 7.19 compares simulation a-2a's most-minimized T_{max} reactor model 9 and simulation a-1b's most-minimized T_{max} reactor model. Figure 7.19 shows that simulation a-2a's most-minimized

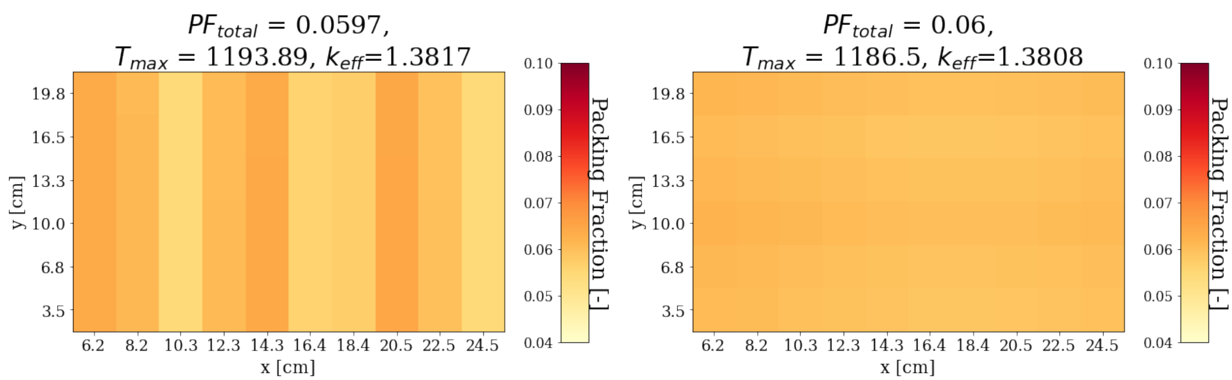

Figure 7.19: Simulation a-2a's most-minimized T_{max} TRISO distribution from Figure 7.7 (left) and simulation a-1b's most-minimized T_{max} TRISO distribution from Figure 7.3 (right).

T_{max} reactor model, and simulation a-1b's most-minimized T_{max} reactor model have similar almost constant TRISO distributions with packing fraction standard deviations of 0.004 and 0.0009, respectively. However, they have different PF_{total} values, and simulation a-2a's most-minimized T_{max}'s TRISO distribution is not as flat as simulation a-1b.

Figure 7.20 shows reactor model 13, which minimized PF_{total} and T_{max} to an equal extent by balancing influences from both objectives. The TRISO distributions on simulation a-2a's Pareto

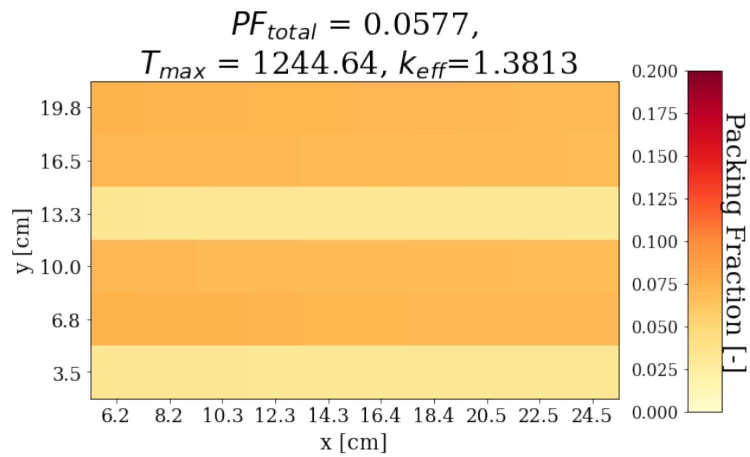

Figure 7.20: Simulation a-2a's reactor model 13 which minimized both PF_{total} and T_{max} to an equal extent (see Pareto Front in Figure 7.7).

front in Figure 7.7 minimize both PF_{total} and T_{max} and vary between the two extreme cases: most-minimized PF_{total} and most-minimized T_{max}. The minimize T_{max} objective influences the TRISO distribution's flatness, as described in Section 7.6.2, while the minimize PF_{total} objective influences the oscillating pattern, as described in Section 7.6.1.

Simulation a-2b

In Section 7.3.2's simulation a-2b, I conducted a two-objective optimization simulation to minimize total fuel packing fraction (PF_{total}) and fuel-normalized power peaking factor (PPF_{fuel}) in a one-third assembly model by varying PF_{total} and TRISO packing fraction distribution. In simulation a-2b's final generation, ROLLO found 12 reactor models on the Pareto Front (Figure 7.8a).

In simulation a-2b, ROLLO found that the one-third assembly model with the most-minimized PF_{total} objective, reactor model 3 (Figure 7.8b), has an oscillating TRISO distribution along the x-axis and y-axis. Figure 7.21 compares simulation a-2b's reactor model 3 and simulation a-1a's most-minimized PF_{total} reactor model. Figure 7.21 shows that simulation a-2b's reactor model 3 and simulation a-1a's most-minimized PF_{total} reactor model have similarly large packing fraction standard deviation of 0.053 and 0.04, respectively. However, they do not follow the same TRISO distribution pattern. Section 6.6.3 described that in the AHTR plank model, the minimize PF_{total} and minimize PPF_{fuel} objectives influence each other resulting in unexpected TRISO distributions at different PF_{total} values. This same effect also applies to the one-third assembly model, explaining

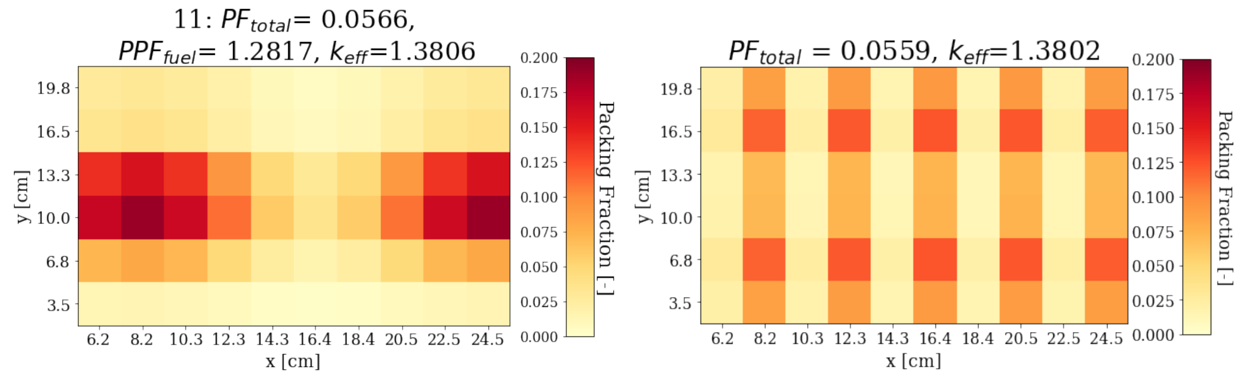

Figure 7.21: Simulation a-2b's most-minimized PF_{total} TRISO distribution from Figure 7.8 (left) and simulation a-1a's most-minimized PF_{total} TRISO distribution from Figure 7.1 (right).

why, unlike simulation a-2a, simulation a-2b's extreme most-minimized PF_{total} and most-minimized PPF_{fuel} do not follow similar TRISO distribution patterns as their single-objective counterparts.

In simulation a-2b, ROLLO found that the one-third assembly model with the most-minimized PPF_{fuel} objective, reactor model 1 (Figure 7.8b), has a TRISO distribution that oscillates along the y-axis and oscillates slightly along the x-axis. Figure 7.21 compares simulation a-2b's most-minimized PPF_{fuel} reactor model 1 and simulation a-1c's most-minimized PPF_{fuel} reactor model. Figure 7.22 shows that simulation a-2b's reactor model 1 and simulation a-1a's most-minimized

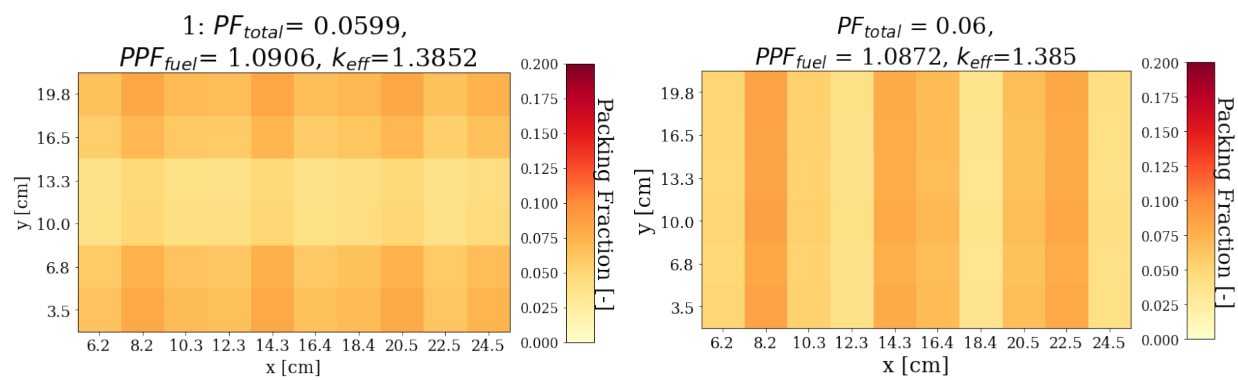

Figure 7.22: Simulation a-2b's most-minimized PPF_{fuel} TRISO distribution from Figure 7.8 (left) and simulation a-1c's most-minimized PPF_{fuel} TRISO distribution from Figure 7.5 (right).

PPF_{fuel} reactor model have similarly small packing fraction standard deviation of 0.013 and 0.017, respectively. However, they do not follow the same TRISO distribution pattern; this is attributed to the PF_{total} and PPF_{fuel} relationship resulting in unexpected TRISO distributions at different PF_{total} values, as mentioned previously. The relationship between the AHTR's PF_{total} and PPF_{fuel}

merits future work of further sensitivity analysis.

To better understand the reactor models on simulation a-2b's Pareto Front, I deep dive into the driving factors for the minimize PF_{total} and minimize PPF_{fuel} objectives.

Driving Factor Quantification Sections 7.6.1 and 7.6.3 verified that, similar to the AHTR plank, the AHTR one-third assembly's minimize PF_{total} objective is driven by maximizing total fission reaction rates, and the minimize PPF_{fuel} objective is driven by flattening the thermal flux distribution. This section compares the total fission reaction rate and thermal flux flatness for 3 reactors models on simulation a-2b's Pareto Front (Figure 7.8a): reactor model 11 with most-minimized PF_{total}, reactor model 1 with most-minimized PPF_{fuel}, and reactor model 5 which minimizes both PF_{total} and PPF_{fuel} to an equal extent. Figure 7.23 shows the TRISO packing fraction distribution for the 3 reactors models.

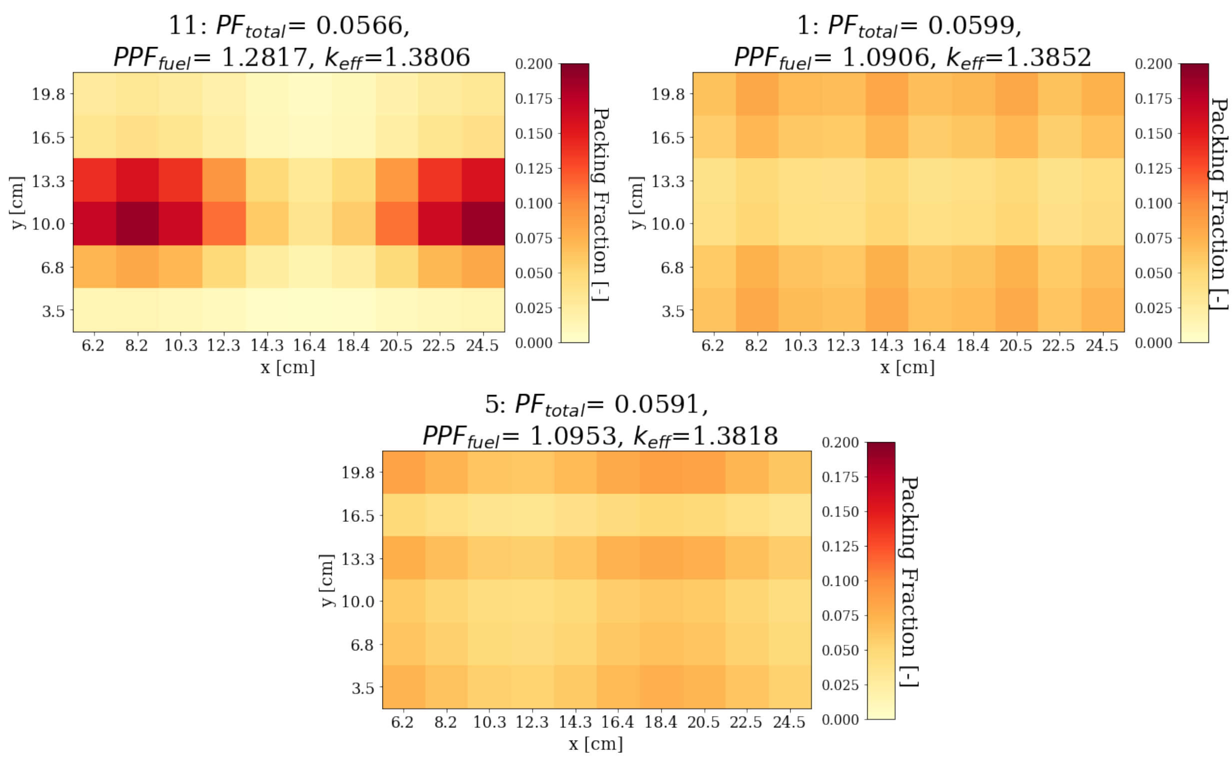

Figure 7.23: TRISO distributions for 3 reactor models on Simulation a-2b's Pareto Front (Figure 7.8a): reactor model 11 with most-minimized PF_{total} (top left), reactor model 1 with most-minimized PPF_{fuel} (top right), and reactor model 5 which minimizes both PF_{total} and PPF_{fuel} to an equal extent (bottom).

Table 7.21 shows the total fission reaction rate, and thermal flux flatness for the three reactor models.

Table 7.21: Total fission reaction rate, and thermal flux flatness ($max(\phi_4)/min(\phi_4)$) for 3 reactor models on simulation a-2b's Pareto Front (Figure 7.8a): reactor model 1 with most-minimized PPF_{fuel}, reactor model 11 with most-minimized PF_{total}, and reactor model 5 which minimizes both PF_{total} and PPF_{fuel} to an equal extent.

Most Minimized Parameter	**Reactor Model**	**Fission [reactions/src]**	% **Diff**	$max(\phi_4)/min(\phi_4)$	% **Diff**
Both	5	0.5471	-	1.2986	-
PF_{total}	11	0.5472	+0.017	1.3168	+1.40
PPF_{fuel}	1	0.5478	+0.12	1.2851	-1.03

The most minimized PPF_{fuel} reactor model 1 has the highest fission reaction rate, followed by the most minimized PF_{total} reactor model 11, and then reactor model 5 which minimizes both PF_{total} and PPF_{fuel} to an equal extent. Reactor model 1 has the highest fission reaction rate since it has the highest PF_{total}. Reactor model 11 has a slightly higher fission reaction rate than reactor model 5, and they have k_{eff} values within error of each other despite reactor model 11 having a lower PF_{total} ($PF_{total,11}$ = 0.0566 vs. $PF_{total,5}$ = 0.0591). Section 7.6.1 verified that maximizing the total fission reaction rate drives the AHTR one-third assembly model's minimize PF_{total} objective. Therefore, reactor model 11's oscillating TRISO distribution enables a lower PF_{total} for the same k_{eff} as reactor model 5 since both have comparable total fission reaction rates.

The most minimized PPF_{fuel} reactor model 1 has the flattest thermal flux, followed by reactor model 5 which minimizes both PF_{total} and PPF_{fuel} to an equal extent, and then the most minimized PF_{fuel} reactor model 11. Section 7.6.3 verified that the AHTR one-third assembly model's minimize PPF_{fuel} objective is driven by flattening thermal (Group 4) flux distribution. Therefore, reactor model 1, with the flattest thermal flux distribution, most minimized PPF_{fuel}.

Simulation a-2c

In Section 7.3.3's simulation a-2c, I conducted a two-objective optimization simulation to minimize maximum temperature (T_{max}) and fuel-normalized power peaking factor (PPF_{fuel}) in a one-third assembly model by varying TRISO distribution. In simulation a-2c, ROLLO found one reactor model on the Pareto Front (Figure 7.9a), demonstrating that the minimize T_{max} and minimize PPF_{fuel} objectives are non-contrasting for the one-third assembly model.

Figure 7.24 compares the single reactor model on simulation a-2c's Pareto Front, simulation a-1b's most-minimized T_{max} reactor model, and simulation a-1c's most-minimized PPF_{fuel} reactor model. All reactor models have PF_{total} = 0.06.

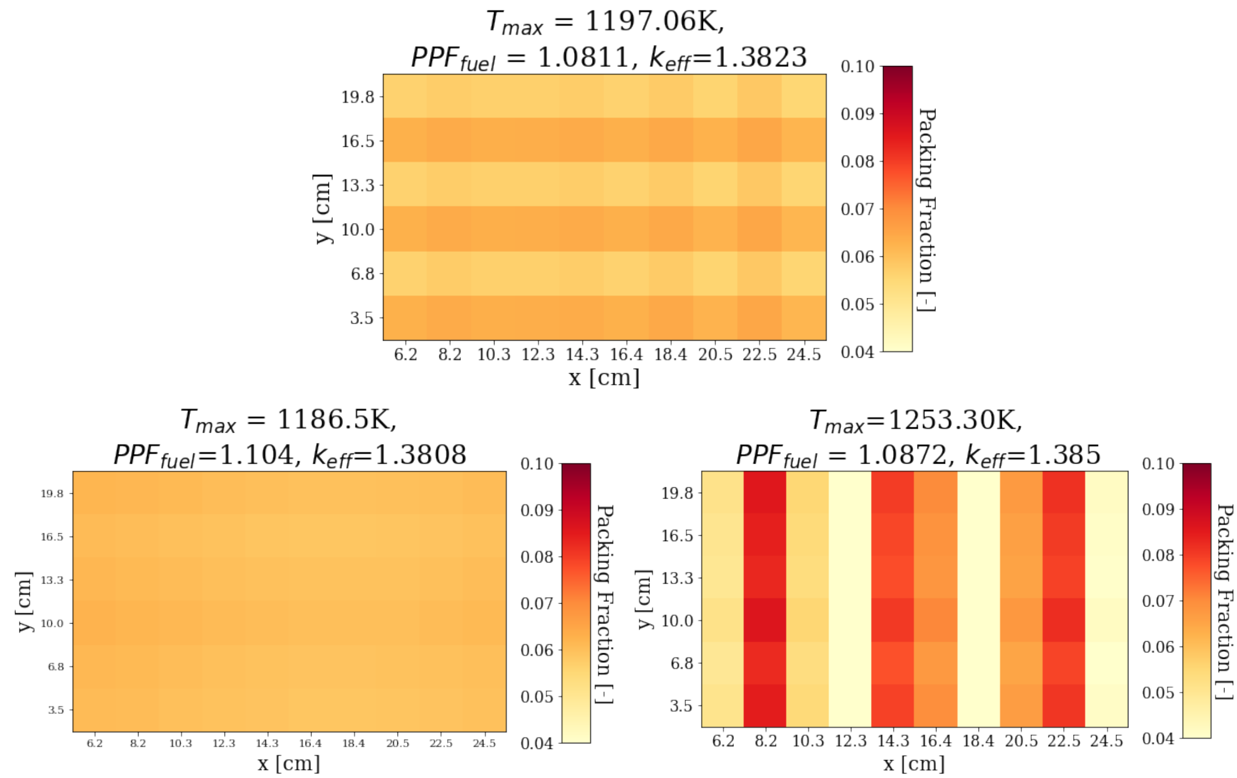

Figure 7.24: Simulation a-2c's single Pareto Front reactor model's TRISO distribution from Figure 7.9 (above), simulation a-1b's most-minimized T_{max} TRISO distribution from Figure 7.3 (lower left), and simulation a-1c's most-minimized PPF_{fuel} TRISO distribution from Figure 7.5 (lower right). All reactor models have PF_{total} = 0.06.

Figure 7.24 shows that the single reactor model on simulation a-2c's Pareto Front's TRISO distributions is more similar to simulation a-1b's most-minimized T_{max} TRISO distribution than simulation a-1c's most-minimized PPF_{fuel} TRISO distribution. Simulation a-1c's most-minimized PPF_{fuel} reactor model has a high T_{max} = 1253.30 K, while simulation a-1b's most-minimized T_{max} reactor model has a low PPF_{fuel} = 1.104. Therefore, influences from the minimize T_{max} objective results in the single reactor model on simulation a-2c's Pareto Front to have a TRISO distribution more similar to simulation a-1b's most-minimized T_{max} reactor model. The minimize T_{max} objective influences the TRISO distribution's flatness, as described in Section 7.6.2, while the minimize PPF_{fuel} objective influences the oscillating pattern, as described in Section 7.6.3.

Simulation a-3a

In Section 7.4.1's simulation a-3a, I conducted a three-objective optimization simulation to minimize total fuel packing fraction (PF_{total}), maximum temperature (T_{max}), and fuel-normalized power peaking factor (PPF_{fuel}) in the one-third assembly model by varying PF_{total} and TRISO distribution. ROLLO found 32 widely spread reactor models on simulation a-3a's Pareto front (Figure 7.10a).

In simulation a-3a, ROLLO found that the one-third assembly model with the most-minimized PF_{total} objective, reactor model 30 (Figure 7.11a), has an oscillating TRISO distribution along the x-axis and y-axis. Figure 7.25 compares simulation a-3a's reactor model 30 and simulation a-1a's most-minimized PF_{total} reactor model. Figure 7.25 shows that simulation a-3a's reactor

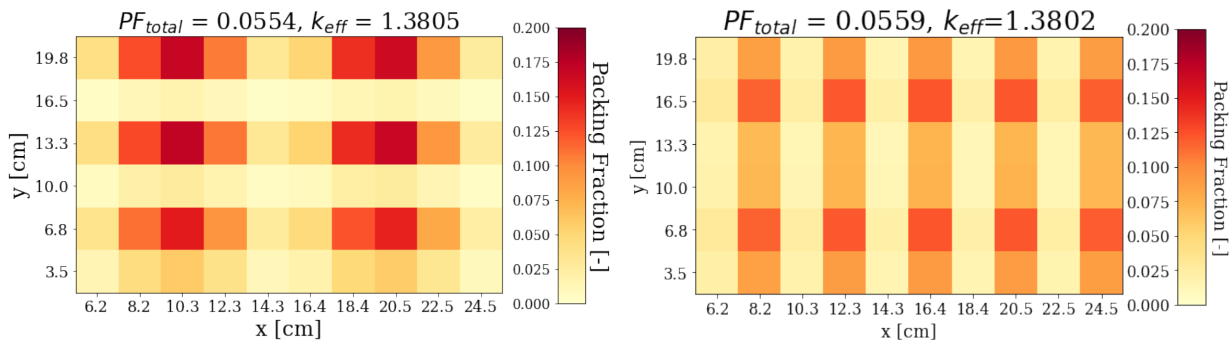

Figure 7.25: Simulation a-3a's most-minimized PF_{total} TRISO distribution from Figure 7.11 (left) and simulation a-1a's most-minimized PF_{total} TRISO distribution from Figure 7.1 (right).

model 30 and simulation a-1a's most-minimized PF_{total} reactor model have similarly large packing fraction standard deviation of 0.052 and 0.04, respectively. However, they do not follow the same TRISO distribution pattern; this is attributed to the PF_{total} and PPF_{fuel} relationship resulting in unexpected TRISO distributions at different PF_{total} values, as mentioned previously.

In simulation a-3a, ROLLO found that the one-third assembly model with the most-minimized T_{max} objective, reactor model 3 (Figure 7.11a), has an almost constant TRISO distribution. Figure 7.26 compares simulation a-3a's most-minimized T_{max} reactor model 3 and simulation a-1b's most-minimized T_{max} reactor model. Figure 7.26 shows that simulation a-3a's most-minimized T_{max} reactor model, and simulation a-1b's most-minimized T_{max} reactor model have similar almost constant TRISO distributions with packing fraction standard deviations of 0.003 and 0.0009,

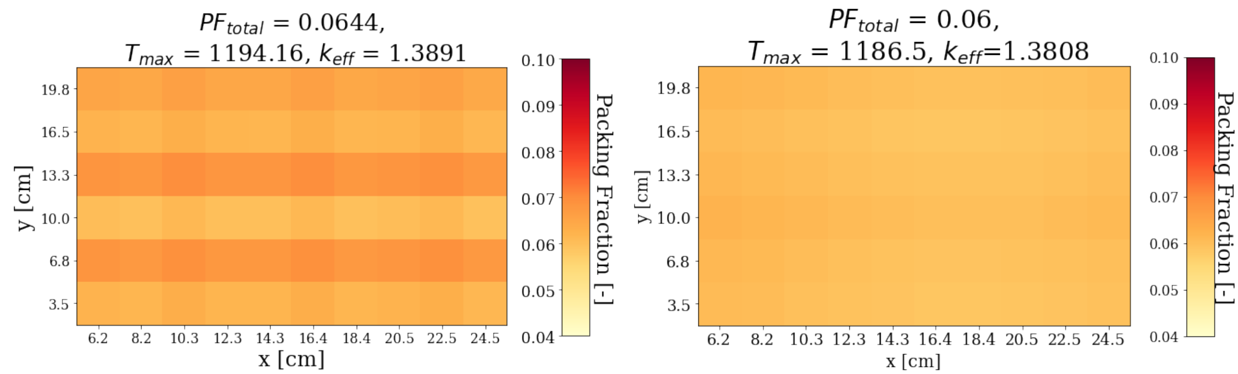

Figure 7.26: Simulation a-3a's most-minimized T_{max} TRISO distribution from Figure 7.11a (left) and simulation a-1b's most-minimized T_{max} TRISO distribution from Figure 7.3 (right).

respectively. However, they have different PF_{total} values, and simulation a-3a's most-minimized T_{max}'s TRISO distribution is not as flat as simulation a-1b.

In simulation a-3a, ROLLO found that the one-third assembly model with the most-minimized PPF_{fuel} objective, reactor model 1 (Figure 7.11a) has an oscillating TRISO distribution along the x-axis and y-axis. Figure 7.27 compares simulation a-3a's most-minimized PPF_{fuel} reactor model 1 and simulation a-1c's most-minimized PPF_{fuel} reactor model. Figure 7.27 shows that simulation

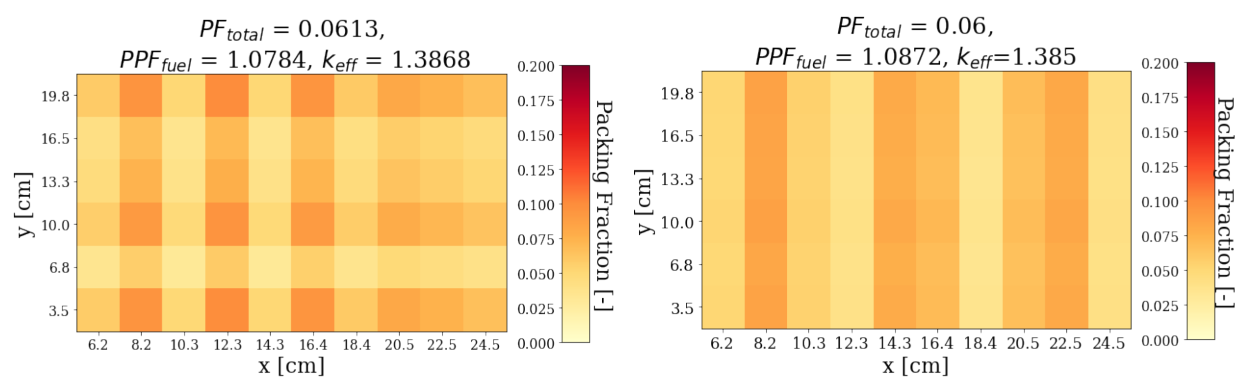

Figure 7.27: Simulation a-3a's most-minimized PPF_{fuel} TRISO distribution from Figure 7.11a (left) and simulation a-1c's most-minimized PPF_{fuel} TRISO distribution from Figure 7.5 (right).

a-3a's reactor model 1 and simulation a-1a's most-minimized PPF_{fuel} reactor model have similarly small packing fraction standard deviation of 0.019 and 0.017, respectively. However, they do not follow the same TRISO distribution pattern; this is attributed to the PF_{total} and PPF_{fuel} relationship resulting in unexpected TRISO distributions at different PF_{total} values, as mentioned previously.

Figure 7.28 shows reactor model 22, which minimized PF_{total}, T_{max}, and PPF_{fuel} to an equal extent by balancing influences from all objectives.

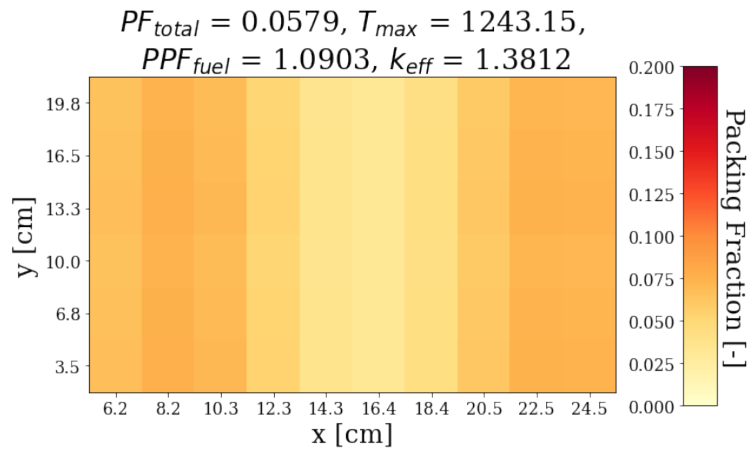

Figure 7.28: Simulation a-3a's reactor model 22 which minimized PF_{total}, T_{max}, and PPF_{fuel} to an equal extent (see Pareto Front in Figure 7.10a).

In all the reactor models on simulation a-3a's Pareto front (Figure 7.10a), the TRISO distribution flatness is influenced by the minimize T_{max} objective. The variations in TRISO distributions are influenced by both the minimize PF_{total} and minimize PPF_{fuel} objectives. However, as mentioned previously, the PF_{total} and PPF_{fuel} relationship result in unexpected TRISO distributions at different PF_{total} values. The minimize PF_{total} objective tries to maximize the fission reaction rate to enable a higher k_{eff} for a lower PF_{total}, and the PPF_{fuel} objective tries to flatten thermal flux.

Simulation a-3b

In Section 7.4.2's simulation a-3b, I conducted a three-objective optimization simulation to minimize total fuel packing fraction (PF_{total}), maximum temperature (T_{max}), and fuel-normalized power peaking factor (PPF_{fuel}) in a one-third assembly model by varying PF_{total}, TRISO distribution, and coolant channel shape (r_1, r_2, r_3, r_4, r_5). ROLLO found 12 reactor models on simulation a-3b's Pareto front (Figure 7.12a).

Compared to simulation a-3a in the previous section, simulation a-3b's reactor models have, on average, a lower T_{max} value due to coolant channel shape variation. In simulation a-3b, ROLLO found that the one-third assembly model with the most-minimized PF_{total} objective, reactor model

11 (Figure 7.13a), has an oscillating TRISO distribution along the x-axis and y-axis. Figure 7.25 compares simulation a-3b's reactor model 11 and simulation a-1a's most-minimized PF_{total} reactor model. Figure 7.29 shows that simulation a-3b's reactor model 11 and simulation a-1a's most-

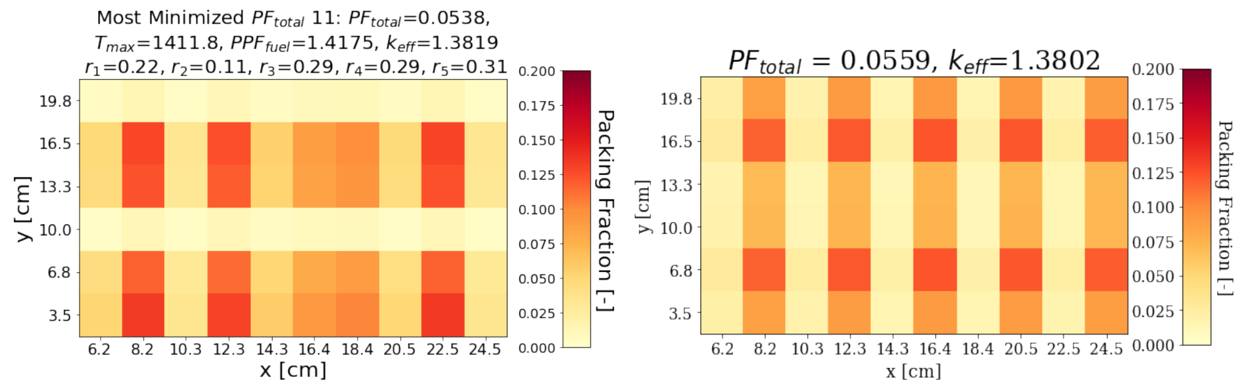

Figure 7.29: Simulation a-3b's most-minimized PF_{total} TRISO distribution from Figure 7.13 (left) and simulation a-1a's most-minimized PF_{total} TRISO distribution from Figure 7.1 (right).

minimized PF_{total} reactor model have similarly large packing fraction standard deviation of 0.044 and 0.04, respectively. However, they do not follow the same TRISO distribution pattern, which is attributed to the PF_{total} and PPF_{fuel} relationship resulting in unexpected TRISO distributions at different PF_{total} values, as mentioned previously.

In simulation a-3b, ROLLO found that the one-third assembly model with the most-minimized T_{max} objective, reactor model 1 (Figure 7.11a), has an almost constant TRISO distribution. Figure 7.30 compares simulation a-3b's most-minimized T_{max} reactor model 1 and simulation a-1b's most-minimized T_{max} reactor model. Figure 7.30 shows that simulation a-3b's most-minimized

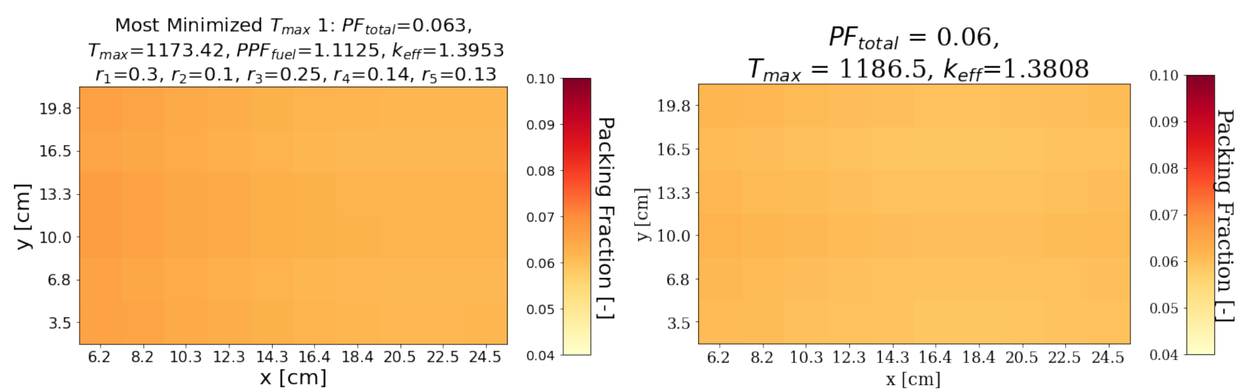

Figure 7.30: Simulation a-3b's most-minimized T_{max} TRISO distribution from Figure 7.11a (left) and simulation a-1b's most-minimized T_{max} TRISO distribution from Figure 7.3 (right).

T_{max} reactor model, and simulation a-1b's most-minimized T_{max} reactor model have similar almost constant TRISO distributions with packing fraction standard deviations of 0.001 and 0.0009, respectively. However, they have different PF_{total} values.

In simulation a-3b, ROLLO found that the one-third assembly model with the most-minimized PPF_{fuel} objective, reactor model 4 (Figure 7.13a), has a slightly oscillating TRISO distribution along the y-axis. Figure 7.27 compares simulation a-3b's most-minimized PPF_{fuel} reactor model 4 and simulation a-1c's most-minimized PPF_{fuel} reactor model. Figure 7.31 shows that simulation

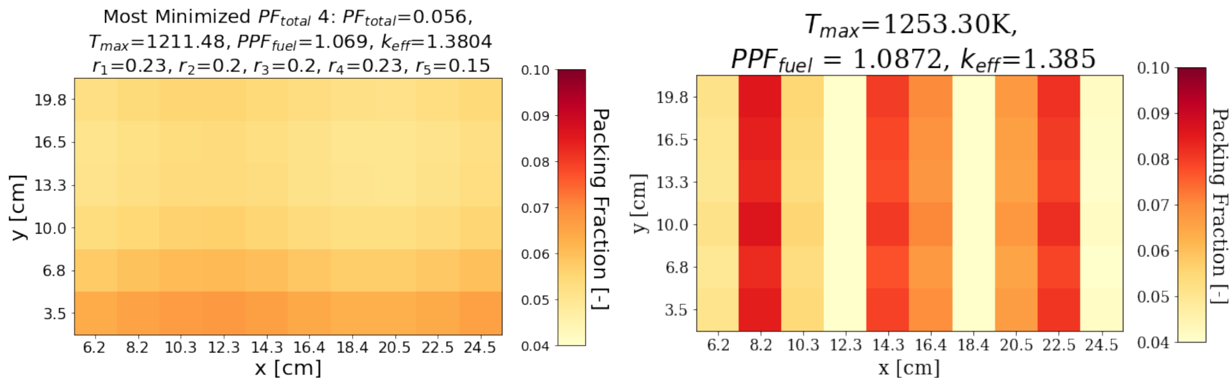

Figure 7.31: Simulation a-3b's most-minimized PPF_{fuel} TRISO distribution from Figure 7.13a (left) and simulation a-1c's most-minimized PPF_{fuel} TRISO distribution from Figure 7.5 (right).

a-3b's reactor model 4 and simulation a-1a's most-minimized PPF_{fuel} reactor models have small packing fraction standard deviation of 0.005 and 0.017, respectively. However, they do not follow the same TRISO distribution pattern; this is attributed to the PF_{total} and PPF_{fuel} relationship resulting in unexpected TRISO distributions at different PF_{total} values, as mentioned previously.

Figure 7.32 shows reactor model 2, which minimized PF_{total}, T_{max}, and PPF_{fuel} to an equal extent by balancing influences from all objectives. Similar to simulation a-3a, for all the reactor models on simulation a-3b's Pareto front (Figure 7.12a), the TRISO distribution flatness is influenced by the minimize T_{max} objective. The variations in TRISO distributions are influenced by both the minimize PF_{total} and minimize PPF_{fuel} objectives. However, as mentioned previously, the PF_{total} and PPF_{fuel} relationship result in unexpected TRISO distributions at different PF_{total} values. The minimize PF_{total} objective tries to maximize the fission reaction rate to enable a higher k_{eff} for a lower PF_{total}, and the PPF_{fuel} objective tries to flatten thermal flux.

Figure 7.33a shows the one-third assembly centerline temperatures for three reactors on sim-

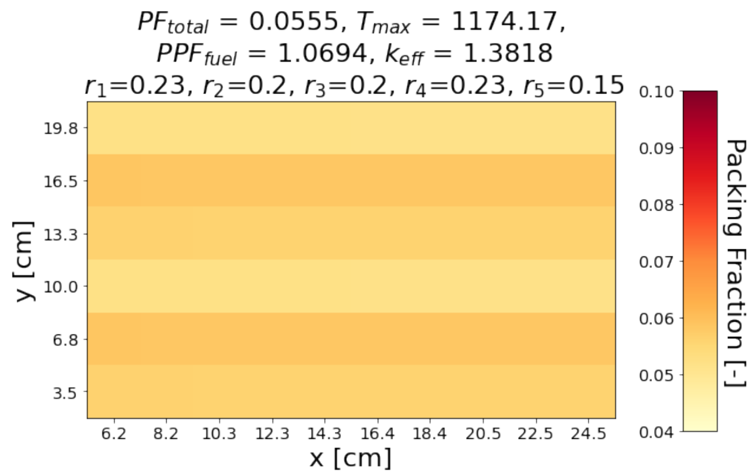

Figure 7.32: Simulation a-3b's reactor model 2 which minimized PF_{total}, T_{max}, and PPF_{fuel} to an equal extent (see Pareto Front in Figure 7.12a).

ulation a-3b's Pareto front: reactor model 11 with most-minimized PF_{total}, reactor model 1 with most-minimized T_{max}, and reactor model 4 with most-minimized PPF_{fuel}. r_1, r_2, r_3, r_4, and r_5 values correspond to the FliBe channel at 18cm, 15cm, 12cm, 8cm, and 6cm, respectively. Section

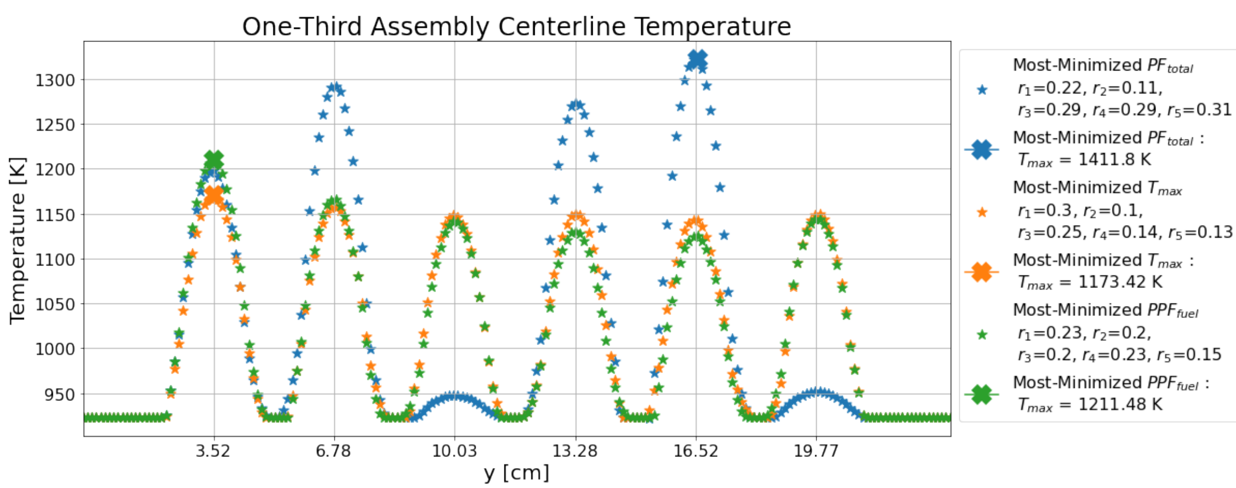

(a) Centerline temperature. AHTR assembly's centerline is the white line in Figure 5.14.

Figure 7.33: Simulation a-3b's one-third assembly reactor models' temperature distribution. Reactor models are on simulation a-3b's Pareto front: reactor model 11 with most-minimized PF_{total}, reactor model 1 with most-minimized T_{max}, and reactor model 4 with most-minimized PPF_{fuel}. r_1, r_2, r_3, r_4, and r_5 values correspond to the FliBe channel at 18cm, 15cm, 12cm, 8cm, and 6cm, respectively.

7.6.2 concluded that the one-third assembly's FLiBe channels (corresponding to r_1, r_2, r_3, r_4, r_5) closest to the temperature peaks are most important to minimizing T_{max}. However, coolant channel shape variation does not have as high of an impact on T_{max} as TRISO distribution variation: the average T_{max} due to TRISO variation decreased by ~ $150K$ over 3 generations, while average T_{max} due to coolant channel shape variation only decreased by ~ $10K$ over 3 generations. Sections 7.6.1, 7.6.2, and 7.6.3 also concluded that only coolant channel shape only correlates with the minimize T_{max} objective.

Figure 7.33a shows that reactor model 11 with most minimized PF_{total} peaks in the 4th graphite plank (at 16.52cm) and has $r_1 = 0.22cm$ and $r_2 = 0.11cm$, reactor model 1 with most minimized T_{max} peaks in the 1st graphite plank (at 3.52cm) and has $r_5 = 0.13cm$, and reactor model 4 with most minimized PPF_{fuel} peaks in the 1st graphite plank (at 3.52cm) and has $r_5 = 0.15cm$. All their radius values are unexpectedly small. This could be due to the coolant channel shape not having a high impact on T_{max} compared to TRISO distribution; thus, ROLLO was more influenced by TRISO distribution when searching for optimal reactor models. This paired with simulation a-3b's 128 individuals per generation possibly being too small to explore reactor models with 12 input parameters. Simulation a-3b has 12 input parameters which is higher than all the other optimization simulations, which have 7 or fewer input parameters. Larger population size will enable ROLLO to explore more reactor model variations and potentially find even more optimal reactor models. To better explore simulation a-3b's design space, I re-run simulation a-3b with 256 individuals per generation.

Simulation a-3b with 256 Population Size

Simulation a-3b-256 has the exact same optimization problem parameters as simulation a-3b (Table 7.16) except for an increase in population size to 256 individuals. Figure 7.34a shows a plot of the final generation's reactor models' PF_{total} against T_{max} against PPF_{fuel}; crosses mark the reactor models that fall on the Pareto front. Figure 7.34b shows the 38 TRISO packing fraction distributions in the final generation that fall on the Pareto front.

Figure 7.34 demonstrates that ROLLO found 38 reactor models on simulation a-3b-256 final generation's Pareto front. Figure 7.35 shows three reactor models on the Pareto front that most minimized each objective and one reactor model on the Pareto front that equally minimized all three objectives. I selected the equally minimized reactor model by visually studying Figure 7.34 and

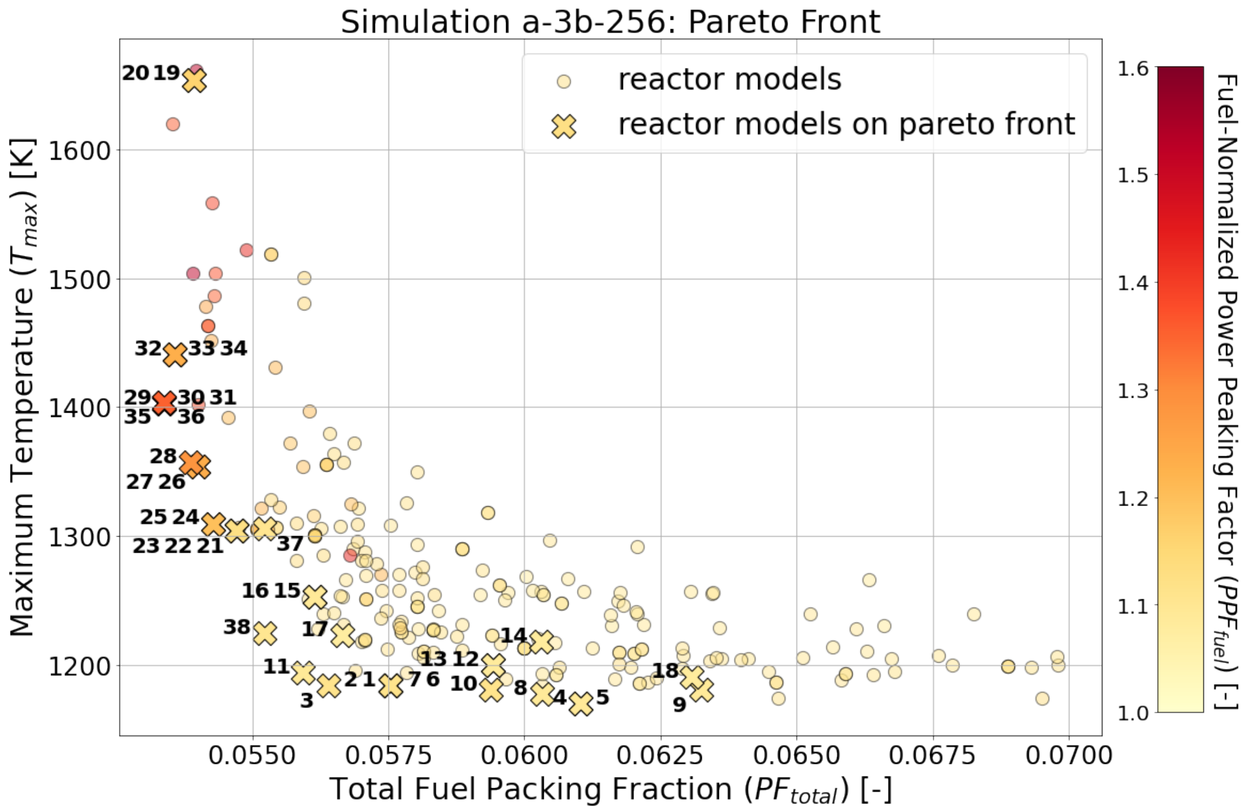

(a) Plot of final generation's reactor models' PF_{total} against T_{max} against PPF_{fuel} as a color dimension. Crosses indicate the reactor models on the Pareto front. Cross numbering correspond to TRISO distributions in Figure 7.12b.

Figure 7.34: Simulation a-3b-256 – ROLLO three-objective optimization with 256 population size to minimize total fuel packing fraction (PF_{total}), maximum temperature (T_{max}), and fuel-normalized power peaking factor (PPF_{fuel}) in the one-third assembly. Input parameters varied: total fuel packing fraction PF_{total}, TRISO packing fraction distribution ($\rho_{TRISO}(\vec{r})$), coolant channel shape (r_1, r_2, r_3, r_4, r_5).

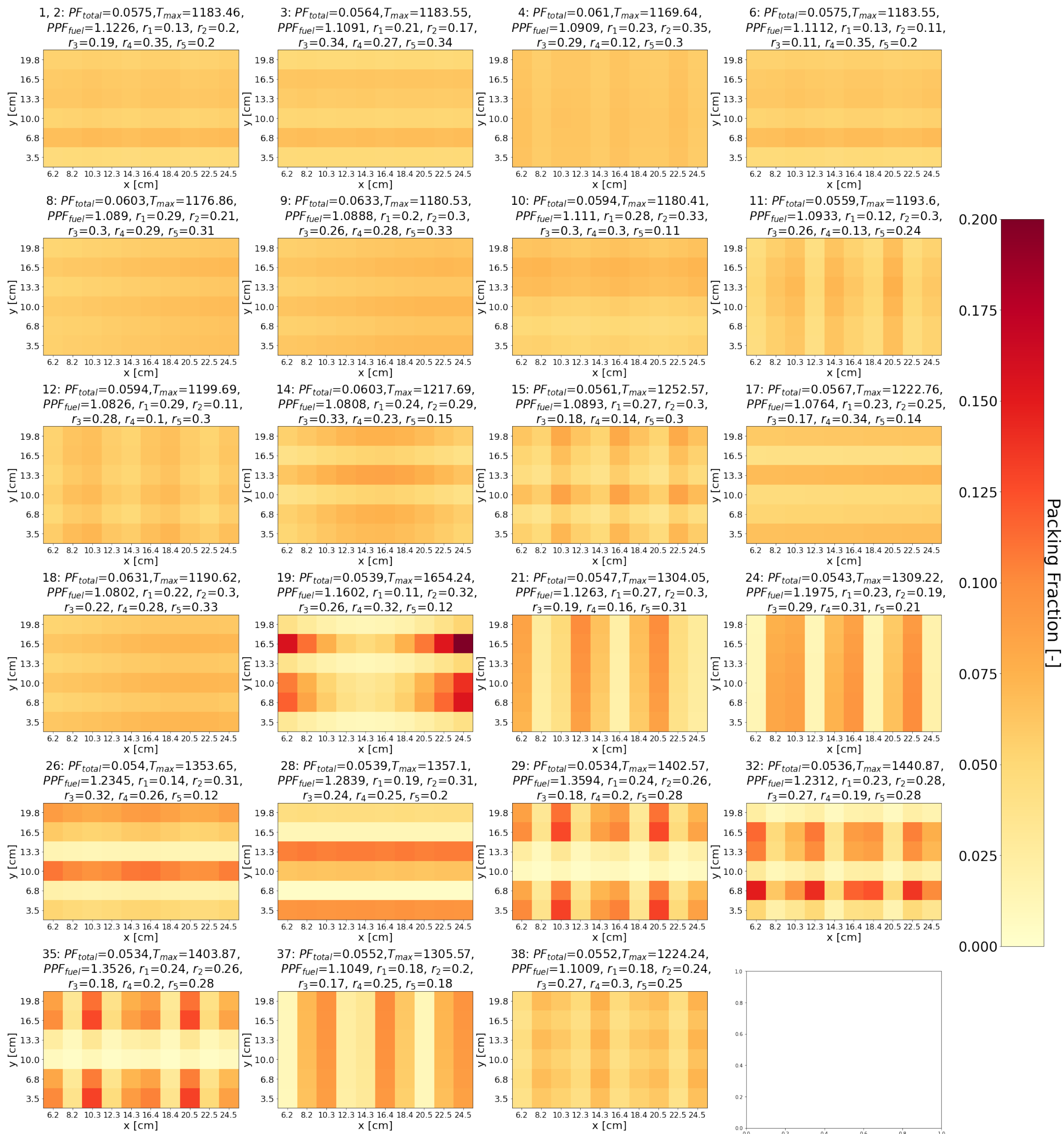

(b) TRISO distributions for the 38 reactor models on the Pareto front. Numbered reactor models correspond to numbered crosses in Figure 7.34a.

Figure 7.34: (contd.) Simulation a-3b-256 – ROLLO three-objective optimization with 256 population size to minimize total fuel packing fraction (PF_{total}), maximum temperature (T_{max}), and fuel-normalized power peaking factor (PPF_{fuel}) in the one-third assembly. Input parameters varied: total fuel packing fraction PF_{total}, TRISO packing fraction distribution ($\rho_{TRISO}(\vec{r})$), coolant channel shape (r_1, r_2, r_3, r_4, r_5).

selecting a reactor model close to the origin with a light yellow color dimension. Reactor model 36 most-minimized PF_{total}, reactor model 4 most-minimized T_{max}, reactor model 17 most-minimized PPF_{fuel}, and reactor model 11 equally minimized all three objectives.

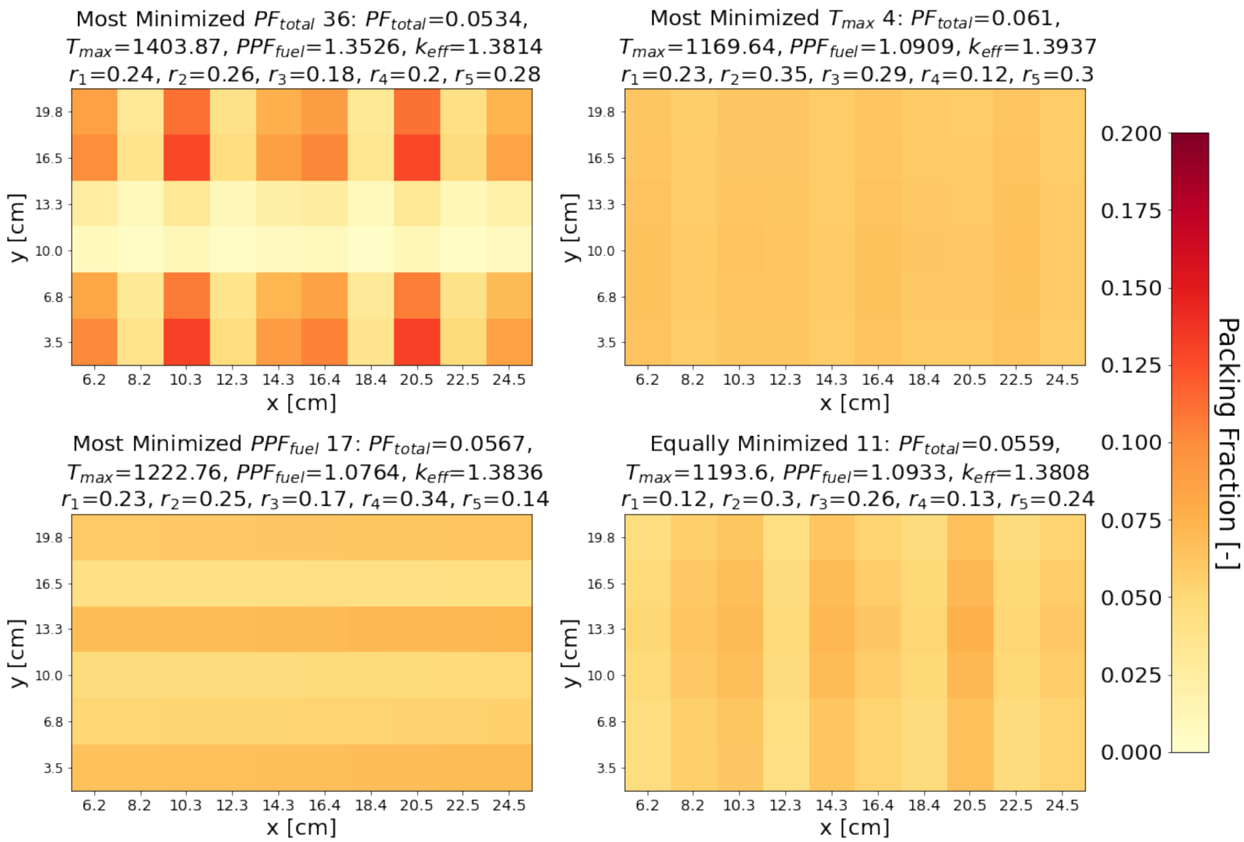

(a) TRISO packing fraction distributions.

Figure 7.35: AHTR one-third assembly models and TRISO distributions for the 3 reactor models on simulation a-3b-256's Pareto front that most-minimized each objective, and 1 reactor model that equally minimized all three objectives. Simulation a-3b – ROLLO three-objective optimization to minimize total fuel packing fraction (PF_{total}), maximum temperature (T_{max}), and fuel-normalized power peaking factor (PPF_{fuel}) in the one-third assembly. Input parameters varied: total fuel packing fraction PF_{total}, TRISO packing fraction distribution ($\rho_{TRISO}(\vec{r})$), coolant channel shape (r_1, r_2, r_3, r_4, r_5).

Figure 7.36 shows the one-third assembly centerline temperatures for three reactors on simulation a-3b-356's Pareto front: reactor model 36 with most-minimized PF_{total}, reactor model 4 with most-minimized T_{max}, and reactor model 17 with most-minimized PPF_{fuel}. r_1, r_2, r_3, r_4, and r_5 values correspond to the FliBe channel at 18cm, 15cm, 12cm, 8cm, and 6cm, respectively. Figure 7.36a shows that all three reactor models peak in the 1st graphite plank (at 3.52cm) with r_1 values

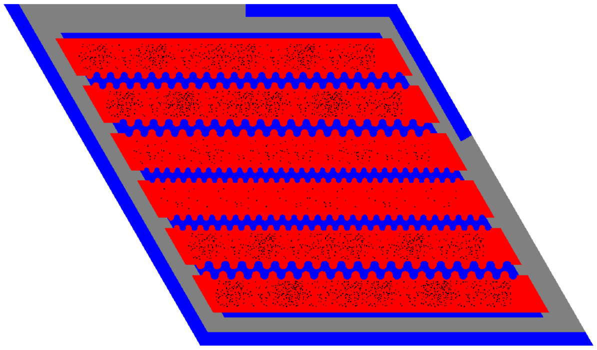

(b) AHTR one-third assembly model with the most-minimized PF_{total} (reactor model 36).

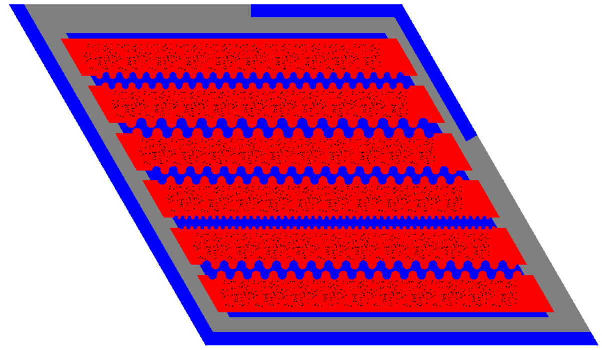

(c) AHTR one-third assembly model with the most-minimized T_{max} (reactor model 4).

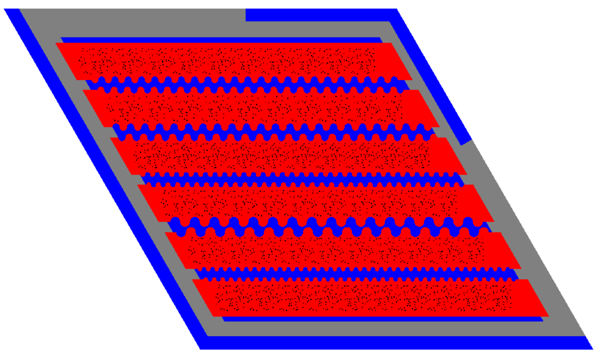

(d) AHTR one-third assembly model with the most-minimized PPF_{fuel} (reactor model 17).

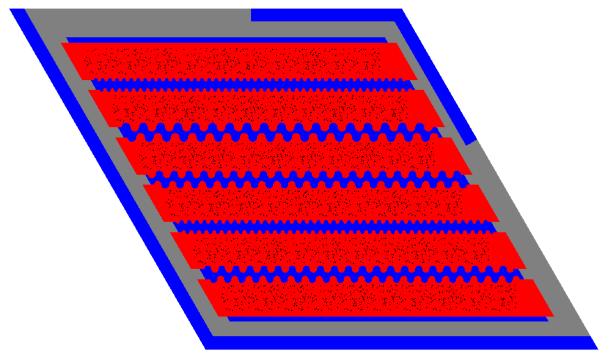

(e) AHTR one-third assembly model that equally minimized all objectives (reactor model 11).

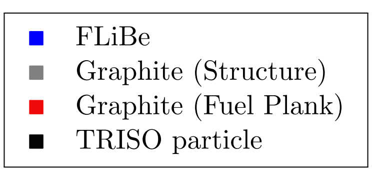

Figure 7.35: (contd.) AHTR one-third assembly models and TRISO distributions for the 3 reactor models on simulation a-3b-256's Pareto front that most-minimized each objective, and 1 reactor model that equally minimized all three objectives. Simulation a-3b – ROLLO three-objective optimization to minimize total fuel packing fraction (PF_{total}), maximum temperature (T_{max}), and fuel-normalized power peaking factor (PPF_{fuel}) in the one-third assembly. Input parameters varied: total fuel packing fraction PF_{total}, TRISO packing fraction distribution ($\rho_{TRISO}(\vec{r})$), coolant channel shape (r_1, r_2, r_3, r_4, r_5).

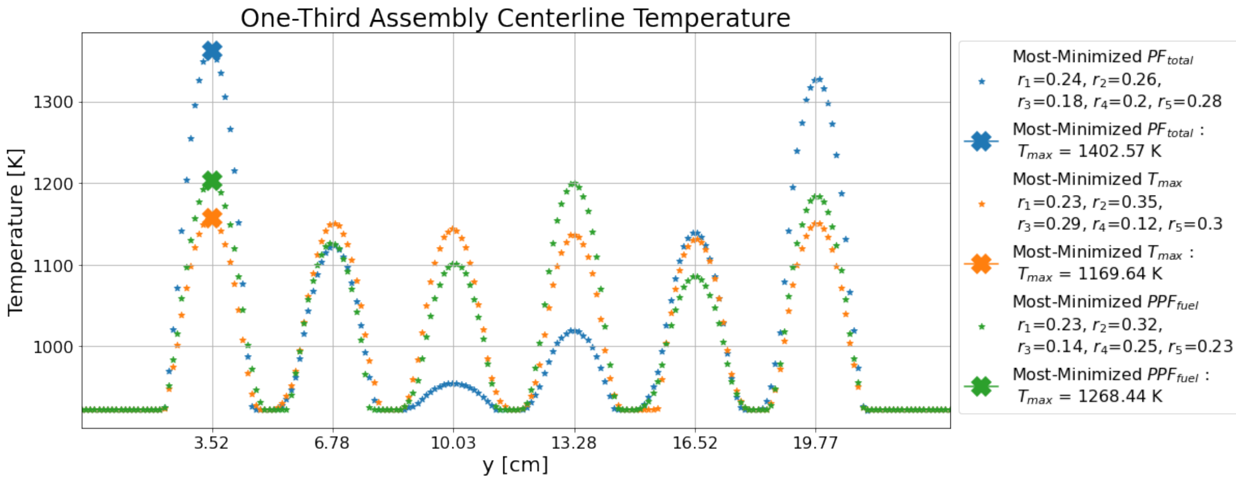

(a) Centerline temperature. AHTR assembly's centerline is the white line in Figure 5.14.

Figure 7.36: Simulation a-3b-256's one-third assembly reactor models' temperature distribution. Reactor models are on simulation a-3b-256's Pareto front: reactor model 36 with most-minimized PF_{total}, reactor model 4 with most-minimized T_{max}, and reactor model 17 with most-minimized PPF_{fuel}. r_1, r_2, r_3, r_4, and r_5 values correspond to the FliBe channel at 18cm, 15cm, 12cm, 8cm, and 6cm, respectively.

of ~ $0.23cm$. The larger radius values closer to temperature peaks enables lower T_{max} values in simulation a-3b-256 compared to simulation a-3b's equivalent reactor models (Figure 7.33a). This suggests that simulation a-3b-256's larger population size enabled ROLLO to explore more reactor model variations and find even more optimal reactor models that further minimized T_{max}.

7.7 Summary

This chapter described the Advanced High-Temperature Reactor (AHTR) one-third assembly's Reactor evOLutionary aLgorithm Optimizer (ROLLO) optimization results. I varied the following AHTR one-third assembly input parameters: Tristructural Isotropic (TRISO) packing fraction distribution ($\rho_{TRISO}(\vec{r})$), total fuel packing fraction (PF_{total}), and coolant channel shape; to minimize the following objectives: PF_{total}, maximum temperature (T_{max}), and fuel-normalized power peaking factor (PPF_{fuel}) in the one-third assembly.

In Section 7.2's single-objective optimization simulations: a-1a, a-1b, a-1c, a-1d, a-1e, a-1f; and Sections 7.6.1, 7.6.2, and 7.6.3 discussions, I verified that each of the one-third assembly objective follows the same driving factors as the AHTR plank optimization objectives (Chapter 6) and described each objective's relationship with each input parameter. I determined that ROLLO flattens TRISO distribution and maximizes the coolant channel shape's radius values (r_1, r_2, r_3, r_4, r_5) that are close to the reactor model's temperature peak to achieve the minimize T_{max} objective. The minimize PF_{total} objective is driven by maximizing the one-third assembly's total fission reaction rate and influences oscillations in the TRISO distribution to achieve the objective. The minimize PPF_{fuel} objective is driven by flattening the one-third assembly's thermal flux distribution and influences PF_{total} and oscillations in the TRISO distribution to achieve the objective. Both the minimize PF_{total} and minimize PPF_{fuel} objectives do not correlate with the coolant channel shape. Simulation a-1b and a-1e results demonstrated that coolant channel shape variation does not have as high of an impact on T_{max} as TRISO distribution variation.

In Sections 7.3 and 7.4's multi-objective optimization simulations: a-2a, a-2b, a-2c, a-3a, a-3b, a-3b-256; and the accompanying discussion in Section 7.6.4, I further analyzed how the objectives' combined effects resulted in the optimal reactor models found by each multi-objective optimization simulation. The multi-objective optimization simulations successfully found a wide spread of reactor models on their Pareto fronts that meet each objective to varying degrees. In the multi-objective optimization simulations, the minimize T_{max} objective continued to influence the flattening of the TRISO distribution and maximizing of the coolant channel shape's radius values (r_1, r_2, r_3, r_4, r_5) that are close to the reactor model's temperature peak. Simulation a-2b results suggested that the minimize PF_{total} objective's driving factor maximize total fission reaction rate and minimize PPF_{fuel} objective's driving factor flattening thermal flux distribution influence each other resulting in unexpected TRISO distributions at different PF_{total} values.

Simulation a-3b-256's multi-objective optimization shows the result of minimizing all three objectives (minimize PF_{total}, T_{max}, and PPF_{fuel}) while varying all the input parameters (PF_{total}, TRISO distribution, and coolant channel shape). Figure 7.34 shows the 38 reactor models on simulation a-3b-256's Pareto front that meet all three objectives. The reactor models on the Pareto Front have different PF_{total}, TRISO distributions, and coolant channel shapes, depending on the extent each objective is minimized due to the nature of multi-objective optimization that results in a tradeoff between objectives. These results demonstrate ROLLO's success in conducting a multi-objective global search of the large AHTR design space to find optimal reactor models that satisfy all the objectives. ROLLO also gives the reactor designer a sense of how sensitive each input parameter is in relation to the objectives. Once the ROLLO search is complete, reactor designers gain a better intuition of the model's reactor physics and can view the narrower reactor design space that meets their defined objectives. From there, reactor designers can determine the importance of each objective for their purposes, then conduct sensitivity analysis and use higher fidelity models to study the optimal design space further.

References

[1] D. Petti, "The future of nuclear energy in a carbon-constrained world," *Massachusetts Institute of Technology Energy Initiative (MITEI)*, p. 272, 2018.

[2] "U.S. Energy Information Administration (EIA)."

[3] "Climate change widespread, rapid, and intensifying – IPCC — IPCC."

[4] *Climate Change and Nuclear Power 2018.* Non-serial Publications, Vienna: INTERNATIONAL ATOMIC ENERGY AGENCY, 2018.

[5] "Nuclear energy and climate change - World Nuclear Association."

[6] "Nuclear Power in a Clean Energy System – Analysis."

[7] J. Simpson, J. Haley, C. Cramer, O. Shafer, A. Elliott, B. Peter, L. Love, and R. Dehoff, "CONSIDERATIONS FOR APPLICATION OF ADDITIVE MANUFACTURING TO NUCLEAR REACTOR CORE COMPONENTS," p. 43, May 2019.

[8] K. A. Terrani, "Transformational Challenge Reactor demonstration program," tech. rep., 2019.

[9] V. Sobes, B. Hiscox, E. Popov, M. Delchini, R. Archibald, P. Laiu, B. Betzler, and K. Terrani, "ARTIFICIAL INTELLIGENCE DESIGN OF NUCLEAR SYSTEMS EMPOWERED BY ADVANCED MANUFACTURING," p. 8, 2020.

[10] A. Bergeron and J. B. Crigger, "Early progress on additive manufacturing of nuclear fuel materials," *Journal of Nuclear Materials*, vol. 508, pp. 344–347, 2018. ISBN: 0022-3115 Publisher: Elsevier.

[11] N. D. See, S. Cetiner, and B. R. Betzler, "Design Optimization of the Transformational Challenge Reactor Outlet Plenum," *Nuclear Science and Engineering*, pp. 1–20, Jan. 2022.

[12] G. J. Y. Chee, "rollo: Reactor Evolutionary Algorithm Optimizer," May 2021.

[13] P. K. Romano, N. E. Horelik, B. R. Herman, A. G. Nelson, B. Forget, and K. Smith, "OpenMC: A state-of-the-art Monte Carlo code for research and development," *Annals of Nuclear Energy*, vol. 82, pp. 90–97, Aug. 2015.

[14] A. Lindsay, G. Ridley, A. Rykhlevskii, and K. Huff, "Introduction to Moltres: An application for simulation of Molten Salt Reactors," *Annals of Nuclear Energy*, vol. 114, pp. 530–540, Apr. 2018.

[15] GIF, "A Technology Roadmap Updtate for Generation IV Nuclear Energy Systems," Tech. Rep. GIF-002-00, US DOE Nuclear Energy Research Advisory Committee and the Generation IV International Forum, 2002.

[16] C. W. Forsberg, K. A. Terrani, L. L. Snead, and Y. Katoh, "Fluoride-Salt-Cooled High-Temperature Reactor (FHR) with Silicon-Carbide-Matrix Coated-Particle Fuel," in *Transactions of the American Nuclear Society*, vol. 107, p. 907, 2012.

[17] M. I. T. Facilitators, U. M. Facilitators, and U. B. Facilitators, "Fluoride-Salt-Cooled, High-Temperature Reactor (FHR) Development Roadmap and Test Reactor Performance Requirements White Paper," 2013.

[18] B. Petrovic, K. Ramey, and I. Hill, "Benchmark Specifications for the Fluoride-salt High-temperature Reactor (FHR) Reactor Physics Calculations," tech. rep., Nuclear Energy Agency, Mar. 2021.

[19] P. K. Romano and B. Forget, "The OpenMC Monte Carlo particle transport code," *Annals of Nuclear Energy*, vol. 51, pp. 274–281, Jan. 2013.

[20] M. B. Chadwick, M. Herman, P. Obložinský, M. E. Dunn, Y. Danon, A. C. Kahler, D. L. Smith, B. Pritychenko, G. Arbanas, R. Arcilla, R. Brewer, D. A. Brown, R. Capote, A. D. Carlson, Y. S. Cho, H. Derrien, K. Guber, G. M. Hale, S. Hoblit, S. Holloway, T. D. Johnson, T. Kawano, B. C. Kiedrowski, H. Kim, S. Kunieda, N. M. Larson, L. Leal, J. P. Lestone, R. C. Little, E. A. McCutchan, R. E. MacFarlane, M. MacInnes, C. M. Mattoon, R. D. McKnight, S. F. Mughabghab, G. P. A. Nobre, G. Palmiotti, A. Palumbo, M. T. Pigni, V. G. Pronyaev, R. O. Sayer, A. A. Sonzogni, N. C. Summers, P. Talou, I. J. Thompson, A. Trkov, R. L. Vogt, S. C. van der Marck, A. Wallner, M. C. White, D. Wiarda, and P. G. Young, "ENDF/B-VII.1 Nuclear Data for Science and Technology: Cross Sections, Covariances, Fission Product Yields and Decay Data," *Nuclear Data Sheets*, vol. 112, pp. 2887–2996, Dec. 2011.

[21] C. Behar, "Technology roadmap update for generation IV nuclear energy systems," in *OECD Nuclear Energy Agency for the Generation IV International Forum, accessed Jan*, vol. 17, pp. 2014–03, 2014. Issue: 2018.

[22] C. W. Forsberg, P. F. Peterson, and P. S. Pickard, "Molten-salt-cooled advanced high-temperature reactor for production of hydrogen and electricity," *Nuclear Technology*, vol. 144, no. 3, pp. 289–302, 2003. ISBN: 0029-5450 Publisher: Taylor & Francis.

[23] M. K. M. Ho, G. H. Yeoh, and G. Braoudakis, "Molten salt reactors," in *Materials and processes for energy: communicating current research and technological developments* (A. Méndez-Vilas, ed.), no. 1 in Energy Book Series, pp. 761–768, Badajoz, Spain: Formatex Research Center, 2013 ed., 2013. http://www.formatex.info/energymaterialsbook/ http://www.energymaterialsbook.org/chapters.html.

[24] M. W. Rosenthal, P. R. Kasten, and R. B. Briggs, "Molten-Salt Reactors - History, Status, and Potential," *Nuclear Applications and Technology*, vol. 8, pp. 107–117, Feb. 1970.

[25] R. O. Scarlat, M. R. Laufer, E. D. Blandford, N. Zweibaum, D. L. Krumwiede, A. T. Cisneros, C. Andreades, C. W. Forsberg, E. Greenspan, L.-W. Hu, and P. F. Peterson, "Design and licensing strategies for the fluoride-salt-cooled, high-temperature reactor (FHR) technology," *Progress in Nuclear Energy*, vol. 77, pp. 406–420, Nov. 2014.

[26] R. O. Scarlat and P. F. Peterson, "The current status of fluoride salt cooled high temperature reactor (FHR) technology and its overlap with HIF target chamber concepts," *Nuclear Instruments and Methods in Physics Research Section A: Accelerators, Spectrometers, Detectors and Associated Equipment*, vol. 733, pp. 57–64, 2014. ISBN: 0168-9002 Publisher: Elsevier.

[27] D. L. Krumwiede, R. O. Scarlat, J. K. Choi, T. M. Phan, and P. F. Peterson, "Three-dimensional modeling of the pebble-bed fluoride-salt-cooled, high-temperature reactor (PB-FHR) commercial plant design," in *Proceedings of the American Nuclear Society 2013 Winter Meeting*, 2013.

[28] L. Liu, D. Zhang, Q. Lu, K. Wang, and S. Qiu, "Preliminary neutronic and thermal-hydraulic analysis of a 2 MW Thorium-based Molten Salt Reactor with Solid Fuel," *Progress in Nuclear Energy*, vol. 86, pp. 1–10, Jan. 2016.

[29] D. E. Holcomb, D. Ilas, V. K. Varma, A. T. Cisneros, R. P. Kelly, and J. C. Gehin, "Core and refueling design studies for the advanced high temperature reactor," *ORNL/TM-2011/365, Oak Ridge National Laboratory, Oak Ridge, TN*, 2011.

[30] V. K. Varma, D. E. Holcomb, F. J. Peretz, E. C. Bradley, D. Ilas, A. L. Qualls, and N. M. Zaharia, "AHTR mechanical, structural, and neutronic preconceptual design," tech. rep., Oak Ridge National Lab.(ORNL), Oak Ridge, TN (United States), 2012.

[31] S. R. Greene, J. C. Gehin, D. E. Holcomb, J. J. Carbajo, D. Ilas, A. T. Cisneros, V. K. Varma, W. R. Corwin, D. F. Wilson, and G. L. Yoder Jr, "Pre-conceptual design of a fluoride-salt-cooled small modular advanced high-temperature reactor (SmAHTR)," *Oak Ridge National Laboratory, ORNL/TM-2010/199*, 2010.

[32] K. M. Ramey and B. Petrovic, "Monte Carlo modeling and simulations of AHTR fuel assembly to support V&V of FHR core physics methods," *Annals of Nuclear Energy*, vol. 118, pp. 272–282, Aug. 2018.

[33] F. Rahnema, D. Diamond, D. Serghiuta, and P. Burke, "Phenomena, gaps, and issues for neutronics modeling and simulation of FHRs," *Annals of Nuclear Energy*, vol. 123, pp. 172–179, Jan. 2019.

[34] F. Rahnema, B. Petrovic, C. Edgar, D. Zhang, P. Avigni, M. Huang, and S. Terlizzi, "The Current Status of the Tools for Modeling and Simulation of Advanced High Temperature Reactor Neutronics Analysis," tech. rep., Georgia Institute of Technology, 2015.

[35] D. E. Holcomb, G. F. Flanagan, G. T. Mays, W. D. Pointer, K. R. Robb, and G. L. Yoder Jr, "Fluoride salt-cooled high-temperature reactor technology development and demonstration roadmap," *ORNL/TM-2013/401, ORNL, Oak Ridge, TN*, 2013.

[36] D. Zhang and F. Rahnema, "Integrated Approach to Fluoride High Temperature Reactor Technology and Licensing Challenges (FHR-IRP)," tech. rep., Georgia Inst. of Technology, Atlanta, GA (United States), 2019.

[37] A. T. Cisneros and D. Ilas, "Neutronics and Depletion Methods for Parametric Studies of Fluoride Salt Cooled High Temperature Reactors with Slab Fuel Geometry and Multi-Batch Fuel Management Schemes," 2012.

[38] L. Mei, X. Cai, D. Jiang, J. Chen, Y. Zhu, Y. Liu, and X. Wang, "The investigation of thermal neutron scattering data for molten salt Flibe," *Journal of Nuclear Science and Technology*, vol. 50, no. 7, pp. 682–688, 2013. ISBN: 0022-3131 Publisher: Taylor & Francis.

[39] Y. Zhu and A. I. Hawari, "Thermal neutron scattering cross section of liquid FLiBe," *Progress in Nuclear Energy*, vol. 101, pp. 468–475, 2017. ISBN: 0149-1970 Publisher: Elsevier.

[40] C. A. Gentry, *Development of a Reactor Physics Analysis Procedure for the Plank-Based and Liquid Salt-Cooled Advanced High Temperature Reactor*. PhD thesis, 2016.

[41] J. Leppanen, M. Pusa, T. Viitanen, V. Valtavirta, and T. Kaltiaisenaho, "The Serpent Monte Carlo code: Status, development and applications in 2013," *Annals of Nuclear Energy*, vol. 82, pp. 142–150, Aug. 2014.

[42] P. Turinsky, R. Al-Chalabi, P. Engrand, H. Sarsour, F. Faure, and W. Guo, "NESTLE: Few-group neutron diffusion equation solver utilizing the nodal expansion method for eigenvalue, adjoint, fixed-source steady-state and transient problems," Tech. Rep. EGG-NRE–11406, 10191160, June 1994.

[43] K. Koebke, "A new approach to homogenization and group condensation," tech. rep., 1980.

[44] H.-C. Lin, *Thermal Hydraulics System-Level Code Validation and Transient Analyses for Fluoride Salt-Cooled High-Temperature Reactors*. PhD thesis, 2020.

[45] "Fluoride Salt-Cooled High-Temperature Reactor (FHR) Benchmark."

[46] B. A. Lindley, J. G. Hosking, P. J. Smith, D. J. Powney, B. S. Tollit, T. D. Newton, R. Perry, T. C. Ware, and P. N. Smith, "Current status of the reactor physics code WIMS and recent developments," *Annals of Nuclear Energy*, vol. 102, pp. 148–157, 2017. ISBN: 0306-4549 Publisher: Elsevier.

[47] B. Petrovic, K. Ramey, I. Hill, E. Losa, M. Elsawi, Z. Wu, C. Lu, J. Gonzales, D. Novog, and G. Chee, "Preliminary Results of the NEA FHR Benchmark Phase IA and IB (Fuel Element 2-D Benchmark)," in *The International Conference on Mathematics and Computational Methods Applied to Nuclear Science and Engineering, Raleigh, NC*, 2021.

[48] B. Petrovic and K. M. Ramey, "FHR/AHTR NEA Benchmark," Oct. 2019.

[49] X.-. M. C. Team, "MCNP — A General Monte Carlo N-Particle Transport Code, Version 5," Tech. Rep. LA-UR-03-1987, LANL, Los Alamos, NM, Apr. 2003.

[50] R. Macfarlane, D. W. Muir, R. M. Boicourt, A. C. Kahler III, and J. L. Conlin, "The NJOY nuclear data processing system, version 2016," tech. rep., Los Alamos National Lab.(LANL), Los Alamos, NM (United States), 2017.

[51] I. Gibson, D. W. Rosen, and B. Stucker, *Additive manufacturing technologies*, vol. 17. Springer, 2014.

[52] A. Standard, "Standard terminology for additive manufacturing technologies," *ASTM International F2792-12a*, 2012.

[53] A. Uriondo, M. Esperon-Miguez, and S. Perinpanayagam, "The present and future of additive manufacturing in the aerospace sector: A review of important aspects," *Proceedings of the Institution of Mechanical Engineers, Part G: Journal of Aerospace Engineering*, vol. 229, no. 11, pp. 2132–2147, 2015. ISBN: 0954-4100 Publisher: SAGE Publications Sage UK: London, England.

[54] "Printed titanium parts expected to save millions in Boeing Dreamliner costs," *Reuters*, Apr. 2017.

[55] "Transformation In 3D: How A Walnut-Sized Part Changed The Way GE Aviation Builds Jet Engines | GE News," 2018.

[56] "Roadmap for Regulatory Acceptance of Advanced Manufacturing Methods in the Nuclear Energy Industry," NEI Report, Nuclear Energy Institute.

[57] N. Sridharan, M. N. Gussev, and K. G. Field, "Performance of a ferritic/martensitic steel for nuclear reactor applications fabricated using additive manufacturing," *Journal of Nuclear Materials*, vol. 521, pp. 45–55, 2019. ISBN: 0022-3115 Publisher: Elsevier.

[58] B. Betzler, B. Ade, A. Wysocki, P. Jain, P. Chesser, M. Greenwood, and K. Terrani, "Transformational Challenge Reactor preconceptual core design studies," *Nuclear Engineering and Design*, vol. 367, p. 110781, Oct. 2020.

[59] M. P. Trammell, B. C. Jolly, M. D. Richardson, A. T. Schumacher, and K. A. Terrani, "Advanced Nuclear Fuel Fabrication: Particle Fuel Concept for TCR," tech. rep., 2019.

[60] J. Rosales, I. J. van Rooyen, and C. J. Parga, "Characterizing surrogates to develop an additive manufacturing process for U3Si2 nuclear fuel," *Journal of Nuclear Materials*, vol. 518, pp. 117–128, 2019. ISBN: 0022-3115 Publisher: Elsevier.

[61] T. Koyanagi, K. Terrani, S. Harrison, J. Liu, and Y. Katoh, "Additive manufacturing of silicon carbide for nuclear applications," *Journal of Nuclear Materials*, vol. 543, p. 152577, 2020. ISBN: 0022-3115 Publisher: Elsevier.

[62] C. Sauder, "Ceramic matrix composites: nuclear applications," *Ceramic matrix composites: materials, modeling and technology*, pp. 609–646, 2014. Publisher: Wiley Online Library.

[63] L. L. Snead, T. Nozawa, Y. Katoh, T.-S. Byun, S. Kondo, and D. A. Petti, "Handbook of SiC properties for fuel performance modeling," *Journal of nuclear materials*, vol. 371, no. 1-3, pp. 329–377, 2007. ISBN: 0022-3115 Publisher: Elsevier.

[64] K. A. Terrani, J. O. Kiggans, C. M. Silva, C. Shih, Y. Katoh, and L. L. Snead, "Progress on matrix SiC processing and properties for fully ceramic microencapsulated fuel form," *Journal of Nuclear Materials*, vol. 457, pp. 9–17, 2015. ISBN: 0022-3115 Publisher: Elsevier.

[65] J. Byrne, P. Cardiff, A. Brabazon, and M. ONeill, "Evolving parametric aircraft models for design exploration and optimisation," *Neurocomputing*, vol. 142, pp. 39–47, Oct. 2014.

[66] H. A. Simon, *The sciences of the artificial.* MIT press, 2019.

[67] K. Deb, *Multi-objective optimization using evolutionary algorithms*, vol. 16. John Wiley & Sons, 2001.

[68] W. F. Sacco and C. M. Pereira, "Two stochastic optimization algorithms applied to nuclear reactor core design," *Progress in Nuclear Energy*, vol. 48, no. 6, pp. 525–539, 2006. ISBN: 0149-1970 Publisher: Elsevier.

[69] W. F. Sacco, H. Alves Filho, N. Henderson, and C. R. de Oliveira, "A Metropolis algorithm combined with Nelder–Mead Simplex applied to nuclear reactor core design," *Annals of Nuclear Energy*, vol. 35, no. 5, pp. 861–867, 2008. ISBN: 0306-4549 Publisher: Elsevier.

[70] F. Y. Odeh and W. S. Yang, "Core design optimization and analysis of the Purdue Novel Modular Reactor (NMR-50)," *Annals of Nuclear Energy*, vol. 94, pp. 288–299, 2016. ISBN: 0306-4549 Publisher: Elsevier.

[71] C. D. Fletcher and R. R. Schultz, "RELAP5/MOD3 code manual," tech. rep., Nuclear Regulatory Commission, 1992.

[72] D. J. Kropaczek and R. Walden, "Large-Scale Application of the Constraint Annealing Method for Pressurized Water Reactor Core Design Optimization," *Nuclear Science and Engineering*, vol. 193, no. 5, pp. 523–536, 2019. ISBN: 0029-5639 Publisher: Taylor & Francis.

[73] D. J. Kropaczek and R. Walden, "Constraint annealing method for solution of multiconstrained nuclear fuel cycle optimization problems," *Nuclear Science and Engineering*, vol. 193, no. 5, pp. 506–522, 2019. ISBN: 0029-5639 Publisher: Taylor & Francis.

[74] B. R. Betzler, D. Chandler, D. H. Cook, E. E. Davidson, and G. Ilas, "Design optimization methods for high-performance research reactor core design," *Nuclear Engineering and Design*, vol. 352, p. 110167, 2019. ISBN: 0029-5493 Publisher: Elsevier.

[75] C. M. Pereira and C. M. Lapa, "Coarse-grained parallel genetic algorithm applied to a nuclear reactor core design optimization problem," *Annals of Nuclear Energy*, vol. 30, no. 5, pp. 555–565, 2003. ISBN: 0306-4549 Publisher: Elsevier.

[76] C. M. Pereira and W. F. Sacco, "A parallel genetic algorithm with niching technique applied to a nuclear reactor core design optimization problem," *Progress in Nuclear Energy*, vol. 50, pp. 740–746, Sept. 2008.

[77] S. Kamalpour and H. Khalafi, "SMART reactor core design optimization based on FCM fuel," *Nuclear Engineering and Design*, p. 110970, 2020. ISBN: 0029-5493 Publisher: Elsevier.

[78] A. Kumar and P. V. Tsvetkov, "A new approach to nuclear reactor design optimization using genetic algorithms and regression analysis," *Annals of Nuclear Energy*, vol. 85, pp. 27–35, Nov. 2015.

[79] S. Krish, "A practical generative design method," *Computer-Aided Design*, vol. 43, pp. 88–100, Jan. 2011.

[80] G. Renner and A. Ekárt, "Genetic algorithms in computer aided design," *Computer-aided design*, vol. 35, no. 8, pp. 709–726, 2003.

[81] D. E. Goldberg, "Genetic algorithms in search," *Optimization, and MachineLearning*, 1989. Publisher: Addison Wesley Publishing Co. Inc.

[82] K. Deb, A. Pratap, S. Agarwal, and T. Meyarivan, "A fast and elitist multiobjective genetic algorithm: NSGA-II," *IEEE transactions on evolutionary computation*, vol. 6, no. 2, pp. 182–197, 2002. ISBN: 1089-778X Publisher: IEEE.

[83] D. E. Goldberg, K. Deb, and D. Thierens, "Toward a better understanding of mixing in genetic algorithms," *Journal of the Society of Instrument and Control Engineers*, vol. 32, no. 1, pp. 10–16, 1993. ISBN: 0453-4662 Publisher: The Society of Instrument and Control Engineers.

[84] A. Ng, K. Katanforoosh, and Y. B. Mourri, "Improving Deep Neural Networks: Hyperparameter Tuning, Regularization and Optimization," 2021.

[85] J. Jordan, "Hyperparameter tuning for machine learning models.," Nov. 2017.

[86] G. Chee, "arfc/fhr-benchmark," 2021.

[87] NCSA, "About Blue Waters: The National Center for Supercomputing Applications at the University of Illinois at Urbana-Champaign," 2017. http://www.ncsa.illinois.edu/.

[88] M. Torabi, A. Lashkari, S. F. Masoudi, and S. Bagheri, "Neutronic analysis of control rod effect on safety parameters in Tehran Research Reactor," *Nuclear Engineering and Technology*, vol. 50, no. 7, pp. 1017–1023, 2018. ISBN: 1738-5733 Publisher: Elsevier.

[89] A. Lindsay, "Moltres, software for simulating Molten Salt Reactors," 2017. https://github.com/arfc/moltres.

[90] J. A. Bucholz, "SCALE: A modular code system for performing standardized computer analyses for licensing evaluation," NUREG NUREG/CR-0200-Vol.2-Bk.2; ORNL/NUREG/CSD-2-Vol.2-Bk.2 ON: DE82013370; TRN: 82-013156, Oak Ridge National Lab., TN (USA), 1982.

[91] C. Geuzaine and J.-F. Remacle, "Gmsh: A 3-D finite element mesh generator with built-in pre- and post-processing facilities," *International Journal for Numerical Methods in Engineering*, vol. 79, no. 11, pp. 1309–1331, 2009. _eprint: https://onlinelibrary.wiley.com/doi/pdf/10.1002/nme.2579.

[92] K. M. Ramey, *Methodology for Coupled Reactor Physics, Thermal Hydraulics, and Depletion of a Fluoride Salt-Cooled High-Temperature Reactor (FHR)*. PhD thesis, Georgia Institute of Technology, 2021.

[93] F.-A. Fortin, F.-M. D. Rainville, M.-A. Gardner, M. Parizeau, and C. Gagné, "DEAP: Evolutionary algorithms made easy," *Journal of Machine Learning Research*, vol. 13, no. Jul, pp. 2171–2175, 2012.

[94] A. Garrett, "inspyred: Bio-inspired Algorithms in Python," *URL: https://pypi. python. org/pypi/inspyred (visited on 11/28/2016)*, 2014.

[95] C. S. Perone, "Pyevolve: a Python open-source framework for genetic algorithms," *Acm Sigevolution*, vol. 4, no. 1, pp. 12–20, 2009.

[96] C. Gagné and M. Parizeau, "Open BEAGLE: A New Versatile C++ Framework for Evolutionary Computation.," in *GECCO Late Breaking Papers*, pp. 161–168, Citeseer, 2002.

[97] G. J. Y. Chee, "Documentation for rollo (Reactor Evolutionary Algorithm Optimizer)," 2021.

[98] Ronacher, "Welcome to Jinja2 - Jinja2 Documentation (2.10)," 2018.

[99] R. Smallshire, "multiprocessing_on_dill 3.5.0a4 : A friendly fork of multiprocessing which uses dill instead of pickle."

[100] D. Ackley, *A connectionist machine for genetic hillclimbing*, vol. 28. Springer Science & Business Media, 2012.

[101] SFU, "Ackley Function."

[102] T. T. Binh and U. Korn, "MOBES: A multiobjective evolution strategy for constrained optimization problems," in *The third international conference on genetic algorithms (Mendel 97)*, vol. 25, p. 27, 1997.

[103] M. Bassi, E. S. d. Cursi, E. Pagnacco, and R. Ellaia, "Statistics of the Pareto front in Multi-objective Optimization under Uncertainties," *Latin American Journal of Solids and Structures*, vol. 15, Nov. 2018. Publisher: Associação Brasileira de Ciências Mecânicas.

[104] A. P. Guerreiro, C. M. Fonseca, and L. Paquete, "The Hypervolume Indicator: Problems and Algorithms," *arXiv:2005.00515 [cs]*, May 2020. arXiv: 2005.00515.

[105] A. Blanchard, K. R. Yates, J. F. Zino, D. Biswas, S. C. Aiken, D. E. Carlson, H. Hoang, and D. Heemstra, "Updated Critical Mass Estimates for Plutonium-238," tech. rep., Savannah River Site, 1999.

[106] "Theta/ThetaGPU | Argonne Leadership Computing Facility."

[107] G. Chee, "Dissertation Results Repository," 2021. https://github.com/gwenchee/dissertation-results.

[108] "Argonne Leadership Computing Facility," 2022.